On a Two-Dimensional Inverse Scattering Problem for a Dielectric

Dissertation

zur Erlangung des Dokorgrades

der Mathematisch-Naturwissenschaftlichen Fakultäten

Georg-August-Universität zu Göttingen

vorgelegt

Ahmet Altundag

aus Mardin, der Türkei

Göttingen January, 2012

D7
Referent: Prof. Dr. R. Kress
Korreferent: Prof. Dr. T. Hohage
Tag der mündlichen Prüfung:

Acknowledgements

Contents

Chapter 1

Introduction

1.1 Introduction

Two problems are said to be inverse to each other if the solution to the first is required to formulate the second and vise-versa. There are several simple examples of inverse problems such as division and multiplication or differentiation and integration. Usually one of them has been studied or investigated for a longer time and is therefore better understood or comprehended than the other. In this way this problem has become easier to solve and is therefore called the direct problem. The inverse problem is then remaining problem of the pair. Solving the inverse problem usually requires harder or even new techniques.

Scattering theory has been studied over the last century (see [6, 7, 40]). Scattering theory is concerned with modeling the effects of objects and inhomogeneities on the propagation of waves. In the direct scattering problem the object is given and it is required to find the scattered wave. In the inverse scattering problem one wants to receive information on the shape or physical parameters of the scattering objects.

For Problems in mathematical physics, in particular for initial and boundary value problems, Hadamard [24] postulated three properties:

1. Existence of a solution.

2. Uniqueness of the solution.

3. Continuous dependence of the solution on the data.

A problem satisfying all three requirements is called well-posed or properly-posed and if one of these properties is violated then the problem is said to be ill-posed or improperly-posed. In most cases the inverse scattering problem is ill-posed. This means it fails to be uniquely solvable or the solution does not continuously depend on data, i.e., small errors in the data cause large errors in the solution. The ill-posedness is a great challenge for numerical methods to solve the inverse scattering

problem since they have to somehow stabilize the ill-posedness of the problem. It is not seldom that mathematical problems arising from applications are ill-posed and therefore this is an area of great interest for several areas of science today.

The mathematical modeling of the application of scattering phenomena in various non-destructive evaluation techniques leads to inverse scattering problems for time-harmonic electromagnetic waves. In principle, in these approaches the effects of scattering objects on the propagation of electromagnetic waves are exploited to obtain images of the nature of the scattering objects, i.e., inverse scattering constitutes a particular method of imaging. As opposed to classical techniques of imaging such as computerized tomography, that is based on the fact that X-rays travel along straight lines, inverse scattering problems take into account that the propagation of electromagnetic waves has to be modeled by a wave equation. This, in particular, implies that inverse scattering leads to nonlinear models whereas inverse X-ray tomography is linear.

The inverse scattering problem that we are consider in this manuscript is in fact ill-posed. We are interested in considering obstacle scattering problems. Roughly speaking, the main concern about these problems are to study the effect that obstacle has on some incident plane waves. Furthermore, we want to observe how this effect is influenced by the property of the obstacle, namely its shape, location and physical constitution. We consider an obstacle D embedded in some known homogeneous background. Knowing the physical properties of the background medium and the obstacle, and considering the total field u is to be the sum of the incident plane wave u^i and the scattered field u^s, then the direct scattering problem consists of determining the scattered field u^s from the knowledge of the obstacle, including the boundary condition, differential equation that governess the propagation of the field. The inverse scattering problem is however much more challenging and interesting than the direct scattering problem. Given information on the scattered field u^s either in the near field or in the far field, and the incident wave u^i, the inverse scattering problem consists of determining some unknown properties of the obstacle, such as its location and shape, or physical constitution. There are a variety of applications since its early statement for radio location, for instance according to Sleeman [46]

- construction of images of tumors (X-ray tomography);

- location of cracks in elastic materials;

- location and identification of discharges in storms for the analysis of the storms themselves and prediction of tornadoes from characteristic source patterns;

- construction of images of aircrafts, missiles, surface vessels and submarines;

- analysis of sound speed variation in water and the sea bed sedimentary layer.

In inverse obstacle scattering problems for time-harmonic waves the scattering object is a homogeneous obstacle and the inverse problem is to obtain an image of the scattering object, i.e., an image of the shape of the obstacle from a knowledge of the scattered wave either at near distances or at large distances, i.e., from the far field pattern. In the current manuscript we deal with dielectric scatterers and confine ourselves to the case of infinitely long cylinders.

We are interested in the special case of time-harmonic acoustic scattering as motivated in section 2.1, i.e., we are interested only in the space dependence u^s of the scattered field. We assume $D \subset \mathbb{R}^2$ is a simply connected bounded domain with C^2-smooth boundary ∂D that represents the cross section of a dielectric infinite cylinder having constant wave number k_d with $Re k_d \geq 0$ and $Im k_d \geq 0$ embedded in a homogeneous background with positive wave number k_0. Denote by ν the outward unit normal vector to ∂D. Then, given an incident plane wave $u^i(x) = e^{ik_0 x \cdot d}$ with incident direction given by the unit vector d, the direct scattering problems for E-polarized electromagnetic waves is modeled by the following transmission problem for the Helmholtz equation: Find solutions $u \in H^1_{\text{loc}}(\mathbb{R}^2 \setminus \bar{D})$ and $v \in H^1(D)$ to the Helmholtz equations

$$\Delta u + k_0^2 u = 0 \quad \text{in } R^2 \setminus \bar{D}, \qquad \Delta v + k_d^2 v = 0 \quad \text{in } D \tag{1.1.1}$$

satisfying the boundary conditions

$$u = v, \qquad \frac{\partial u}{\partial \nu} = Bv \quad \text{on} \quad \partial D \tag{1.1.2}$$

in the trace sense such that $u = u^i + u^s$ with the scattered wave u^s. The operator B defines the boundary condition that is to be satisfied and is related to physical properties of domain D. For $Bv = \dfrac{\partial v}{\partial \nu}$ and for $Bv = \dfrac{\partial v}{\partial \nu} + i\eta v$ the boundary condition (1.1.2) turn out to be transmission boundary condition and conductive boundary condition respectively. The function η is called conductive function. Since these are exterior problems, to ensure uniqueness of the solution for each problem a condition at infinity needs to be imposed. Sommerfeld [47] suggested the radiation condition

$$\lim_{r \to \infty} \sqrt{r}\left(\frac{\partial u^s}{\partial r} - ik_0 u^s\right) = 0, \quad r = |x| \tag{1.1.3}$$

the limit holds uniformly in all directions $\frac{x}{|x|}$. The physical meaning of this condition is that energy is radiating to infinity, in another words, no energy sources are at infinity. With this radiation condition the direct problems are well-posed, since they are uniquely solvable and the scattered wave depends continuously on the incident plane wave u^i.

It can also be shown that the solution u^s to the direct scattering problems can be represented by Green's formula

$$u^s(x) = \int_{\partial D} \left\{ u^s(y) \frac{\partial \Phi(x,y)}{\partial \nu(y)} - \frac{\partial u^s}{\partial \nu}(y)\Phi(x,y) \right\} ds(y) \quad x \in \mathbb{R}^2 \setminus \bar{D}.$$

under appropriate assumptions(see Theorem 2.1.5). Here Φ stands for the fundamental solution to the Helmholtz equation. Moreover, one can show (see Theorem 2.2.1) that the solution u^s has an asymptotic behavior of an outgoing cylindrical wave of the form

$$u^s(x) = \frac{e^{ik|x|}}{\sqrt{|x|}}\{u_\infty(\hat{x}) + O(\frac{1}{|x|})\}, \quad |x| \to \infty,$$

where the function u_∞ defined on a unit circle Ω is called the far-field of the scattered field u^s. Furthermore, by Rellich's lemma(see Lemma 2.3) it uniquely determines the scattered field u^s.

The inverse scattering problems we are interested in are to determine some property of the obstacle from the knowledge of the scattered field u^s either at the large distances or at near distances generated by a known incident plane wave. In this sense we assume that the near field pattern obtained from the scattered field at near distances or far field pattern is the given data. We also assume the priori knowledge that the obstacle is a dielectric and satisfies transmission or conductive boundary condition. Now the inverse scattering problems can be formulated as follows: Given an incident plane wave u^i and the corresponding near field pattern or far field pattern u_∞, determine shape, interior wave number k_d, and simultaneously shape and interior wave number k_d, and the conductive function η for the first, second, third, and fourth problems respectively. More generally, we also consider the reconstruction of these properties from the far field patterns for a small finite number of incident plane waves with different incident directions. These inverse problems are non-linear and ill-posed, since the solution of the scattering problem (1.1.1)-(1.1.3) is non-linear with respect to the boundary and since the mapping from the boundary to the far field pattern is extremely smoothing. To find an approximating solution to these inverse problems in a stable way we will use Tikhonov regularization.

We summarize the four problems we are interested in:

Problem 1 : Given the far field pattern u_∞ for one incident field u^i, determine the shape of the boundary ∂D of the dielectric scatterer D.

Problem 2 : Given the far field pattern u_∞ for one incident field u^i, determine the interior wave number k_d of the dielectric scatterer D.

Problem 3 : Given the far field pattern u_∞ for one incident field u^i, simultaneously determine the shape of the boundary ∂D and the interior wave k_d of the dielectric scatterer D.

Problem 4 : The inverse scattering problem is formulated as follows: Given the far field pattern u_∞ for one incident field u^i, determine the conductive function η of the dielectric scatterer D.
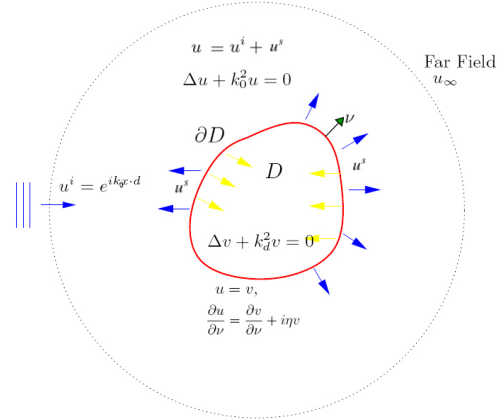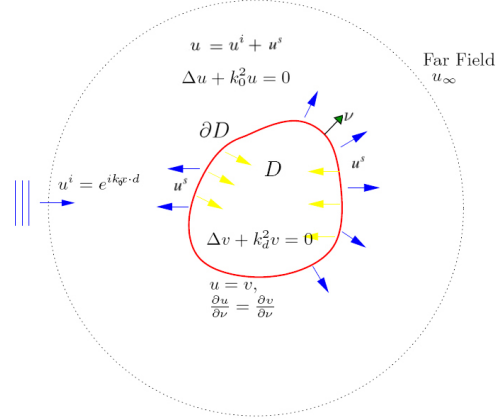
The first three problems have the same direct problem,i.e., the scattered field is obtained from (1.1.1) with transmission boundary condition and the scattered field for the fourth problem is founded from (1.1.1) with conductive boundary condition.

At this point we note that uniqueness results for this inverse transmission problem are only available for the case of infinitely many incident waves (see [28]). A general uniqueness result based on the far field pattern for one or finitely many incident waves is still lacking. In this manuscript we will include a uniqueness result for recovering a dielectric disk from the far field pattern for scattering of one incident plane wave. We also give an overview of some classical and some more recent uniqueness results in section 3.2.1.

In the literature, there exists a large number of numerical methods for solving inverse scattering problems. According to Kress [33], their classification can be split into three groups: iterative, decomposition and sampling or probe methods. Iterative methods interpret the inverse obstacle scattering problem as a nonlinear

ill-posed operator equation in the form

$$F(\partial D) = u_\infty \qquad\qquad (1.1.4)$$

where the operator F maps the boundary ∂D of the obstacle D onto far field pattern u_∞ of the scattered field u^s for a fixed incident field u^i. The operator equation (1.1.4) can be solved by regularized Newton iteration methods because of the availability of Frechet differentiability of the operator F. The regularized Newton iteration methods converge to a local minimum and therefore a good initial guess is required. Furthermore, these methods suffer from high computational effort because they require direct solver at each iteration step. On the other hand, the main advantage of these methods is that the reconstructions are generally very good. For details on how these methods are implemented for such an operator equation (1.1.4), we refer the Colton and Kress [7], Hohage [14], and Kress [30, 31].

Decomposition methods split the ill-posedness and non-linearity of the inverse scattering problem into two parts. In the first part, the scattered field is reconstructed from the ill-posed measured far field data. This is done by representing the scattered field u^s as a suitable layer potential over some appropriate closed curve. The density for the layer potential is found from the given measured far field data. In the second part, the boundary of the scatterer is found by the location where the boundary condition is satisfied. This is done by linearizing L^2-norm of the boundary condition and finding a curve that is minimal with respect to this linearized equation in a least square sense. The main advantage of that method is that it does not require a direct solver. However, the reconstructions obtained by this method are generally worse than the reconstruction obtained from iterative methods. For details we refer to Colton and Monk [8, 9] and Potthast [43].

Sampling or probe methods are based on the numerical evaluation of a criteria in terms of indicator functions that determine whether a point lies inside or outside of the obstacle. In the literature, there exists subclasses of these methods, for instance, the linear sampling method suggested by Colton and Kirsch [5], the factorization method suggested by Kirsch [27], the point source method suggested by Potthast [43], and the probe method suggested by Ikehata [16]. The main advantage of these methods is that they do not require a priori knowledge on the boundary condition. However, a big drawback occurs for these type of methods since they require a huge amount of data in order to obtain a reasonable reconstruction. In addition to this, they usually just reconstruct the obstacle and not the boundary condition.

Recently three new iterative methods were proposed and so far mainly considered for impenetrable scatterers. The first method was suggested by Kress [32] and further investigated by Kress and Serranho [37, 38, 45] and denoted as hybrid method. The second method suggested by Kress and Rundell [36] and developed for inverse scattering problems by Ivanyshyn and Kress [19, 21, 23] and named simultaneous linearization method, and the third method was suggested by Johansson and Sleeman [25].

The aim of this manuscript is to extend these approaches to penetrable scatterers.

- Firstly, we numerically solve the inverse scattering problems for an infinitely long dielectric cylinder embedded in homogeneous background via the hybrid method [37, 38, 45], the simultaneous linearization method [19, 21, 23], and the Johansson and Sleeman method [25] and illustrate their numerical feasibility via synthetic and experimental data.

- Secondly, we include a uniqueness result for recovering a disc from the far field pattern for scattering of one incident plane wave.

- Thirdly, we show connections and differences to the traditional regularized Newton type iterations as applied to the boundary to far field map, including alternatives for the implementation of these Newton iterations.

For the first three problems we represent the solution v and u^s to the forward scattering in terms of single-layer potentials in D and in $\mathbb{R}^2 \setminus \bar{D}$ with densities φ_d and φ_0, respectively. The boundary condition (1.1.2) with *transmission condition* provides a system of two boundary integral equations on ∂D for the corresponding densities, that in the sequel we will denote as field equations. The inverse problem for the first problem,i.e., for the shape reconstruction, the required coincidence of the far field of the single-layer potential representing u^s and the given far field u_∞ provides a further equation that we denote as data equation. The system of the field and data equations can be viewed as three equations for three unknowns, i.e., the two densities and the boundary curve. They are linear with respect to the densities and nonlinear with respect to the boundary curve. This opens up a variety of approaches to solve the system by linearization and iteration.

For the first problem,i.e., for the shape reconstruction, three methods were implemented for this system in the current manuscript. In the spirit of the Johansson and Sleeman method [25], given an approximation $\partial D_{\text{approx}}$ for the boundary ∂D in a first step the well-posed field equations can be solved for two densities on $\partial D_{\text{approx}}$. Then in a second step, keeping the densities fixed, the ill-posed data equation can be linearized with respect to the boundary and the solution of the ill-posed linearized equation can be utilized to update the boundary approximation. Because of the ill-posedness the solution of this update equation requires stabilization, for example, by Tikhonov regularization. These two steps can be iterated until some suitable stopping criterion is satisfied.

In the spirit of the simultaneous linearization method [19, 21, 23, 32, 36] given an approximation $\partial D_{\text{approx}}$ for the boundary ∂D and for the densities $\varphi_{d_{approx}}, \varphi_{0_{approx}}$, all three equations are simultaneously linearized with respect to the boundary and the densities. The solution of the ill-posed linearized equations can be utilized both update the densities and the boundary approximation. This can be iterated until some suitable stopping criterion is satisfied. Because of the ill-posedness the

solution of this update equations require stabilization, for instance, Tikhonov regularization. Note that in order to obtain a suitable initial guess for the densities we solve the well-posed field equations on ∂D_{approx}.

In the spirit of the hybrid method [32, 37, 38, 45] given an approximation $\partial D_{\mathrm{approx}}$ for the boundary ∂D in a first step from the ill-posed data equation, regularized by Tikhonov regularization as above, z density φ_0 can now be found on $\partial D_{\mathrm{approx}}$. Then, in a second step, keeping the density φ_0 fixed, we find the density φ_d from one of the field equations. Then in a third step, keeping the densities fixed, we linearize the remaining field equation with respect to the boundary and the solution of the ill-posed linearized equation can be utilized to update the boundary approximation. Because of the ill-posedness the solution of this update equation requires stabilization, for example, by Tikhonov regularization. These three steps can be iterated until some suitable stopping criterion is satisfied. Here we note that the linearized equation is ill-posed because this ill-posedness is inherited by linearization from the original equation.

For the shape reconstruction, experimental data were also implemented. We obtained the data from the following system and used that data to obtain reconstruction via all three methods.

The experimental system which can be seen in the photo was conducted at the faculty of Electronics and Communication of Istanbul Technical University. For a sufficiently long dielectric obstacle we used a circular cylindrical wood with radius 3 cm. In this system, the transmitter sends electromagnetic plane waves with the frequency one GHz polarized in the direction of the cylinder axis. The distance between the transmitter and the cylinder axis is one meter. The receiver is located one meter away from cylindrical wood and rotates around it and collects data. In order to decrease the reflection of the waves and noise, absorbers are settled around the system.

We used electromagnetic waves with frequency one GHz which means that the exterior wave number k_0 is equal to 20.944 and the interior wave number is taken $k_d = \sqrt{3}k_0$. Since we obtain the data from the near distance, it requires to use near field pattern instead of far field pattern.

For the second and the third problems only the simultaneous linearization and the hybrid method can be used, since the data equation does not include the interior wave number. For the second problem, the simultaneous linearization and the hybrid methods proceed the same line as the shape reconstruction with difference that the unknown boundary ∂D is replaced by interior wave number k_d. For the third problem, the simultaneous linearization and the hybrid methods proceed the same line as the shape reconstruction with the difference that the interior wave number k_d is included as an unknown parameter.

For the fourth problem we represent the solution v and u^s to the forward scattering in terms of single-layer potentials in D and in $\mathbb{R}^2 \setminus \bar{D}$ with densities φ_d and φ_0, respectively, the (1.1.2) with *conductive* boundary condition provides a system of two boundary integral equations on ∂D for the corresponding densities, that in the sequel we will denote as field equations. The inverse problem, the required coincidence of the far field of the single-layer potential representing u^s and the given far field u_∞ provides a further equation that we denote as data equation. The system of the field and data equations can be viewed as three equations for three unknowns, i.e., the two densities and the conductive function η. This inverse problem is ill-posed determination of η does not depend continuously on the far field pattern. Furthermore, it is non-linear in the sense that the scattered field depends non-linearly on the conductive function η. The inverse problem is formulated as follows: Given an incident plane wave and corresponding far field pattern u_∞ is to determine conductive function η.

In the sense of the hybrid method [32, 37, 38, 45], in a first step, the ill-posed data equation is regularized, for instance, by Tikhonov regularization then density φ_d is solved from regularized data equation on ∂D. In a second step, the density φ_d is solved from the first field equation. And in a third step, the conductive function is reconstructed from the second field equation. However, reconstruction of the conductive function is not straightforward because of ill-posedness of the inverse problem and of sensitivity to the errors in the vicinity of zeros. In the spirit of Akduman and Kress [1], to obtain more stable solution, we express the unknown impedance function in terms of some basis functions. Then, we satisfy the second field equation in a least square sense. For the ill-posedness we will use Tikhonov regularization.

1.1.1 Organization

This manuscript consists of six chapters. In the second chapter some results about scattering theory is given. In the first section, we begin with the Helmholtz equation

and give some motivation on it and then we proceed by the Green's formula and theorems. In the second section, some properties of far-field pattern are discussed and some related theorems are given and Rellich's lemma is stated. In the third section, we present single- and double-layer potentials and some related theorems and corollaries are stated. Moreover, We give definition of Hölder and Sobolev spaces and some related theorems are stated. In addition, we introduce the single- and double-layer operators and state their mapping properties in these spaces. In the fourth section, we give some information about ill-posedness and regularization, and state some related theorems. We mainly focus on Tikhonov regularization and its theorems. In the fifth section, we state Riesz theorems because they will be vital tools for showing well-posedness of the direct problems. Furthermore, we also state definition of the Fréchet differentiability and give some properties and related theorems.

In the third chapter, in the first section, we present the direct scattering problems for the first three problems. The direct scattering problems are stated and related theorems are stated and proved. In the second section, some classical uniqueness results for penetrable and impenetrable obstacles are stated. In addition, we also include a uniqueness result for recovering a dielectric disc from the far field pattern for scattering of one incident plane wave. In the third section, the inverse scattering problems are stated and related theorems are stated and discussed. Moreover, iterative schemes for three problems are deeply discussed for the hybrid, the simultaneous linearization, and the Johansson and Sleeman method.

In the fourth chapter, we numerically solve the direct and inverse scattering problems. We also illustrate numerical feasibility of the hybrid, the simultaneous linearization, the Johansson and Sleeman method and establish their advantages and disadvantages. Moreover, we compare these methods via the quality of their reconstructions, tolerance to noise level, and computational effort. In addition, we also obtain some reconstructions via experimental data and include some numerical examples. We illustrate the experimental result and examples at the end of this chapter.

In the fifth chapter, we present the direct and inverse scattering problem for the fourth problem. In the first section, the direct scattering problem is stated and related theorems established and proved. Furthermore, its numerical solution is stated and as mentioned above, we obtain field equations,i.e., system of integral equations and we solve this system of integral equations approximately via collocation method combined with numerical quadrature based on approximation by trigonometric polynomials. In the second section, the inverse scattering problem stated and related theorem stated and proved. Moreover, its numerical solution is established. In addition, the solution of the problem is deeply described. In the third section, the numerical feasibility is stated and discussed.

In the final chapter, we make some considerations and final conclusion on methods and present some future perspectives.

Chapter 2

Acoustic Scattering Theory

In this chapter we mainly follow the sources [6, 7, 31].

2.1 The Helmholtz Equation

Consider the propagation of sound waves of small amplitude in a homogeneous isotropic medium in $\mathrm{I\!R}^2$ which can be seen as an inviscid fluid. Assume $v = v(x, t)$ is the velocity field and assume $S = S(x, t)$, $p = p(x, t)$, and $\rho = \rho(x, t)$ denote the specific entropy, pressure, and density, respectively, of the fluid. Then, the motion of the field is given by Euler's equation

$$\frac{\partial v}{\partial t} + v \cdot \nabla v + \frac{1}{\rho} \nabla p = 0,$$

the equation of continuity

$$\frac{\partial \rho}{\partial t} + \nabla \cdot (\rho v) = 0,$$

and the state equation

$$p = f(\rho, S),$$

where f depends on the nature of the fluid. Let v, p, ρ and S be small perturbations of the initial value $v_0 = 0$, $p_0 = $ constant, $\rho_0 = $ constant and $S_0 = $ constant then the linearized Euler equation is obtained as

$$\frac{\partial v}{\partial t} + \frac{1}{\rho_0} \nabla p = 0,$$

and the linearized equation of continuity turns out to be of the form

$$\frac{\partial \rho}{\partial t} + \rho_0 \nabla \cdot v = 0,$$

and the linearized state equation has of the form

$$\frac{\partial p}{\partial t} = \frac{\partial f}{\partial \rho}(\rho_0, S_0)\frac{\partial \rho}{\partial t}.$$

From this equation we obtain the *wave* equation

$$\frac{1}{c^2}\frac{\partial^2 p}{\partial^2 t} = \Delta p$$

where the speed of the sound c is defined by

$$c^2 = \frac{\partial f}{\partial \rho}(\rho_0, S_0).$$

From the linearized Euler equation, we see that there exist a velocity potential $U = U(x,t)$ such that

$$v = \frac{1}{\rho_0}\nabla U \quad and \quad p = -\frac{\partial U}{\partial t}.$$

We observe that the velocity potential U also satisfies the function

$$\frac{1}{c^2}\frac{\partial^2 U}{\partial^2 t} = \Delta U.$$

For the time-harmonic acoustic waves of the form

$$U(x,t) = Re\{u(x)e^{-iwt}\}$$

with frequency $w > 0$, we conclude that the complex valued time independent part u satisfies the reduced *wave equation* or *Helmholtz equation*

$$\Delta u + k^2 u = 0$$

where the wave number k is given by the positive constant $k = \frac{w}{c}$.

2.2   Green's Theorem and Formula

A domain $D \subset \mathbb{R}^2$, i.e., an open and connected set, with boundary ∂D is said to have a boundary of class C^n, $n \in \mathbb{N}$, if for each point x_0 of the boundary ∂D there exist neighborhood V of x_0 with following properties:

- Firstly, the intersection $V \cap \bar{D}$ can be mapped bijectively onto the half disk

$$\{z \in \mathbb{R}^2 : |z| < 1, z_2 \geq 0\};$$

- secondly, this mapping and its inverse have continuous partial derivatives up to order n;

- thirdly, the intersection $V \cap \partial D$ is mapped onto the interval

$$\{z \in \mathbb{R}^2 : |z| < 1, z_2 = 0\}.$$

This mapping generates a parametrization

$$x(t) = (x_1(t), x_2(t)), \qquad 0 \leq t \leq T,$$

of a curve patch of ∂D containing x_0. We denote by $C^n(D)$ the linear space of real- or complex-valued functions defined on the domain D for which the partial derivatives up to order n exist and are continuous. In addition we denote by $C^n(\bar{D})$ the subspace of all functions in $C^n(D)$ which together with all their derivatives up to order n can be extended continuously from D into the closure $\bar{D} := D \cup \partial D$.

Now we can state Green's first and second integral theorem

Theorem 2.2.1 *Let $D \subset \mathbb{R}^2$ be a bounded domain of class C^2 and let ν denote the unit normal vector to the boundary ∂D directed into the exterior of D. For functions $u \in C^1(\bar{D})$ and $v \in C^2(\bar{D})$ the equality*

$$\int_D \{u\Delta v + \nabla u \cdot \nabla v\}dx = \int_{\partial D} u\frac{\partial v}{\partial \nu}ds, \qquad (2.2.1)$$

holds.

Theorem 2.2.2 *Let $D \subset \mathbb{R}^2$ be a bounded domain of class C^2 and let ν denote the unit normal vector to the boundary ∂D directed into the exterior of D. For functions $u \in C^2(\bar{D})$ and $v \in C^2(\bar{D})$ the equality*

$$\int_D \{u\Delta v - v\Delta u\}dx = \int_{\partial D} \{u\frac{\partial v}{\partial \nu} - v\frac{\partial u}{\partial \nu}\}ds, \qquad (2.2.2)$$

holds.

Most of the basic properties of solutions to the Helmholtz equation

$$\Delta u + k^2 u = 0$$

with positive wave number k can be produced from its fundamental solution that we are going to introduce now.

Definition 2.1 *Solution to the Helmholtz equation satisfying the Sommerfeld radiation condition (1.1.3) are called radiating solutions.*

The fundamental solution of the Helmholtz equation in $\mathbb{R}^2$ is given by

$$\Phi(x,y) := \frac{i}{4} H_0^{(1)}(k|x - y|), \qquad x \neq y, \tag{2.2.3}$$

where the function $H_0^{(1)}$ denotes the Hankel function of first kind and of order zero. It can be shown that for fixed $y \in \mathbb{R}^2$ the fundamental solution satisfies the Helmholtz equation in $\mathbb{R}^2 \setminus \{y\}$. In addition,it satisfies the radiation condition uniformly with respect to y on compact subsets of $\mathbb{R}^2$. Physically speaking, the fundamental solution represents an acoustic point source located at the point y (see[7]). The Hankel functions of the first and the second kind of order n are defined by

$$H_n^{(1,2)} := J_n \pm iY_n, \qquad n = 0, 1, 2, ... \tag{2.2.4}$$

with the Bessel functions of order n

$$J_n(t) := \sum_{p=0}^{\infty} \frac{(-1)^p}{(n+p)!p!} (\frac{t}{2})^{n+2p}, \tag{2.2.5}$$

and the Neumann functions of order n

$$Y_n(t) := \frac{2}{\pi} \{ ln(\frac{t}{2}) + C_E \} J_n(t) - \frac{1}{\pi} \sum_{j=0}^{\infty} \frac{(-1)^p}{(n+p)!p!} (\frac{t}{2})^{n+2p} \{ \psi(p+n) + \psi(p) \}$$

$$- \frac{1}{\pi} \sum_{p=0}^{n-1} \frac{(n-1-p)!}{p!} (\frac{2}{t})^{n-2p} \tag{2.2.6}$$

Here $\psi(0) := 0$,

$$\psi(p) = \sum_{m=1}^{p} \frac{1}{m}, \qquad p = 1, 2, ...$$

and $C_E \approx 0.57721$ denotes Euler constant

$$C_E = \lim_{p \to \infty} \{ \sum_{m=1}^{p} \frac{1}{m} - \ln p \}.$$

From the series (2.2.5) and (2.2.6) it can be seen that

$$J_n(t) = \frac{t^n}{2^n n!} (1 + O(\frac{1}{n})), \qquad n \to \infty, \tag{2.2.7}$$

uniformly on compact subset of $\mathbb{R}$ and

$$H_n^{(1)}(t) = \frac{2^n(n-1)!}{i\pi t^n} (1 + O(\frac{1}{n})), \qquad n \to \infty, \tag{2.2.8}$$

uniformly on compact subsets of $(0, \infty)$. For the large arguments the Hankel functions have the following asymptotic behavior

$$H_n^{(1,2)}(t) = \sqrt{\frac{2}{\pi t}} e^{\pm i(t - \frac{n\pi}{2} - \frac{\pi}{4})}(1 + O(\frac{1}{t})), \qquad t \to \infty, \qquad (2.2.9)$$

From the expansions (2.2.5) and (2.2.6) we yield that

$$\Phi(x, y) = \frac{1}{2\pi} ln\frac{1}{|x - y|} + \frac{i}{4} - \frac{1}{2\pi} ln\frac{k}{2} - \frac{C_E}{2\pi} + O(|x - y|^2 ln\frac{1}{|x - y|}. \qquad (2.2.10)$$

for $|x - y| \to 0$. Therefore, the fundamental solution to the Helmholtz equation in two dimensions has the same singular behavior as the fundamental solution of Laplace's equation. This will be used later on in deriving Green's representation formula and the jump relation for the single- and double-layer potentials. Using Green's integral theorems one can derive representation formulas for the solution to the Helmholtz equation.

Theorem 2.2.3 *Let $u \in C^2(\mathbb{R}^2 \setminus D) \cap C^1(\mathbb{R}^2 \setminus \bar{D})$ be a solution to the Helmholtz equation*

$$\Delta u + k^2 u = 0 \quad in \ D.$$

Then

$$u(x) = \int_{\partial D} \{\frac{\partial u}{\partial \nu}(y)\Phi(x, y) - u(y)\frac{\partial \Phi(x, y)}{\partial \nu(y)}\}ds(y) \quad x \in D \qquad (2.2.11)$$

Proof: See Theorem 2.1 in [7]

Theorem 2.2.4 *(Holmgren)*
let $u \in C^2(D) \cap C^1(\bar{D})$ be a solution to the Helmholtz equation in D such that

$$u = 0 \quad and \quad \frac{\partial u}{\partial \nu} = 0 \quad on \quad \Gamma \qquad (2.2.12)$$

for some open arc $\Gamma \subset \partial D$. Then u vanishes identically in D.

Proof: We use the Green's representation formula (2.2.11) to extend the definition of u by setting

$$u(x) = \int_{\partial D \setminus \Gamma} \{\frac{\partial u}{\partial \nu}(y)\Phi(x, y) - u(y)\frac{\partial \Phi(x, y)}{\partial \nu(y)}\}ds(y) \qquad (2.2.13)$$

for $x \in (\mathbb{R}^2 \setminus \bar{D}) \cup \Gamma$. The equation (2.2.13) can be written as

$$u(x) = \int_{\partial D} \{\frac{\partial u}{\partial \nu}(y)\Phi(x, y) - u(y)\frac{\partial \Phi(x, y)}{\partial \nu(y)}\}ds(y) - \int_{\Gamma} \{\frac{\partial u}{\partial \nu}(y)\Phi(x, y) - u(y)\frac{\partial \Phi(x, y)}{\partial \nu(y)}\}ds(y) \qquad (2.2.14)$$

Now if we use hypothesis of the theorem the equation (2.2.14) has of the form

$$u(x) = \int_{\partial D} \{\frac{\partial u}{\partial \nu}(y)\Phi(x,y) - u(y)\frac{\partial \Phi(x,y)}{\partial \nu(y)}\}ds(y), \quad x \in (\mathbb{R}^2 \setminus \bar{D}) \cup \Gamma. \quad (2.2.15)$$

Now we apply Green's second theorem (2.2.2) to (2.2.15) we have that

$$u(x) = \int_D \Phi(x,y)\{\Delta u + k^2 u\}ds(y), \quad x \in (\mathbb{R}^2 \setminus \bar{D}) \cup \Gamma. \quad (2.2.16)$$

The equation (2.2.16) implies that $u = 0$ in $\mathbb{R}^2 \setminus \bar{D}$. Let G denote a complement of $\mathbb{R}^2 \setminus \bar{D}$ with $\Gamma \cap \partial G \neq \emptyset$. We observe that u solves the Helmholtz equation in $(\mathbb{R}^2 \setminus \partial D) \cup \Gamma$ and therefore $u = 0$ in D, since D and G are connected through the gap Γ in D. □

Theorem 2.2.5 *Let $u \in C^2(\mathbb{R}^2 \setminus \bar{D}) \cap C(\mathbb{R}^2 \setminus D)$ be a radiating solution to the Helmholtz equation*

$$\Delta u + k^2 u = 0 \quad \text{in } \mathbb{R}^2 \setminus \bar{D}.$$

Then the following formula

$$u(x) = \int_{\partial D} \{u(y)\frac{\partial \Phi(x,y)}{\partial \nu(y)} - \frac{\partial u}{\partial \nu}(y)\Phi(x,y)\}ds(y) \quad x \in \mathbb{R}^2 \setminus \bar{D}, \quad (2.2.17)$$

holds.

Proof : See Theorem 2.4 in [7].

Definition 2.2 *Solutions of the Helmholtz equation which are defined in all of $\mathbb{R}^2$ are said to be entire solutions.*

Theorem 2.2.6 *An entire solution to the Helmholtz equation satisfying the Sommerfeld radiation condition vanishes identically.*

Proof : Let u satisfy the Sommerfeld radiation condition and be an entire solution. And let ∂D be a circle of radius R with outward drawn unit normal vector ν. Since u is the solution of the Helmholtz equation in D, from the Green's formula (2.2.17) we have that

$$u(x) = \int_{\partial D} \{u(y)\frac{\partial \Phi(x,y)}{\partial \nu(y)} - \frac{\partial u}{\partial \nu}(y)\Phi(x,y)\}ds(y), \quad x \in \mathbb{R}^2 \setminus \bar{D}. \quad (2.2.18)$$

If we use Green's second theorem (2.2.2) then equation (2.2.18) has of the form

$$u(x) = \int_D \Phi(x,y)\{\Delta u + k^2 u\}dy \quad x \in \mathbb{R}^2 \setminus \bar{D}. \quad (2.2.19)$$

Since u is entire solution it satisfies Helmholtz equation in D. Hence, $u = 0$ in $\mathbb{R}^2 \setminus \bar{D}$. From the analyticity of u we conclude that $u = 0$ in $\mathbb{R}^2$. □

2.3 Far Field Pattern

We are now in a position to introduce the notion of the $far-field$ $pattern$ or the $scattering$ $amplitude$ of radiating solutions to the Helmholtz equation.

Theorem 2.3.1 *Every radiation solution u to the Helmholtz equation has an asymptotic behavior of an outgoing spherical wave*

$$u(x) = \frac{e^{ik|x|}}{\sqrt{|x|}}\{u_\infty(\hat{x}) + O(\frac{1}{|x|})\}, \quad |x| \to \infty, \tag{2.3.1}$$

uniformly in all directions $\hat{x} = x/|x|$, where the function u_∞ defined on the unit circle

$$\Omega := \{\hat{x} \in \mathbb{R}^2 : |\hat{x}| = 1\}$$

is called the far field pattern of u. Under the assumption of Theorem (2.2.5) we have

$$u_\infty(\hat{x}) = \gamma \int_{\partial D}\{u(y)\frac{\partial e^{-ik\hat{x}\cdot y}}{\partial \nu(y)} - \frac{\partial u}{\partial \nu}(y)e^{-ik\hat{x}\cdot y}\}ds(y) \tag{2.3.2}$$

where $\gamma := \dfrac{e^{i\frac{\pi}{4}}}{\sqrt{8\pi k}}$ and $\hat{x} \in \Omega$.

Proof: The proof can be found for the 3 dimensional case in [6] and for the 2 dimensional case in [13] respectively.

Lemma 2.3 *(Rellich)*
Assume the bounded domain D is the open complement of an unbounded domain and let $u \in C^2(\mathbb{R}^2 \setminus \bar{D})$ be a solution to the Helmholtz equation satisfying

$$\lim_{r\to\infty}\int_{|x|=r}|u(x)|^2 ds = 0. \tag{2.3.3}$$

Then $u = 0$ in $\mathbb{R}^2 \setminus \bar{D}$.

Proof: See Lemma 2.11 in [7].

Theorem 2.3.2 *Assume $u \in C^2(\mathbb{R}^2 \setminus \bar{D}) \cap C^2(\mathbb{R}^2 \setminus D)$ is a radiating solution to the Helmholtz equation with wave number $k > 0$ such that*

$$Im \int_{\partial D} u\frac{\partial \bar{u}}{\partial \nu}ds \geq 0. \tag{2.3.4}$$

Then $u = 0$ in $\mathbb{R}^2 \setminus \bar{D}$.

Proof: See Theorem 2.12 in [7]
Rellich's lemma also establishes a one-to-one correspondence between radiating waves and their far field patterns.

Theorem 2.3.3 *Let $u \in C^2(\mathrm{I\!R}^2 \setminus \bar{D})$ be a radiating solution to the Helmholtz equation for which the far field pattern u_∞ vanishes identically. Then $u = 0$ in $\mathrm{I\!R}^2 \setminus \bar{D}$.*

Proof: See Theorem 2.13 in [7].

2.4   Single- and Double-layer Potentials

Assume that $D \subset \mathrm{I\!R}^2$ is a bounded domain with boundary ∂D of class C^2. We denote by ν the unit normal vector to the boundary ∂D directed into exterior of D.

Given an integrable function φ, the integral

$$u(x) := \int_{\partial D} \Phi(x, y)\varphi(y)ds(y), \qquad x \in \mathrm{I\!R}^2 \setminus \partial D,$$

and

$$v(x) := \int_{\partial D} \frac{\partial \Phi(x, y)}{\partial \nu(y)}ds(y), \qquad x \in \mathrm{I\!R}^2 \setminus \partial D,$$

are called, respectively, acoustic single-layer and acoustic double-layer potentials with density φ. They are solutions to the Helmholtz equation in D and in $\mathrm{I\!R}^2 \setminus \bar{D}$ and satisfy the Sommerfeld radiation condition (1.1.3). Their far field patterns are given by

$$u_\infty(\hat{x}) = \gamma \int_{\partial D} e^{-ik\hat{x}\cdot y}\varphi(y)ds(y), \qquad \hat{x} \in \Omega,$$

$$v_\infty(\hat{x}) = \gamma \int_{\partial D} \frac{\partial e^{-ik\hat{x}\cdot y}}{\partial \nu(y)}\varphi(y)ds(y), \qquad \hat{x} \in \Omega,$$

respectively. Physically speaking, the single- and double- layer potential correspond to a layer of acoustic monopoles and dipoles, respectively. Green's formulas (2.2.11) and (2.2.17) show that any solution to the Helmholtz equation can be represented as a combination of single- and double-layer potentials in terms of the boundary values and the normal derivatives on the boundary.

The behavior of the curve potentials at the boundary is described by the following regularity and jump relations. By

$$\| f \|_{\infty,G} := \sup_{x \in G} |f(x)|$$

we denote the supremum norm of a real- or complex-valued bounded continuous function f defined on a subset $G \subset \mathrm{I\!R}^2$.

Theorem 2.4.1 *Let ∂D be of class C^2 and let φ be continuous. Then the single-layer potential u with the density φ is continuous throughout $\mathbb{R}^2$ and*

$$\| u \|_{\infty,\mathbb{R}^2} \leq C \| \varphi \|_{\infty,\partial D}$$

for some constant C depending on ∂D. On the boundary we have

$$u(x) = \int_{\partial D} \Phi(x,y)\varphi(y)ds(y), \qquad x \in \partial D, \tag{2.4.1}$$

and

$$\frac{\partial u_{\pm}}{\partial \nu}(x) = \int_{\partial D} \frac{\partial \Phi(x,y)}{\partial \nu(x)}\varphi(y)ds(y) \mp \frac{1}{2}\varphi(x), \qquad x \in \partial D, \tag{2.4.2}$$

where

$$\frac{\partial u_{\pm}}{\partial \nu}(x) := \lim_{h \to +0} \nu(x) \cdot \mathrm{grad}u(x \pm h\nu(x))$$

is to be understood in the sense of uniform convergence on ∂D and where the integrals exist as improper integrals. The double layer potential v with the density φ can be continuously extended from D to $\bar{D}$ and from $\mathbb{R}^2 \setminus \bar{D}$ to $\mathbb{R}^2 \setminus D$ with limiting values

$$v_{\pm}(x) = \int_{\partial D} \frac{\partial \Phi(x,y)}{\partial \nu(y)}\varphi(y)ds(y) \pm \frac{1}{2}\varphi(x), \qquad x \in \partial D, \tag{2.4.3}$$

where

$$v_{\pm}(x) := \lim_{h \to +0} v(x \pm h\nu(x))$$

and where the integral exists as an improper integral. Furthermore,

$$\| v \|_{\infty,\bar{D}} + \| v \|_{\infty,\mathbb{R}^2 \setminus D} \leq C \| \varphi \|_{\infty,\partial D}$$

for some constant C depending on ∂D and

$$\lim_{h \to +0}\{\frac{\partial v}{\partial \nu}(x + h\nu(x)) - \frac{\partial v}{\partial \nu}(x - h\nu(x))\} = 0 \tag{2.4.4}$$

uniformly for $x \in \partial D$.

Proof: See Theorem 3.1 [7].

Corollary 2.4 *We have jump relations*

$$u_+ = u_-, \qquad \text{and} \qquad \frac{\partial u_+}{\partial \nu} - \frac{\partial u_-}{\partial \nu} = -\varphi \quad \text{on} \quad \partial D, \tag{2.4.5}$$

for the single-layer potential and

$$v_+ - v_- = \varphi, \qquad \text{and} \qquad \frac{\partial v_+}{\partial \nu} = \frac{\partial v_-}{\partial \nu} \quad \text{on} \quad \partial D, \tag{2.4.6}$$

for the double-layer potential with the continuity of the normal derivative to be understood in the sense (2.4.4).

Since the fundamental solution to the Helmholtz equation has the same singular behavior as fundamental solution to the Laplacian equation, the above regularity and jump relations for the Helmholtz equation can be deduced from those for the Laplace equation.

Definition 2.5 *(Hölder Continuity)*
A real- or complex-valued function φ defined on set $\Gamma \subset \mathbb{R}^2$ is called uniformly Hölder continuous with Hölder exponent $0 < \alpha \leq 1$ if there exists a constant C such that

$$|\varphi(x) - \varphi(y)| \leq C|x - y|^\alpha, \quad \text{for all} \quad x, y \in \Gamma.$$

The Hölder space $C^{0,\alpha}(\Gamma)$ is the space of all bounded and uniformly Hölder continuous functions on Γ with exponent α. The norm in $C^{0,\alpha}(\Gamma)$ is defined by

$$\| \varphi \|_{\alpha,\Gamma} := \sup_{x \in \Gamma} |\varphi(x)| + \sup_{x,y \in \Gamma, x \neq y} \frac{|\varphi(x) - \varphi(y)|}{|x - y|^\alpha}.$$

Here, we will use the Hölder spaces in the cases where $\Gamma = \bar{D}$, $\Gamma = \mathbb{R}^2 \setminus D$, $\Gamma = \partial D$. In addition, we need to introduce the Hölder space $C^{1,\alpha}(\partial D)$ as the space of all uniformly Hölder continuously differentiable functions on ∂D, i.e., of all real- or complex-valued functions φ on ∂D that have a derivative $\dfrac{d\varphi}{ds} \in C^{0,\alpha}(\partial D)$ with respect to arclength s. The norm on $C^{1,\alpha}(\partial D)$ is defined by

$$\| \varphi \|_{1,\alpha,\partial D} := \| \varphi \|_\infty + \| \frac{d\varphi}{ds} \|_{\alpha,\partial D} .$$

Definition 2.6 *The single- and double-layer operators S and K are defined by*

$$(S\varphi)(x) := 2 \int_{\partial D} \Phi(x,y)\varphi(y)ds(y), \quad x \in \partial D, \tag{2.4.7}$$

$$(K\varphi)(x) := 2 \int_{\partial D} \frac{\partial \Phi(x,y)}{\partial \nu(y)} \varphi(y)ds(y), \quad x \in \partial D, \tag{2.4.8}$$

and the normal derivative operators K' and T are defined by

$$(K'\varphi)(x) := 2 \int_{\partial D} \frac{\partial \Phi(x,y)}{\partial \nu(x)} \varphi(y)ds(y), \quad x \in \partial D, \tag{2.4.9}$$

$$(T\varphi)(x) := 2 \frac{\partial}{\partial \nu(x)} \int_{\partial D} \frac{\partial \Phi(x,y)}{\partial \nu(y)} \varphi(y)ds(y), \quad x \in \partial D. \tag{2.4.10}$$

In terms of these operators the above jump relations can be written in short hand in the form

$$u_\pm = \frac{1}{2}S\varphi \qquad (2.4.11)$$

and

$$\frac{\partial u_\pm}{\partial \nu} = \frac{1}{2}K'\varphi \mp \frac{1}{2}\varphi \qquad (2.4.12)$$

for the single-layer potential u with continuous density φ and

$$v_\pm = \frac{1}{2}K\varphi \pm \frac{1}{2}\varphi \qquad (2.4.13)$$

and

$$\frac{\partial v_\pm}{\partial \nu} = \frac{1}{2}T\varphi \qquad (2.4.14)$$

for the double-layer potential v with continuous density φ; the relation (2.4.14) involving T requires that $\varphi \in C^{1,\alpha}(\partial D)$.

The operators S, K, and K' are integral operators with weakly singular kernels, since for C^2 curves one can be prove an estimate of the form

$$|\nu(x) \cdot \{x - y\}| \leq C|x - y|^2$$

for all $x, y \in \partial D$ and some positive constant C depending on ∂D (see Theorem 2.2 in [7]). However, the operator T representing the normal derivative of the double-layer potential is not weakly singular; it is a hyper-singular operator as expressed in the following theorem.

Theorem 2.4.2 *Let ∂D be of class C^2.*

- *The operators S, K, and K' are bounded operators from $C(\partial D)$ into $C^{0,\alpha}(\partial D)$.*

- *The operators S and K are also bounded from $C^{0,\alpha}$ into $C^{1,\alpha}$.*

- *The operator T is bounded from $C^{1,\alpha}(\partial D)$ into $C^{0,\alpha}$.*

- *The operators S, K, and K' are compact operators from $C(\partial D)$ into $C(\partial D)$ and from $C^{0,\alpha}(\partial D)$ into $C^{0,\alpha}(\partial D)$.*

- *The operators S and K are compact operators from $C^{1,\alpha}(\partial D)$ into $C^{1,\alpha}(\partial D)$.*

Proof:.   See Theorems 2.12, 2.15, 2.16, 2.17, 2.22, 2.23, and 2.30 in [6]

The hyper-singular operator T defined by (2.4.14) can be expressed by following theorem

Theorem 2.4.3 *(Maue's formula)*
Assume that $\varphi \in C^{1,\alpha}(\partial D)$ then

$$T\varphi = \frac{d}{ds}S\frac{d\varphi}{ds} + k^2 \nu \cdot S(\nu\varphi), \qquad (2.4.15)$$

where $\dfrac{d}{ds}$ denotes tangential derivative along ∂D.

Proof: See [41] and for the numerical solution of a hyper-singular integral equation see also [29].

As a basis of our presentation of Sobolev spaces we begin with a brief review on the classical Fourier series expansion. For a function $\varphi \in L^2[0, 2\pi]$ the series

$$\sum_{m=-\infty}^{\infty} a_m e^{imt} \qquad (2.4.16)$$

where

$$a_m := \frac{1}{2\pi} \int_0^{2\pi} \varphi(t)e^{-imt}dt$$

is called the *Fourier series* of φ, its coefficient a_m are called the *Fourier* coefficients of φ. On $L^2[0, 2\pi]$, as usual, we introduce the mean square norm by the scalar product

$$(\varphi, \psi) := \int_0^{2\pi} \varphi(t)\bar{\psi}(t)dt. \qquad (2.4.17)$$

Definition 2.7 *(The Sobolev Space $H^p[0, 2\pi]$)*
Let $0 \leq p < \infty$. By $H^p[0, 2\pi]$ we denote the space of all functions $\varphi \in L^2[0, 2\pi]$ with the property

$$\sum_{-\infty}^{\infty}(1 + m^2)^p|a_m|^2 < \infty$$

for the Fourier coefficients a_m of φ. The space $H^p[0, 2\pi]$ is called a Sobolev space. Note that $H^0[0, 2\pi]$ coincides with $L^2[0, 2\pi]$.

Theorem 2.4.4 *The Sobolev space $H^p[0, 2\pi]$ is a Hilbert space with the scalar product defined by*

$$(\varphi, \psi)_p := \sum_{-\infty}^{\infty}(1 + m^2)^p a_m \bar{b}_m$$

for $\varphi, \psi \in H^p[0, 2\pi]$ with Fourier coefficients a_m and b_m, respectively. In addition, the trigonometric polynomials are dense in $H^p[0, 2\pi]$.

Proof: See Theorem 8.2 in [31].

Definition 2.8 (*The dual space of the Sobolev space*)
For $0 \leq p < \infty$ by $H^{-p}[0, 2\pi]$ we denote the dual space of $H^p[0, 2\pi]$, that is, the space of bounded linear functionals on $H^p[0, 2\pi]$.

Theorem 2.4.5 *For $F \in H^{-p}[0, 2\pi]$ there holds*

$$\| F \|_p = \{\sum_{-\infty}^{\infty} (1 + m^2)^{-p} |c_m|^2\}^{\frac{1}{2}}$$

where $c_m = F(e^{imt})$. Conversely, to each sequence (c_m) satisfying

$$\sum_{-\infty}^{\infty} (1 + m^2)^{-p} |c_m|^2 < \infty$$

there exists a bounded linear functional $F \in H^{-p}[0, 2\pi]$ with $F(e^{imt}) = c_m$.

Proof: See Theorem 8.9 in [31].

Theorem 2.4.6 *For each function $g \in L^2[0, 2\pi]$ the duality pairing*

$$G(\varphi) := \frac{1}{2\pi} \int_0^{2\pi} \varphi(t) \bar{g}(t) dt, \qquad \varphi \in H^p[0, 2\pi],$$

canonically defines a linear functional $G \in H^{-p}[0, 2\pi]$. In this sense, $L^2[0, 2\pi]$ is a subspace of each dual space $H^{-p}[0, 2\pi]$, and trigonometric polynomials are dense in $H^{-p}[0, 2\pi]$.

Proof: See Theorem 8.10 in [31].
Let ∂D be the boundary of simply connected bounded domain $D \subset \mathbb{R}^2$ of class C^k, $k \in \mathbb{N}$. With the aid of a regular and k times continuously differentiable parametric representation
$$x(t) = (x_1(t), x_2(t)), \qquad t \in [0, 2\pi].$$

Definition 2.9 (*The Sobolev space $H^p(\partial D)$*)
For $0 \leq p \leq k$ the Sobolev space $H^p(\partial D)$ is the space of all functions $\varphi \in L^2(\partial D)$ with the property that $\varphi \circ x \in H^p[0, 2\pi]$. The scalar product and norm on $H^p(\partial D)$ are defined through the scalar product on $H^p[0, 2\pi]$ by

$$(\varphi, \psi)_{H^p(\partial D)} := (\varphi \circ x, \psi \circ x)_{H^p[0, 2\pi]}.$$

Theorem 2.4.7 *The operators $K : H^{1/2}(\partial D) \to H^{1/2}(\partial D)$ defined by the double-layer potential (2.4.8) and $K' : H^{-1/2}(\partial D) \to H^{-1/2}(\partial D)$ defined by the normal derivative of single-layer potential (2.4.9) are compact and adjoint in the dual system $(H^{1/2}(\partial D), H^{-1/2}(\partial D))_{L^2(\partial D)}$, that is,*

$$(K\varphi, \psi)_{L^2(\partial D)} = (\varphi, K'\psi)_{L^2(\partial D)}$$

for all $\varphi \in H^{1/2}(\partial D)$ and $\psi \in H^{-1/2}(\partial D)$.

Proof: The proof is the same as the proof of Theorem 8.20 in [31].

Theorem 2.4.8 *The operator $S : H^{-1/2}(\partial D) \to H^{1/2}(\partial D)$ defined by the single-layer potential (2.4.7) and $T : H^{1/2}(\partial D) \to H^{-1/2}(\partial D)$ defined by the normal derivative of double-layer potential (2.4.10) are bounded. The operator S is self ad-joint with respect to dual systems $(H^{-1/2}(\partial D), H^{1/2}(\partial D))_{L^2(\partial D)}$ and $(H^{1/2}(\partial D), H^{-1/2}(\partial D))_{L^2(\partial D)}$, that is,*

$$(S\varphi, \psi)_{L^2(\partial D)} = (\varphi, S\psi)_{L^2(\partial D)}$$

for all $\varphi, \psi \in H^{-1/2}(\partial D)$. The operator T is self adjoint with respect to dual systems $(H^{1/2}(\partial D), H^{-1/2}(\partial D))_{L^2(\partial D)}$ and $(H^{-1/2}(\partial D), H^{1/2}(\partial D))_{L^2(\partial D)}$, that is,

$$(T\varphi, \psi)_{L^2(\partial D)} = (\varphi, T\psi)_{L^2(\partial D)}$$

for all $\varphi, \psi \in H^{1/2}(\partial D)$.

Proof: The proof is the same as the proof of Theorem 8.21 in [31].

2.5   Ill-Posed Problems and Regularization

For Problems in mathematical physics, in particular for initial and boundary value problems, Hadamard [24] postulated three properties:

1. Existence of a solution.

2. Uniqueness of the solution.

3. Continuous dependence of the solution on the data.

The third postulate is motivated by the fact that in all applications the data will be measured quantities. Therefore, one wants to make sure that small errors in the data will cause only small errors in the solution. A problem satisfying all three requirements is called well-posed or properly posed. If one of these requirements is violated then the problem is said to be ill-posed or improperly-posed. We will make Hadamard's concept of well-posedness more precise through the following

Definition 2.10 *Let $A : X \to Y$ be an operator from a normed space X into a normed space Y.*

$$A\varphi = f \tag{2.5.1}$$

is called well-posed or properly-posed if A is bijective and the inverse operator $A^{-1} : Y \to X$ is continuous. Otherwise the equation is said to be ill-posed or improperly-posed.

One of the primary interest in the study of ill-posed problem is the case of instability, that is, when the third requirement is violated. To handle this problem, regularization methods have been implemented, which approximate the unbounded inverse operator $A^{-1} : A(X) \to X$ by a bounded linear operator $R : Y \to X$.

Definition 2.11 *Let $A : X \to Y$ be an injective bounded linear operator. Then a family of bounded linear operators $R_\alpha : Y \to X$, $\alpha > 0$, with the property of point-wise convergence*

$$\lim_{\alpha \to 0} R_\alpha A \varphi = \varphi \qquad (2.5.2)$$

for all $\varphi \in X$ is called a regularization scheme for the operator A. The parameter α is called the regularization parameter.

The (2.5.2) is equivalent to $R_\alpha f \to A^{-1} f$ as $\alpha \to 0$, for all $f \in A(X)$. The regularization scheme approximates the solution φ of (2.5.1) by the regularized solution

$$\varphi_\alpha^\delta := R_\alpha f^\delta. \qquad (2.5.3)$$

Then, for the approximation error, writing

$$\varphi_\alpha^\delta - \varphi = R_\alpha f^\delta - R_\alpha f + R_\alpha A \varphi - \varphi,$$

by the triangle inequality we have the estimate for the approximation error

$$\| \varphi^\delta - \varphi \| \leq \delta \| R_\alpha \| + \| R_\alpha A \varphi - \varphi \| . \qquad (2.5.4)$$

This estimate illustrates the error consists of two parts: the first term reflects the influence of the incorrect data and second term is due to the approximation error between R_α and A^{-1}. To achieve an acceptable total error for the regularized solution we need to have a strategy for choosing the regularization parameter α depending on the error level δ. On one hand, the accuracy of the approximation asks for small error $\| R_\alpha A \varphi - \varphi \|$,i.e., for a small parameter α. On the other hand, the stability requires for a large parameter α in order to make $\| R_\alpha \|$ small. An optimal choice would try to make the right hand side of (2.5.4) minimal. The corresponding parameter then kind of compromises between the accuracy and stability. One expects from the regularization strategy that the regularization converges to the exact solution when the error level δ tends to zero.

Definition 2.12 *A strategy for a regularization scheme R_α, $\alpha \geq 0$, i.e., the choice of the regularization parameter $\alpha = \alpha(\delta)$ depending on the error level δ and the data f^δ, is called regular if for all $f \in A(X)$ and for all $f^\delta \in Y$ with $\| f^\delta - f \| \leq \delta$ we have*

$$R_{\alpha(\delta)} f^\delta \to A^{-1} f, \quad \delta \to 0.$$

Definition 2.13 *(Discrepancy Principle)*
The regularization parameter α for the error level δ should be chosen

$$\| A R_\alpha f^\delta - f^\delta \| = \tau \delta$$

with some fixed parameter $\tau \geq 1$.

2.5.1   Tikhonov Regularization

Theorem 2.5.1 *Let $A : X \to Y$ be a compact linear operator. Then for each $\alpha > 0$ the operator $\alpha I + A^*A : X \to X$ is bijective and has a bounded inverse. Furthermore, if A is injective then*

$$R_\alpha := (\alpha I + A^*A)^{-1} A^*$$

describes a regularization scheme with $\| R_\alpha \| \leq \frac{1}{2\sqrt{\alpha}}$.

Proof: See Theorem 4.13 in [7]

Theorem 2.5.2 *Let $A : X \to Y$ be a compact linear operator and let $\alpha > 0$. Then for each $f \in Y$ there exists a unique $\varphi_\alpha \in X$ such that*

$$\| A\varphi_\alpha - f \|^2 + \alpha \| \varphi_\alpha \|^2 = \inf_{\varphi \in X} \{\| A\varphi - f \|^2 + \alpha \| \varphi \|^2\}. \qquad (2.5.5)$$

The minimizer φ_α is given by the unique solution of the equation

$$\alpha \varphi_\alpha + A^*A\varphi_\alpha = A^*f \qquad (2.5.6)$$

and dependence continuously on f.

Proof: See Theorem 4.14 in [7].

Theorem 2.5.3 *Let $A : X \to Y$ be an injective compact linear operator with dense range in Y and let $f \in Y$ with $0 < \delta < \| f \|$. Then there exists a unique parameter α such that*

$$\| AR_\alpha f - f \| = \delta.$$

Proof: See the Theorem 4.15 in [7].

2.6   Riesz Theory and Fréchet Differentiability

We now present the basic theory for an operator equation

$$\varphi - A\varphi = f$$

of the second kind with a compact linear operator $A : X \to X$ mapping a normed space X into itself.

2.6.1   Riesz Theory for Compact Operators

We define

$$L : I - A$$

where I denotes the identity operator.

Theorem 2.6.1 *(First Riesz Theorem)*
The null space of the operator L

$$N(L) := \{\varphi \in X : L\varphi = 0\} \tag{2.6.1}$$

is a finite dimensional subspace.

Proof: See Theorem 3.1 in [31].

Theorem 2.6.2 *(Second Riesz Theorem)*
The range of the operator L

$$L(X) := \{L\varphi : \varphi \in X\}$$

is a closed linear subspace.

Proof: See Theorem 3.2 in [31].

Theorem 2.6.3 *(Third Riesz Theorem)*
There exists a uniquely determined non-negative integer r, called the Riesz number of the operator A, such that

$$\{0\} = N(L^0) \subsetneqq N(L^1) \subsetneqq \cdots \subsetneqq N(L^r) = N(L^{r+1}) = \cdots ,$$

$$X = L^0(X) \supsetneqq L^1(X) \supsetneqq \cdots \supsetneqq L^r(X) = L^{r+1} = \cdots .$$

Furthermore,

$$X = N(L^r) \oplus L^r(X).$$

Proof: See Theorem 3.3 in [31].

Theorem 2.6.4 *(Fundamental result of the Riesz Theory)*
Let X be a normed space, $A : X \to X$ a compact operator, and let $I - A$ be injective. Then the inverse operator $(I - A)^{-1} : X \to X$ exists and is bounded.

Proof: See Theorem 3.4 in [31].

Corollary 2.14 *Let X be a normed space and $A : X \to X$ a compact linear operator. If the homogeneous equation*

$$\varphi - A\varphi = 0$$

only has the trivial solution $\varphi = 0$, then for all $f \in X$ the inhomogeneous equation

$$\varphi - A\varphi = f$$

has a unique solution $\varphi \in X$ and this solution depends continuously on f.

2.6.2   Fréchet Differentiability

Definition 2.15 *Let X, Y be normed spaces, and let U be an open subset of X. A mapping $A : X \to Y$ is called Fréchet differentiable at $\varphi \in U$ if there exists a bounded linear operator $A'[\varphi] : X \to Y$ such that*

$$\| A(\varphi + h) - A\varphi - A'[\varphi]h \| = \circ(\| h \|)$$

uniformly as $\| h \| \to 0$. $A'[\varphi]$ is called the Fréchet derivative of A at φ. A is called Fréchet differentiable if it is differentiable at every point $\varphi \in U$.

Theorem 2.6.5 *Let $A : U \subset X \to Y$ be Fréchet differentiable and Z be a normed space.*

1. *The Fréchet derivative of A is uniquely determined.*

2. *If $B : U \to Y$ is Fréchet differentiable then $\lambda_1 A + \lambda_2 B$ is differentiable for all $\lambda_1, \lambda_2 \in C$ and*

$$(\lambda_1 A + \lambda_2 B)'[\varphi] = \lambda_1 A'[\varphi] + \lambda_2 B'[\varphi], \quad \varphi \in U.$$

3. *If $B : Y \to Z$ is Fréchet differentiable, then $B \circ A : U \to Z$ is Fréchet differentiable and*

$$(B \circ A)'[\varphi] = B'[A(\varphi)]A'[\varphi], \quad \varphi \in U.$$

4. *If A^{-1} exists, then the mapping A^{-1} is Fréchet differentiable and*

$$(A^{-1})'[\varphi] = -A^{-1}A'[\varphi]A^{-1}, \quad \varphi \in U.$$

Proof: For the first three statements see [26] and for the last statement see [7].

Theorem 2.6.6 *Let $A : U \subset X \to Y$ be a completely continuous operator from an open subset U of a normed space X into a Banach space Y and assume A to be Fréchet differentiable at $\psi \in U$. Then the derivative $A'[\psi]$ is compact.*

Proof: See Theorem 4.19 in [7].
Note that the above theorem shows that ill-posedness of a non-linear problem is inherited by its linearization.

Chapter 3

The Inverse Scattering Problem for a Dielectric

3.1 The Direct Problem

Let the simply connected bounded domain $D \subset \mathbb{R}^2$ with C^2 boundary ∂D represent the cross section of an infinite dielectric cylinder having constant wave number k_d with $\mathrm{Re}\{k_d\}, \mathrm{Im}\{k_d\} \geqslant 0$ and denote the exterior wave number of the background by $k_0 \in \mathbb{R}$. Denote by ν the outward unit normal vector to ∂D. Then, given an incident plane wave $u^i = e^{ik_0 x.d}$ with incident direction given by the unit vector d, the direct scattering problem for E-polarized electromagnetic waves by the dielectric D is modeled by the following transmission problem for the Helmholtz equation: Find solutions u, v to the Helmholtz equations

$$\Delta u + k_0^2 u = 0 \quad \text{in } \mathbb{R}^2 \setminus \bar{D}, \qquad \Delta v + k_d^2 v = 0 \quad \text{in } D \tag{3.1.1}$$

$$u = v, \qquad \frac{\partial u}{\partial \nu} = \frac{\partial v}{\partial \nu} \quad \text{on} \quad \partial D \tag{3.1.2}$$

such that $u = u^i + u^s$ with the scattered wave u^s fulfilling the Sommerfeld radiation condition (1.1.3).

The following uniqueness and existence results follow from Kress and Roach [34] and the book [6].

Theorem 3.1.1 *The scattering problem* (3.1.1)–(3.1.2) *has at most one solution.*

Proof: Let (u_1, v_1) and (u_2, v_2) be two solutions (3.1.1)–(3.1.2). And let $u^s = u_1^s - u_2^s$ and $v = v_1 - v_2$. Then, we have

$$\Delta u^s + k_0^2 u^s = 0 \quad \text{in } \mathbb{R}^2 \setminus \bar{D}, \qquad \Delta v + k_d^2 v = 0 \quad \text{in } D \tag{3.1.3}$$

$$u^s = v, \qquad \frac{\partial u^s}{\partial \nu} = \frac{\partial v}{\partial \nu} \quad \text{on} \quad \partial D \tag{3.1.4}$$

and u^s satisfies the Sommerfeld radiation condition. Let ∂B_R be a circle of radius R with outward drawn unit normal vector ν. Assume that ∂B_R contains ∂D in its interior and let $B_R := \{x \in \mathbb{R}^2 \setminus \bar{D} : |x| < R\}$. Applying Green's theorems over B_R and D and using the differential equation (3.1.3) and the boundary condition (3.1.4) we obtain

$$\int_{\partial B_R} u^s \frac{\partial \bar{u}^s}{\partial \nu} ds = -k_0^2 \int_{B_R} |u^s|^2 dx + \int_{B_R} |\nabla u^s|^2 dx - \bar{k}_d^2 \int_D |v|^2 dx + \int_D |\nabla v|^2 dx \quad (3.1.5)$$

Now we write the interior wave number as $k_d := \alpha + i\beta$ with $\alpha, \beta \geq 0$ due to the assumption on k_d. If we take the imaginary part of (3.1.5) we get

$$Im \int_{\partial B_R} u^s \frac{\partial \bar{u}^s}{\partial \nu} ds = 2\alpha\beta \int_D |v|^2 dx \qquad (3.1.6)$$

The equation (3.1.6) implies that

$$Im \int_{\partial B_R} u^s \frac{\partial \bar{u}^s}{\partial \nu} ds \geq 0 \qquad (3.1.7)$$

Hence from Theorem (2.3.4) we obtain $u^s = 0$ in $\mathbb{R}^2 \setminus \bar{D}$ and from (3.1.4) we have $v = 0$ and $\dfrac{\partial v}{\partial \nu}$ on ∂D. From Green's theorems we conclude that $v = 0$ in D. $\square$

For the case $k_0 \in \mathbb{C}$ we refer to [34] and see also Theorem 3.40 in [6].

In order to show the existence of a solution to the transmission problem we seek the solution in the form of combined double- and single-layer potentials

$$u^s(x) = \int_{\partial D} [\frac{\partial \Phi_{k_0}(x, y)}{\partial \nu(y)} \psi(y) + \Phi_{k_0}(x, y)\phi(y)] ds(y), \quad x \in \mathbb{R}^2 \setminus \bar{D},$$

$$(3.1.8)$$

$$v(x) = \int_{\partial D} [\frac{\partial \Phi_{k_d}(x, y)}{\partial \nu(y)} \psi(y) + \Phi_{k_d}(x, y)\phi(y)] ds(y), \quad x \in D,$$

with continuous densities ψ and ϕ. Φ_{k_d} and Φ_{k_0} denote fundamental solutions of Helmholtz equation in D and in $\mathbb{R}^2 \setminus \bar{D}$ as given by (2.2.3) with wave numbers k_d and k_0 respectively. Clearly, u^s and v satisfy the respective Helmholtz equations and u^s satisfies the Sommerfeld radiation condition (1.1.3). Define $f := -u^i$ and $g := -\dfrac{\partial u^i}{\partial \nu}$ on ∂D and we rewrite (3.1.2) in the form

$$u^s - v = f, \qquad \frac{\partial u^s}{\partial \nu} - \frac{\partial v}{\partial \nu} = g \quad \text{on} \quad \partial D. \qquad (3.1.9)$$

If we approach to the boundary ∂D and use jump relation on ∂D, for the potentials (3.1.8) we get

$$u^s|_{\partial D} = \frac{1}{2}K_{k_0}\psi + \frac{1}{2}\psi + \frac{1}{2}S_{k_0}\phi,$$

$$(3.1.10)$$

$$v|_{\partial D} = \frac{1}{2}K_{k_d}\psi - \frac{1}{2}\psi + \frac{1}{2}S_{k_d}\phi,$$

We distinguish boundary operators as in definition 2.6 for the two wave numbers k_0 and k_d by corresponding subscripts.

If we take the normal derivative of th potentials (3.1.8) and approach the boundary and use the jump relation on the boundary, then we obtain

$$\frac{\partial u^s}{\partial \nu} = \frac{1}{2}T_{k_0}\psi + \frac{1}{2}K'_{k_0}\phi - \frac{1}{2}\phi \quad \text{on} \quad \partial D,$$

$$\frac{\partial v}{\partial \nu} = \frac{1}{2}T_{k_d}\psi + \frac{1}{2}K'_{k_d}\phi + \frac{1}{2}\phi \quad \text{on} \quad \partial D. \tag{3.1.11}$$

Using equations (3.1.9), (3.1.10), and (3.1.11) we observe that the potentials (3.1.8) satisfy the transmission conditions (3.1.2) provided the densities satisfy the system of integral equations

$$2\psi + (K_{k_0} - K_{k_d})\psi + (S_{k_0} - S_{k_d})\phi = 2f \quad \text{on} \quad \partial D,$$

$$2\phi - (T_{k_0} - T_{k_d})\psi - (K'_{k_0} - K'_{k_d})\phi = -2g \quad \text{on} \quad \partial D. \tag{3.1.12}$$

Theorem 3.1.2 *The potential* (3.1.8) *solve the direct scattering problem provided the densities ψ and ϕ solve the system of integral equation* (3.1.12).

On the product space $C(\partial D) \times C)\partial D)$ equipped with $\left\| \begin{pmatrix} \psi \\ \phi \end{pmatrix} \right\| := max(\|\psi\|_\infty, \|\phi\|_\infty)$, we introduce the operator A defined by

$$A := \begin{bmatrix} -(K_{k_0} - K_{k_d}) & -(S_{k_0} - S_{k_d}) \\ (T_{k_0} - T_{k_d}) & (K'_{k_0} - K'_{k_d}) \end{bmatrix}$$

We can rewrite the system of integral equation of (3.1.12) in the abbreviated form

$$2\chi - A\chi = 2h \quad \text{on} \quad \partial D, \tag{3.1.13}$$

where $\chi = \begin{pmatrix} \psi \\ \phi \end{pmatrix}$ and $h = \begin{pmatrix} f \\ -g \end{pmatrix}$.

Theorem 3.1.3 *The equation* (3.1.13) *has a unique solution.*

Proof : Let $\chi = \begin{pmatrix} \psi \\ \phi \end{pmatrix}$ be a solution to the homogeneous equation $\chi - A\chi = 0$. Then the potentials u^s and v given by (3.1.8) solve the homogeneous scattering problem. Therefore, by the uniqueness Theorem 3.1.1, we have that $u^s = 0$ in $\mathbb{R}^2 \backslash \bar{D}$ and $v = 0$ in D. Now we define,

$$p^s(x) := \int_{\partial D} [\frac{\partial \Phi_{k_d}(x,y)}{\partial \nu(y)} \psi(y) + \Phi_{k_d}(x,y)\phi(y)] ds(y), \quad x \in \mathbb{R}^2 \backslash \bar{D},$$

$$q(x) := -\int_{\partial D} [\frac{\partial \Phi_{k_0}(x,y)}{\partial \nu(y)} \psi(y) + \Phi_{k_0}(x,y)\phi(y)] ds(y), \quad x \in D.$$

If we use jump relation on the boundary ∂D, we get

$$p^s - v = \psi, \quad \text{and} \quad q + u^s = \psi \quad \text{on} \quad \partial D,$$

$$\frac{\partial p^s}{\partial \nu} - \frac{\partial v}{\partial \nu} = -\phi, \quad \text{and} \quad \frac{\partial u^s}{\partial \nu} + \frac{\partial q}{\partial \nu} = -\phi, \quad \text{on} \quad \partial D. \tag{3.1.14}$$

Since we have that $v = 0$, $u^s = 0$, $\frac{\partial u^s}{\partial \nu} = 0$, and $\frac{\partial v}{\partial \nu} = 0$ on the boundary ∂D, the equations (3.1.14) imply that

$$p^s = q, \quad \text{and} \quad \frac{\partial p^s}{\partial \nu} = \frac{\partial q}{\partial \nu} \quad \text{on} \quad \partial D. \tag{3.1.15}$$

We also have that

$$\Delta p^s + k_d^2 p^s = 0 \quad \text{in } \mathbb{R}^2 \setminus \bar{D}, \qquad \Delta q + k_0^2 q = 0 \quad \text{in } D, \tag{3.1.16}$$

where p^s satisfies Sommerfeld radiation condition(1.1.3). From (3.1.15), (3.1.16) and Theorem 3.1.1 we obtain

$$p^s = 0 \quad \text{in} \quad \mathbb{R}^2 \backslash \bar{D}, \quad \text{and} \quad q = 0 \quad \text{in} \quad D. \tag{3.1.17}$$

Now the equations (3.1.17) also imply that $q = 0$, $p^s = 0$, $\frac{\partial p^s}{\partial \nu} = 0$, and $\frac{\partial q}{\partial \nu} = 0$ on the boundary ∂D. Hence, from the equations (3.1.14) we conclude that $\psi = 0$ and $\phi = 0$, i.e., $\chi = 0$. Clearly, the operator A is compact since all its components are compact (see Theorem 2.4.2). In particular, $T : C(\partial D) \to C(\partial D)$ is a hyper-singular operator that is only defined on subspace $V \subset C(\partial D)$ of sufficiently smooth function. However, the difference operator $T_0 - T_d : C(\partial D) \to C(\partial D)$ again has a weakly singular kernel and therefore it is compact (see Theorem 2.21 in [31]). Since the null space $N(I - \frac{1}{2}A) = \{0\}$, i.e., the operator $I - \frac{1}{2}A$ is injective, existence of a solution follows from fundamental Riesz Theorem 2.6.4

Theorem 3.1.4 *The direct scattering problem has a unique solution.*

Proof: The proof follows from the Theorems 3.1.1 and 3.1.3.

As one of the ingredients of our inverse algorithm, we provide an alternative existence proof and suggest a single-layer approach. Since this leads to an integral equation of the first kind, the existence analysis requires either Hölder or Sobolev spaces. Here we choose the Sobolev spaces. In Sobolev space setting, for $k = k_0$ and $k = k_d$, we introduce the single-layer potential operators

$$S_k : H^{-1/2}(\partial D) \to H^{1/2}(\partial D)$$

by

$$(S_k \varphi)(x) := 2 \int_{\partial D} \Phi_k(x, y)\varphi(y)ds(y), \quad x \in \partial D, \tag{3.1.18}$$

and the normal derivative operators

$$K'_k : H^{-1/2}(\partial D) \to H^{-1/2}(\partial D)$$

by

$$(K'_k \varphi)(x) := 2 \int_{\partial D} \frac{\partial \Phi_k(x, y)}{\partial \nu(x)}\varphi(y)ds(y), \quad x \in \partial D, \tag{3.1.19}$$

Now we try to find the solution in the form of the single-layer potentials

$$u^s(x) = \int_{\partial D} \Phi_{k_0}(x, y)\varphi_0(y)ds(y), \quad x \in \mathbb{R}^2 \backslash \bar{D},$$

$$\tag{3.1.20}$$

$$v(x) = \int_{\partial D} \Phi_{k_d}(x, y)\varphi_d(y)ds(y), \quad x \in D,$$

with $\varphi_0, \varphi_d \in H^{-1/2}(\partial D)$. If we approach to the boundary ∂D and use the jump relation on the boundary for the single layer potential(3.1.20) we obtain

$$u^s = \frac{1}{2}S_{k_0}\varphi_0, \qquad \text{on} \quad \partial D,$$

$$v = \frac{1}{2}S_{k_d}\varphi_d, \qquad \text{on} \quad \partial D. \tag{3.1.21}$$

Now if we take normal derivative of potentials (3.1.20) and approach to the boundary ∂D, use the jump relation on the boundary, and use the boundary data then we obtain

$$\frac{\partial u^s}{\partial \nu} = \frac{1}{2}K'_{k_0}\varphi_0 - \frac{1}{2}\varphi_0, \quad \text{on} \quad \partial D$$

$$\tag{3.1.22}$$

$$\frac{\partial v}{\partial \nu} = \frac{1}{2}K'_{k_d}\varphi_d + \frac{1}{2}\varphi_d, \quad \text{on} \quad \partial D.$$

From the equations (3.1.21),(3.1.22) it can be seen that the single layer potentials (3.1.20) satisfy the boundary conditions (3.1.2) provided the densities φ_0, φ_d satisfy

the system of integral equation,

$$S_{k_d}\varphi_d - S_{k_0}\varphi_0 = 2u^i, \qquad \text{on} \quad \partial D,$$

$$\varphi_d + \varphi_0 + K'_{k_d}\varphi_d - K'_{k_0}\varphi_0 = 2\frac{\partial u^i}{\partial \nu}, \quad \text{on} \quad \partial D. \tag{3.1.23}$$

We denote these system of integral equations (3.1.23) as field equations.

We assume that k_0 is not a Dirichlet eigenvalue for D, that is, for each solution w to $\Delta w + k_0^2 w = 0$ in D with $w = 0$ on ∂D, we have that $w = 0$ in D. As a consequence of this assumption, the operator $S_{k_0} : H^{-1/2}(\partial D) \to H^{1/2}(\partial D)$ has a bounded inverse.

Theorem 3.1.5 *Provided k_0 is not a Dirichlet eigenvalue for the domain D the system of integral equation (3.1.23) has a unique solution in $H^{-1/2}(\partial D) \times H^{-1/2}(\partial D)$.*

Proof: We first establish that (3.1.23) has at most one solution. If φ_0 and φ_d satisfy the homogeneous form of (3.1.23), then single-layer potentials (3.1.20) solve the scattering problem with zero incident field. Therefore we have that

$$\Delta u^s + k_0^2 u = 0 \quad \text{in} \ \mathbb{R}^2 \setminus \bar{D}, \qquad \Delta v + k_d^2 v = 0 \quad \text{in} \ D,$$

$$u^s = v, \qquad \frac{\partial u^s}{\partial \nu} = \frac{\partial v}{\partial \nu} \quad \text{on} \quad \partial D. \tag{3.1.24}$$

In the proof of the Theorem 3.1.1 we have shown that equations (3.1.24) have only the trivial solution. That is, $u^s = 0$, in $\mathbb{R}^2\setminus\bar{D}$ and $v = 0$ in D. Hence these results imply that $u^s = 0$, $v = 0$, $\frac{\partial u^s}{\partial \nu} = 0$, and $\frac{\partial v}{\partial \nu} = 0$ on the boundary ∂D. Now we define

$$w_1(x) := \int_{\partial D} \Phi_{k_0}(x,y)\varphi_0(y)ds(y) \quad x \in D,$$

$$w_2(x) := \int_{\partial D} \Phi_{k_d}(x,y)\varphi_d(y)ds(y) \quad x \in \mathbb{R}^2\setminus\bar{D}, \tag{3.1.25}$$

where w_1 and w_2 solve the Helmholtz equation in D and in $\mathbb{R}^2\setminus D$ respectively, and w_2 satisfies the Sommerfeld radiation condition(1.1.3). From the jump relation we have that

$$w_1 = u^s \qquad \text{on} \quad \partial D. \tag{3.1.26}$$

Hence, $w_1 = 0$ on the boundary ∂D. Since k_0 is not a Dirichlet eigenvalue in D and w_1 vanishes on the boundary ∂D, we conclude that $w_1 = 0$ in D. Therefore, we have $\frac{\partial w_1}{\partial \nu} = 0$ on the boundary ∂D. From the jump relation, we have

$$\varphi_0 = \frac{\partial u^s}{\partial \nu} - \frac{\partial w_1}{\partial \nu} \quad \text{on} \quad \partial D. \tag{3.1.27}$$

(3.1.27) implies that $\varphi_0 = 0$ on the boundary ∂D.

Now it remains to show that the density φ_d vanishes. If we again use the jump relation we have that

$$w_2 = v \qquad \text{on} \quad \partial D. \tag{3.1.28}$$

(3.1.28) implies that $w_2 = 0$ on the boundary ∂D. If k_d is real, then w_2 satisfies the Sommerfeld radiation condition (1.1.3). The boundary condition $w_2 = 0$ on ∂D then implies that $w_2 = 0$ in $\mathbb{R}^2 \setminus D$. If $Imk_d > 0$, then $w_2(x)$ decays exponentially as $|x| \to \infty$ because of the exponential decay of the Hankel function $H_0^{(1)}(k_d|x|)$ as $|x| \to \infty$. Hence, we can apply Green's integral theorem 2.2.2 in $\mathbb{R}^2 \setminus D$ to obtain

$$\int_{\mathbb{R}^2 \setminus D} \{k_d^2 |w_2|^2 - |\nabla w_2|^2\} dx = \int_{\partial D} w_2 \frac{\partial w_2}{\partial \nu} ds = 0.$$

Taking the imaginary part, gives

$$\int_{\mathbb{R}^2 \setminus D} |w_2|^2 dx = 0,$$

and consequently we deduce $w = 0$ in $\mathbb{R}^2 \setminus D$ also in this case. Hence in both case we have

$$w_2 = 0 \qquad \text{in} \qquad \mathbb{R}^2 \setminus \bar{D}. \tag{3.1.29}$$

(3.1.29) also implies that $\dfrac{\partial w_2}{\partial \nu} = 0$ on the boundary ∂D. Now if we use the jump relation, we obtain

$$\varphi_d = \frac{\partial w_2}{\partial \nu} - \frac{\partial v}{\partial \nu}, \qquad \text{on} \quad \partial D. \tag{3.1.30}$$

Finally, (3.1.30) implies that $\varphi_d = 0$.

To establish a solution, we note that due to the assumption on k_0 the inverse operator

$$S_{k_0}^{-1} : H^{1/2}(\partial D) \to H^{-1/2}(\partial D),$$

exists and bounded. With its aid, if we multiply the equation (3.1.23) by the operator $S_{k_0}^{-1}$ from the left-hand-side, add and subtract φ_d we obtain the equivalent system

$$\varphi_d - \varphi_0 + S_{k_0}^{-1}[S_{k_d} - S_{k_0}]\varphi_d = 2S_{k_0}^{-1}u^i \quad \text{on} \quad \partial D$$

$$\varphi_d + \varphi_0 + K'_{k_d}\varphi_d - K'_{k_0}\varphi_0 = 2\frac{\partial u^i}{\partial \nu} \quad \text{on} \quad \partial D. \tag{3.1.31}$$

We can rewrite the equations (3.1.31) of the form

$$\mathcal{A} \begin{pmatrix} \varphi_d \\ \varphi_0 \end{pmatrix} + \mathcal{K} \begin{pmatrix} \varphi_d \\ \varphi_0 \end{pmatrix} = 2 \begin{pmatrix} S_{k_0}^{-1} u^i |_{\partial D} \\ \dfrac{\partial u^i}{\partial \nu} \Big|_{\partial D} \end{pmatrix}$$

with the matrix operators

$$\mathcal{A}, \mathcal{K} : H^{-1/2}(\partial D) \times H^{-1/2}(\partial D) \to H^{-1/2}(\partial D) \times H^{-1/2}(\partial D)$$

given by

$$\mathcal{A} = \begin{pmatrix} I & -I \\ I & I \end{pmatrix} \quad \text{and} \quad \mathcal{K} = \begin{pmatrix} S_{k_0}^{-1}[S_{k_d} - S_{k_0}] & 0 \\ K'_{k_d} & -K'_{k_0} \end{pmatrix}.$$

Clearly, $\mathcal{A}$ has a bounded inverse and given by

$$\mathcal{A}^{-1} = \frac{1}{2} \begin{pmatrix} I & I \\ -I & I \end{pmatrix}.$$

$\mathcal{K}$ is compact since its components are compact (see the Theorem (2.4.7)). In particular, $S_{k_d} - S_{k_0} : H^{-1/2}(\partial D) \to H^{1/2}(\partial D)$ is compact because of cancellation of singularities in the two single-layer operators, i.e., $S_{k_d} - S_{k_0} : H^{-1/2}(\partial D) \to H^{1/2}(\partial D)$ has continuous kernel therefore it is compact (see Theorem 2.20 in [31]). The operator $\mathcal{A}^{-1}\mathcal{K} : H^{-1/2}(\partial D) \times H^{-1/2}(\partial D) \to H^{-1/2}(\partial D) \times H^{-1/2}(\partial D)$ is compact (see Theorem 2.15 in [31]). Since the null space $N(I - \mathcal{A}^{-1}\mathcal{K}) = \{0\}$, i.e.,the operator $I - \mathcal{A}^{-1}\mathcal{K}$ is injective, existence of a solution follows from the fundamental Riesz Theorem 2.6.4.   □

From the asymptotic for the Hankel functions, it can be deduced that the far field pattern of the single-layer potential u^s with density φ_0 is given by

$$u_\infty(\hat{x}) = \gamma \int_{\partial D} e^{-ik_0 \hat{x} \cdot y} \varphi_0(y) \, ds(y), \quad \hat{x} \in \Omega, \tag{3.1.32}$$

where $\gamma = \dfrac{e^{i\frac{\pi}{4}}}{\sqrt{8\pi k_0}}$ and φ_0 is the solution of the field equation (3.1.23).

3.2   The Inverse Scattering Problem

Problem 3.1 *(Inverse Scattering Problems)*
Given the far field pattern u_∞ for one or finitely many incident plane waves u^i and knowing that the scatterer either is sound-soft or sound-hard or dielectric, determine either the shape and location of the scatterer D,i.e., reconstruction the boundary ∂D or the conductive function of the scatterer D.

Note that these inverse problems are nonlinear since the scattered wave u^s depends nonlinearly on the scatterer D. In addition, they are ill-posed. Example 2.51 in [19] illustrates ill-posedness for the case of sound-soft scatterer. We rewrite that example below.

Example 3.2 *Let D be a sound-soft disk of radius r centered at the origin and $d = (1, 0)$ the direction of the incident plane wave. Then using the polar coordinates (ρ, θ) for $x \in \mathbb{R}^2$ we write the Jacobi-Anger(see [7]) expansion*

$$e^{ikx \cdot d} = \sum_{n=-\infty}^{\infty} i^n J_n(k\rho) e^{in\theta}, \qquad x \in \mathbb{R}^2. \tag{3.2.1}$$

From this expansion we find that the total field $u = u^i + u^s$ can be represented in the form

$$u(x) = \sum_{n=-\infty}^{\infty} \frac{i^n}{H_n^{(1)}(kr)} \{J_n(k\rho) H_n^{(1)}(kr) - J_n(kr) H_n^{(1)}(k\rho)\} \quad |x| \geq r.$$

the asymptotic of the Hankel functions give

$$u_\infty(\hat{x}) = -\gamma \sum_{n=-\infty}^{\infty} \frac{J_n(kr)}{H_n^{(1)}(kr)} e^{in\theta},$$

where $\gamma = \frac{e^{i\frac{\pi}{4}}}{\sqrt{8\pi k}}$, $\hat{x} \in \Omega$, J_n is the Bessel function defined by (2.2.5) and $H_n^{(1)}$ is the Hankel function defined by (2.2.4). To illustrate the ill-posedness we consider a perturbed far field pattern

$$u_\infty^\delta(\hat{x}) = u_\infty(\hat{x}) + \delta e^{in\theta},$$

with $\delta > 0$, $n \in \mathbb{N}$. Then, due to the asymptotic behavior of the Hankel functions for large arguments (2.2.8), the corresponding total field is given by

$$u^\delta(x) = u(x) + \delta \sqrt{\frac{\pi k}{2}} e^{i\frac{\pi}{4}(2n+1)} H_n^{(1)}(k|x|).$$

By the asymptotic of the Hankel functions for large orders this implies the estimate

$$|u^\delta(x) - u(x)| \approx \delta \sqrt{\frac{\pi k}{2}} (n-1)! \left(\frac{2}{kR}\right)^n, \qquad |x| = R.$$

Hence, small changes in the data u_∞ lead to large errors in the solution of the inverse problem.

The inverse scattering problems that we are interested in are formulated as follows:

Problem 1 : Given the far field pattern u_∞ for one incident field u^i, determine the shape of the boundary ∂D of the dielectric scatterer D.

Problem 2 : Given the far field pattern u_∞ for one incident field u^i, determine the interior wave number k_d of the dielectric scatterer D.

Problem 3 : Given the far field pattern u_∞ for one incident field u^i, simultaneously determine the shape of the boundary ∂D and the interior wave k_d of the dielectric scatterer D.
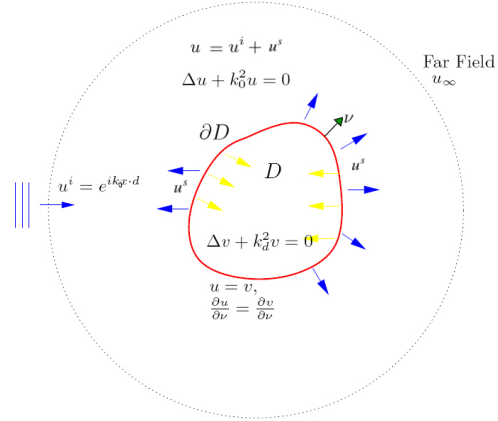
3.2.1 Uniqueness for impenetrable obstacles

An important question in inverse problems is uniqueness, which settles the identifiability, i.e., whether there is enough information to uniquely determine the obstacle from its far field pattern for incident plane waves. The following classical uniqueness result due to Schiffer is concerned with inverse scattering from a sound-soft obstacle.

Theorem 3.2.1 *(Schiffer)*
Assume that $D_1 \subset \mathbb{R}^2$ and $D_2 \subset \mathbb{R}^2$ are two sound-soft scatterers such that the far field patterns coincide for an infinite number of incident plane waves with distinct directions and one fixed wave number. Then $D_1 = D_2$.

Proof: Assume that $D_1 \neq D_2$. Since by Rellich's lemma 2.3 the far field pattern uniquely determines the scattered field, for each plane wave $u^i(x, d) = e^{ikx \cdot d}$ the scattered wave u^s for both obstacles coincides in the unbounded domain G of the complement of $D_1 \cup D_2$ and the total field vanishes on ∂G. Assume that $D^* := (\mathbb{R}^2 \setminus G) \setminus \bar{D}_2$ is non-empty. Then u^s is defined in D^* since it describes the scattered waves for D_2, i.e., the total field satisfies the Helmholtz equation in D^* with homogeneous boundary condition on ∂D^*. Hence, the total field u is a Dirichlet eigenfunction for the negative Laplacian in the domain D^* with eigenvalue k^2. This implies that the total field u is an element of the Sobolev space $H^1(D^*)$. Now, our aim is to show these total fields are linearly independent for distinct incoming incident plane waves. To do so, assume that

$$\sum_{n=1}^{N} c_n u(x, d_n) = 0 \tag{3.2.2}$$

in D^* for some constants c_n and N distinct incident direction d_n. Then, by analyticity, (3.2.2) is satisfied in exterior of some circle containing D_1 and D_2. The total field can be written as the sum of incident plane with distinct incident direction and scattered field of the form

$$u(x, d_n) = e^{ikx \cdot d_n} + u^s(x, d_n)$$

and using the finiteness $u^s(x, d_n) = O(1/|x|)$, from (3.2.2) we yield,

$$\lim_{R \to \infty} \frac{1}{R} \sum_{n=1}^{N} c_n \int_{|x|=R} e^{ikx \cdot (d_n - d_m)} ds(x) = 0.$$

On the other hand, we apply the Funk-Hecke formula (see [7] for $\mathbb{R}^3$)

$$\lim_{R \to \infty} \frac{1}{R} \sum_{n=1}^{N} c_n \int_{|x|=R} e^{ikx \cdot (d_n - d_m)} ds(x) = 2\pi c_m.$$

Therefore, $c_m = 0$ for $m = 1, \ldots, N$, that is, the total functions $u(x, d_n)$, $n = 1, \ldots, N$ are linearly independent. Whereas, there exist only finitely many Dirichlet eigenfunction of the negative Laplacian in $H^1(D^*)$. This is contradiction and therefore we conclude that $D_1 = D_2$. $\qquad \square$

Theorem 3.2.2 *Let D_1 and D_2 be two scatterers which are contained in a disk of radius R, let*

$$N := \sum_{n=0}^{\infty} (2n + 1) z_n,$$

where z_n is the number of zeros of the Bessel functions J_n lying in the interval $(0, kR)$ and assume that the far field patterns coincide for $N + 1$ incident plane waves with distinct directions and wave number k. Then $D_1 = D_2$.

Proof: The proof is based on the strong monotonicity property of the eigenvalues the negative Laplacian with Dirichlet boundary condition, see [10]

Corollary 3.3 *Let D_1 and D_2 be two planar scatterers contained in a disk of radius R such that $kR < \lambda_0$, where λ_0 is the smallest positive zero of the Bessel function J_0 ($\lambda_0 \approx 2.4048$), and assume that the far field patterns coincide for one incident field with wave number k. Then $D_1 = D_2$.*

More recently the bound in Corollary 3.3 was improved to $kR < 3.8322$ by Gintides [12]. Schiffer's proof can not be generalized to the other boundary conditions. This due to the fact that the finiteness of the dimension of the eigenspaces for eigenvalues of the negative Laplacian for the Neumann or impedance boundary condition requires the boundary of a domain to be sufficiently smooth.

Isakov [17] has obtained uniqueness results on inverse scattering for penetrable obstacles by using techniques different from Schiffer's method. The following theorem stated by Kirsch and Kress [28] simplified version of Isakov's approach to prove a uniqueness with respect to impenetrable sound-hard obstacles.

Theorem 3.2.3 *Assume that D_1 and D_2 are two sound-soft scatterers such that for a fixed wave number the far-field patterns for both scatters coincide for all incident directions. Then $D_1 = D_2$.*

Proof: See Theorem 3.3 in [28].

3.2.2   Uniqueness for Penetrable obstacles

The following theorem was stated by Kirsch and Kress [28] who simplified version of Isakov's approach [17] to prove a uniqueness for penetrable obstacles.

Theorem 3.2.4 *Assume that D_1 and D_2 are two penetrable scatterers such that for a fixed wave number the far field patterns for both scatters coincide for all incident directions. Then $D_1 = D_2$.*

Proof: See Theorem 4.1 in [28].

We do not have general uniqueness result for one or finitely many incident plane waves yet. However, if we restrict the scatterer to a disk then we have a uniqueness result. The following theorem express that fact (see [3])

Theorem 3.2.5 *A dielectric disk is uniquely determined by the far field pattern for one incident plane wave.*

Proof: Using the Jacobi–Anger expansion (3.2.1), it can be seen that the scattered field u^s and the transmitted field v for scattering from a disk of radius R centered at the origin have the form

$$u^s(x) = \sum_{n=-\infty}^{\infty} i^n \, \frac{k_0 J_n(k_d R) J_n'(k_0 R) - k_d J_n(k_0 R) J_n'(k_d R)}{k_d H_n^{(1)}(k_0 R) J_n'(k_d R) - k_0 J_n(k_d R) H_n^{(1)\prime}(k_0 R)} \, H_n^{(1)}(k_0 \rho) e^{in\theta}$$

$$(3.2.3)$$

for $|x| \geq R$ and

$$v(x) = \frac{2}{\pi R} \sum_{n=-\infty}^{\infty} \frac{i^{n-1}}{k_d H_n^{(1)}(k_0 R) J_n'(k_d R) - k_0 J_n(k_d R) H_n^{(1)\prime}(k_0 R)} \, J_n^{(1)}(k_d \rho) e^{in\theta}$$

$$(3.2.4)$$

for $|x| \leq R$. Here the $H_n^{(1)}$ denote the Hankel functions of the first kind of order n and in (3.2.4) we have used the Wronskian for the Bessel and Hankel functions. As a consequence of the uniqueness of the solution to the forward scattering problem, the determinant in the denominator in (3.2.3) and (3.2.4) is different from zero. From

the asymptotic of the Bessel and Hankel functions for large n (see [7]) uniform convergence can be established for the series (3.2.3) in compact subsets of $\mathbb{R}^2 \setminus \{0\}$ and for the series (3.2.4) in compact subsets of $\mathbb{R}^2$. In particular, this implies that the scattered wave u^s has an extension as solution to the Helmholtz equation across the boundary into the interior of the disk with the exception of the center. Now assume that two disks D_1 and D_2 with centers z_1 and z_2 have the same far field pattern $u_{\infty,1} = u_{\infty,1}$ for scattering of one incident plane wave. Then by Rellich's lemma (see [7]) the scattered waves coincide $u_1^s = u_2^s$ in $\mathbb{R}^2 \setminus (D_1 \cup D_2)$ and we can identify $u^s = u_1^s = u_2^s$ in $\mathbb{R}^2 \setminus (D_1 \cup D_2)$. Now assume that $z_1 \neq z_2$. Then u_1^s has an extension into $\mathbb{R}^2 \setminus \{z_1\}$ and u_2^s an extension into $\mathbb{R}^2 \setminus \{z_2\}$. Therefore, u^s can be extended from $\mathbb{R}^2 \setminus (D_1 \cup D_2)$ into all of $\mathbb{R}^2$, that is, u^s is an entire solution to the Helmholtz equation. Consequently, since u^s also satisfies the radiation condition it must vanish identically $u^s = 0$ in all of $\mathbb{R}^2$. Without loss of generality we set $D = D_1$, assume its center at the origin and denote its radius by R and have the expansions (3.2.3) and (3.2.4) available. Equating Fourier coefficients in the uniformly convergent series (3.2.1) and (3.2.4) and the corresponding series for the normal derivatives on $|x| = R$, we observe that associated pairs of terms in the series (3.2.1) and (3.2.4) satisfy the transmission condition (3.1.2) separately, i.e., each pair constitutes an eigenfunction pair for an interior transmission eigenvalue for the piecewise constant refractive index with values one in $\mathbb{R}^2 \setminus \bar{D}$ and k_d/k_0 in D. Clearly, these eigenfunctions are linearly independent. However, for a complex-valued refractive index no interior transmission eigenvalues exist (this is a straightforward consequence of Green's second integral theorem) and for a real-valued refractive index interior transmission eigenvalues have finite multiplicity (see [4] and also the proof of Theorem 8.32 in [7]). Hence we arrived at a contradiction and therefore the two disks must have the same center. In order to show that D_1 and D_2 have the same radius, we observe that by symmetry, or by inspection of the explicit solution given above, the far field pattern for scattering of plane waves at a dielectric disk depends only on the angle between the observation direction and the incident direction. Hence, knowledge of the far field pattern for one incident direction implies knowledge of the far field pattern for all incident directions. Now the statement follows from the uniqueness result for infinitely many incident waves in [28]. $\square$

3.2.3   Reconstruction Algorithm

We proceed describing an iterative algorithm for approximately solving the inverse scattering problem by extending the methods proposed by Johansson and Sleeman [25], Ivanyshyn, Kress and Rundell [19, 21, 23, 36], and Kress and Serranho[32, 37, 38, 45]. After introducing the far field operator $S_\infty : H^{-1/2}(\partial D) \to L^2(\Omega)$ by

$$(S_\infty \varphi)(\hat{x}) := \gamma \int_{\partial D} e^{-ik_0 \, \hat{x} \cdot y} \varphi(y) \, ds(y), \quad \hat{x} \in \Omega, \tag{3.2.5}$$

from (3.1.20) and (3.1.32) we observe that the far field pattern for the solution to
the scattering problem (3.1.1)–(1.1.3) is given by

$$u_\infty = S_\infty \varphi_0 \qquad (3.2.6)$$

in terms of the solution to (3.1.23). Therefore we can state the following theorem
as theoretical basis of our inverse algorithm. For this we note that all our integral
operators depend on the boundary curve ∂D.

Theorem 3.2.6 *For a given incident field u^i and a given far field pattern u_∞,
assume that ∂D and the densities φ_d and φ_0 satisfy the system of three integral
equations*

$$S_{k_d}\varphi_d - S_{k_0}\varphi_0 = 2u^i,$$

$$\varphi_d + K'_{k_d}\varphi_d + \varphi_0 - K'_{k_0}\varphi_0 = 2\,\frac{\partial u^i}{\partial \nu}\,, \qquad (3.2.7)$$

$$S_\infty \varphi_0 = u_\infty.$$

Then ∂D solves the inverse problem.

The ill-posedness of the inverse problem is reflected through the ill-posedness of
the third integral equation, the far field equation that we denote as *data equation*.
Note that (3.2.7) is linear with respect to the densities and nonlinear with respect
to the boundary ∂D. This opens up a variety of approaches to solve (3.2.7) by
linearization and iteration.

3.2.4   The Johansson and Sleeman Method

We now proceed with describing in detail the extension of the Johansson and Slee-
man Method [25] from the case of impenetrable scatterers to the case of scattering
from a dielectric.

Given a current approximation for the unknown boundary ∂D we solve the first
two equations, that is, the system (3.1.23) that we denote as *field equations* for the
unknown densities φ_d and φ_0. Then, keeping φ_0 fixed we linearize the data equation
with respect to the boundary ∂D to update the approximation. To describe this in
more detail, we chose a parametrization

$$\partial D = \{z(t) = r(t)(\cos t, \sin t) : t \in [0, 2\pi]\}, \qquad (3.2.8)$$

with a 2π periodic positive smooth function r. Then, via $\psi = \varphi \circ z$ emphasizing the
dependence of the operators on the boundary curve, we introduce the parametrized
single-layer operator

$$\widetilde{S}_k : H^{-1/2}[0, 2\pi] \times C^2[0, 2\pi] \to H^{1/2}[0, 2\pi],$$

by

$$\widetilde{S}_k(\psi, z)(t) := \frac{i}{2} \int_0^{2\pi} H_0^{(1)}(k|z(t) - z(\tau)|)\psi(\tau)|z'(\tau)|d\tau, \qquad (3.2.9)$$

where $\psi := \varphi o z$, $S_k \varphi \circ z := \widetilde{S}_k(\psi, z)$ and parametrized normal derivative operators

$$\widetilde{K}'_k : H^{-1/2}[0, 2\pi] \times C^2[0, 2\pi] \to H^{-1/2}[0, 2\pi]$$

by

$$\widetilde{K}'_k(\psi, z)(t) := \frac{ik}{2} \int_0^{2\pi} \frac{[z'(t)]^\perp \cdot (z(\tau) - z(t))}{|z'(t)||z(t) - z(\tau)|}|z'(\tau)| \, H_1^{(1)}(k|z(t) - z(\tau)|)\psi(\tau)d\tau,$$

$$(3.2.10)$$

for $t \in [0, 2\pi]$ and where $K'_k \varphi \circ z := \widetilde{K}'_k(\psi, z)(t)$. Here we made use of $H_0^{(1)'} = -H_1^{(1)}$ with the Hankel function $H_1^{(1)}$ of order one and of the first kind. Furthermore, we write $v^\perp = (v_2, -v_1)$ for any vector $v = (v_1, v_2)$, that is, $v^\perp$ is obtained by rotating clockwise by 90 degrees.

We also need the parameterized version

$$\widetilde{S}_\infty : H^{-1/2}[0, 2\pi] \times C^2[0, 2\pi] \to L^2(\Omega)$$

of the far field operator as given by

$$\widetilde{S}_\infty(\psi, z)(\hat{x}) := \gamma \int_0^{2\pi} e^{-ik_0 \, \hat{x} \cdot z(\tau)}|z'(\tau)|\psi(\tau) \, d\tau, \quad \hat{x} \in \Omega. \qquad (3.2.11)$$

Then the parameterized form of (3.2.7) is given by

$$\widetilde{S}_{k_d}(\psi_d, z) - \widetilde{S}_{k_0}(\psi_0, z) = 2u^i \circ z,$$

$$\psi_d + \psi_0 + \widetilde{K}'_{k_d}(\psi_d, z) - \widetilde{K}'_{k_0}(\psi_0, z) = \frac{2}{|z'|}[z'(t)]^\perp \cdot \mathrm{grad}u^i \circ z,$$

$$(3.2.12)$$

$$\widetilde{S}_\infty \psi_0 = u_\infty.$$

For a fixed ψ the Fréchet derivative $\widetilde{S}'_\infty$ of the operator $\widetilde{S}_\infty$ with respect to the boundary curve z in the direction h is given by

$$\widetilde{S}'_\infty(\psi, z; h)(\hat{x}) := \gamma \int_0^{2\pi} e^{-ik_0 \, \hat{x} \cdot z(\tau)} \left[-ik_0 \, \hat{x} \cdot h(\tau) + \frac{z'(\tau) \cdot h'(\tau)}{|z'(\tau)|^2} \right] |z'(\tau)|\psi(\tau) \, d\tau$$

$$(3.2.13)$$

for $\hat{x} \in \Omega$. Then the linearization of the third equation in (3.2.12) at z with respect to the direction h reads

$$\widetilde{S}_\infty(\psi_0, z) + \widetilde{S}'_\infty(\psi_0, z; h) = u_\infty \qquad (3.2.14)$$

and is a linear equation for the update h.

Iterative Scheme for the Johansson and Sleeman Method

Now, given an approximation for the boundary curve ∂D with parameterization z, each iteration step of the proposed inverse algorithm consists of two parts.

1. We solve the first two well-posed equations of (3.2.12), i.e., the field equations for the densities ψ_d and ψ_0. This can be done through the numerical method as described in the next chapter.

2. Then we solve the ill-posed linearized equation (3.2.14) for h and obtain an updated approximation for ∂D with the parameterization $z + h$. Since the kernels of the integral operators in (3.2.14) are smooth, for its numerical approximation the composite trapezoidal rule can be employed. Because of the ill-posedness the solution of (3.2.14) requires stabilization, for example, by Tikhonov regularization.

These two steps are now iterated until some stopping criterion is satisfied. The stopping criterion for the iterative scheme is given by the relative error

$$\frac{\parallel u_{\infty;N} - u_\infty \parallel}{\parallel u_\infty \parallel} \le \epsilon, \tag{3.2.15}$$

where $u_{\infty;N}$ is the computed far field pattern after N iteration steps.
The above algorithm has a straightforward extension for the case of more than one incident wave. Assume that $u_1^i, \ldots, u_M^i$ are M incident waves with different incident directions and $u_{\infty,1}, \ldots, u_{\infty,M}$ the corresponding far field patterns for scattering from ∂D. Then the inverse problem to determine the unknown boundary ∂D from these given far field patterns and incident fields is equivalent to solving

$$\tilde{S}_{k_d}(\psi_{d,m}, z) - \tilde{S}_{k_0}(\psi_{0,m}, z) = 2u_m^i \circ z,$$

$$\psi_{d,m} + \psi_{0,m} + \tilde{K}'_{k_d}(\psi_{d,m}, z) - \tilde{K}'_{k_0}(\psi_{0,m}, z) = \frac{2}{|z'|}[z']^\perp \cdot \mathrm{grad} u_m^i \circ z, \tag{3.2.16}$$

$$\tilde{S}_\infty(\psi_{0,m}, z) = u_{\infty,m}.$$

for $m = 1, \ldots, M$. Given an approximation z for the boundary we first solve the first two equations in (3.2.16) for $m = 1, \ldots, M$ to obtain $2M$ densities $\psi_{d,1}, \ldots, \psi_{d,M}$ and $\psi_{0,1}, \ldots, \psi_{0,M}$. Then we solve the linearized equations

$$\widetilde{S}_\infty(\psi_{0,m}, z) + \widetilde{S}'_\infty(\psi_{0,m}, z; h) = u_{\infty,m}, \quad m = 1, \ldots, M, \tag{3.2.17}$$

for the update h by interpreting them as one ill-posed equation with an operator from $H^p[0, 2\pi] \mapsto (L^2[0, 2\pi])^M$ and applying Tikhonov regularization. The stopping

criterion for the iterative scheme is given by the relative error

$$\frac{\| u_{\infty,m;N} - u_{\infty,m} \|}{\| u_{\infty,m} \|} \leq \epsilon, \tag{3.2.18}$$

for $m = 1, \ldots, M$ where $u_{\infty,m;N}$ are the computed far field patterns after N iteration steps.

Corresponding to (3.2.8) the perturbations are of the form

$$h(t) = \{q(t)(\cos t, \sin t) : t \in [0, 2\pi]\}, \tag{3.2.19}$$

with a real function q. In the approximations we assume r and its update q to have the form of a trigonometric polynomial of degree J, in particular,

$$q(t) = \sum_{j=0}^{J} a_j \cos jt + \sum_{j=1}^{J} b_j \sin jt. \tag{3.2.20}$$

Then the update equation (3.2.14) is solved in the least squares sense, penalized via Tikhonov regularization, for the unknown coefficients $a_0, \ldots, a_J$ and $b_1, \ldots, b_J$ of the trigonometric polynomial representing the update q. As experienced in the application of the above approach for related problems, it is advantageous to use an H^p Sobolev penalty term rather than an L^2 penalty in the Tikhonov regularization, i.e, to interpret $\widetilde{S}'_\infty$ as an ill-posed linear operator

$$\widetilde{S}'_\infty : H^p[0, 2\pi] \to L^2[0, 2\pi] \tag{3.2.21}$$

for some small $p \in \mathbb{N}$.

As a theoretical basis for the application of Tikhonov regularization from [20] we cite that, after the restriction to star-like boundaries, the operator $\widetilde{S}'_\infty$ is injective provided k_0^2 is not a Neumann eigenvalue for the negative Laplacian in D.

We note that, in principle, we also could incorporate arc length into the parameterized densities, i.e., parametrize via $\psi = |z'| \varphi \circ z$ instead of $\psi = \varphi \circ z$. In particular, this would avoid the second term in the Fréchet derivative (3.2.13). However, in our numerical experiments we observed that this leads to a poorer accuracy in the numerical reconstructions.

We can relate the above approach to traditional Newton iterations for solving the inverse obstacle scattering problem as described in [15]. Denoting by $F : z \to u_\infty$ the operator that maps the boundary ∂D represented by the parameterization z onto the far field pattern for scattering of the incident wave u^i from the dielectric D, the inverse problem is equivalent to solving the nonlinear operator equation

$$F(z) = u_\infty. \tag{3.2.22}$$

With the above notations, in the case when k_0^2 is not a Dirichlet eigenvalue of the negative Laplacian in D, we can represent

$$F(z) = \widetilde{S}_\infty(\psi_0(z), z) \tag{3.2.23}$$

where $\psi_0(z)$ is the second component of the solution of the first two equations of (3.2.12) depending on z. By the product and chain rule this implies that the Fréchet derivative of F at z in the direction h is given by

$$F'(z; h) = \widetilde{S}'_\infty(\psi_0(z), z; h)) + \widetilde{S}_\infty(\psi'_0(z; h), z) \tag{3.2.24}$$

with the Fréchet derivative $\psi'_0(z; h)$ of ψ_0 at z in the direction h. Hence, we have established an interrelation between our proposed iterative scheme and the traditional Newton iterations for the boundary to far field map as expressed by the following theorem.

Theorem 3.2.7 *The iteration scheme as given through the first two equations, or field equations, of (3.2.12) and the linearization of the data equation (3.2.14) can be interpreted as Newton iterations for (3.2.22) with the derivate of F approximated through the first term in the representation (3.2.24) only.*

3.2.5   The Simultaneous Linearization Method

In this section, we describe the extension of the simultaneous linearization method [19, 22, 21, 23, 36] from the case of impenetrable scatterer to the case of a dielectric.

In the spirit of the simultaneous linearization method, given an approximation $\partial D_{\text{approx}}$ parametrized by z for boundary ∂D and for densities ψ_d and ψ_0, we simultaneously linearize the system (3.2.12) with respect to all three variables. For fixed z, ψ_0 and ψ_d, the linearized system of integral equations obtains the form

$$\widetilde{S}_{k_d}(\psi_d, z) + \widetilde{S}_{k_d}(\eta_d, z) + \widetilde{S}'_{k_d}(\psi_d, z; h) - \widetilde{S}_{k_0}(\psi_0, z) - \widetilde{S}_{k_0}(\eta_0, z)$$

$$-\widetilde{S}'_{k_0}(\psi_0, z; h) = 2u^i \circ z + 2\text{grad}u^i \circ z \cdot h,$$

$$\psi_d + \eta_d + \psi_0 + \eta_0 + \widetilde{K}'_{k_d}(\psi_d, z) + \widetilde{K}'_{k_d}(\eta_d, z) + (\widetilde{K}'_d)'(\psi_d, z; h)$$

$$-\widetilde{K}'_{k_0}(\psi_0, z) - \widetilde{K}'_{k_0}(\eta_0, z) - (\widetilde{K}'_{k_0})'(\psi_0, z; h) = \frac{2}{|z'|}[z']^\perp \cdot \text{grad}u^i \circ z + 2\xi(z) \cdot h,$$

$$\widetilde{S}_\infty(\psi_0, z) + \widetilde{S}_\infty(\eta_0, z) + \widetilde{S}'_\infty(\psi_0, z; h) = u_\infty. \tag{3.2.25}$$

Here the term $\xi(z) \cdot h$ is the form (see [45])

$$\xi(z) \cdot h = -\frac{\partial u^i}{\partial \tau}\frac{\nu \cdot h'}{|z'|} + (\frac{\partial^2 u^i}{\partial \nu \partial \tau} - H\frac{\partial u^i}{\partial \tau})\tau \cdot h + \frac{\partial^2 u^i}{\partial \nu^2}\nu \cdot h \tag{3.2.26}$$

and τ and H stand for the tangential vector and the mean curvature respectively. They are given by

$$\tau = \frac{z'}{|z'|}, \qquad \text{and} \qquad H = -\frac{z'' \cdot \nu}{|z'|^2} \tag{3.2.27}$$

In the system (3.2.25) the operators $\widetilde{S}_k'(\psi, z; h)$ and $(\widetilde{K}_k')'(\psi, z; h)$ stand for the Fréchet derivative of the parametrized single-layer operators (3.2.9) and the parametrized normal derivative of single-layer operator (3.2.10) with respect to the boundary z in the direction h. The Fréchet derivative of the operators $\widetilde{S}_k$ and $\widetilde{K}_k'$ with respect to the boundary z in the direction h are given by (see [42])

$$\widetilde{S}_k'(\psi, z; h)(t) = -\frac{ik}{2} \int_0^{2\pi} \frac{(z(t) - z(\tau)) \cdot (h(t) - h(\tau))}{|z(t) - z(\tau)|} |z'(\tau)| \, H_1^{(1)}(k|z(t) - z(\tau)|) \psi(\tau) d\tau$$

$$+ \frac{i}{2} \int_0^{2\pi} \frac{z'(\tau) \cdot h'(\tau)}{|z'(\tau)|} H_0^{(1)}(k|z(t) - z(\tau)|) \psi(\tau) d\tau, \tag{3.2.28}$$

and

$$(\widetilde{K}_k')'(\psi, z; h)(t) =$$

$$-\frac{ik}{2|z'(t)|} \int_0^{2\pi} \frac{[z'(t)]^\perp \cdot (h(t) - h(\tau)) + [h'(t)]^\perp \cdot (z(t) - z(\tau))}{|z(t) - z(\tau)|} |z'(\tau)| H_1^{(1)}(k|z(t) - z(\tau)|) \psi(\tau) d\tau$$

$$+\frac{ik}{|z'(t)|} \int_0^{2\pi} \frac{[z'(t)]^\perp \cdot (z(t) - z(\tau))(h(t) - h(\tau)) \cdot (z(t) - z(\tau))}{|z(t) - z(\tau)|^3} |z'(\tau)| H_1^{(1)}(k|z(t) - z(\tau)|) \psi(\tau) d\tau$$

$$-\frac{ik^2}{2|z'(t)|} \int_0^{2\pi} \frac{[z'(t)]^\perp \cdot (z(t) - z(\tau))(h(t) - h(\tau)) \cdot (z(t) - z(\tau))}{|z(t) - z(\tau)|^2} |z'(\tau)| H_0^{(1)}(k|z(t) - z(\tau)|) \psi(\tau) d\tau$$

$$+\frac{ik}{2} \frac{h'(t) \cdot z'(t)}{|z'(t)|^2} \int_0^{2\pi} \frac{[z'(t)]^\perp \cdot (z(t) - z(\tau))}{|z(t) - z(\tau)|} |z'(\tau)| H_1^{(1)}(k|z(t) - z(\tau)|) \psi(\tau) d\tau$$

$$-\frac{ik}{2|z'(t)|} \int_0^{2\pi} \frac{[z'(t)]^\perp \cdot (z(t) - z(\tau)) h'(\tau) \cdot z'(\tau)}{|z(t) - z(\tau)||z'(\tau)|} H_1^{(1)}(k|z(t) - z(\tau)|) \psi(\tau) d\tau, \tag{3.2.29}$$

respectively for $t \in [0, 2\pi]$. Here we made use of $H_1^{(1)'}(z) = H_0^{(1)} - \frac{1}{z} H_1^{(1)}$.

For fixed boundary z densities ψ_d and ψ_0 we obtain the linear system with unknowns h, η_d, and η_0. If we rearrange (3.2.25) with respect to the unknown variables

we arrive at

$$\widetilde{S}'_{k_d}(\psi_d,z;h) - \widetilde{S}'_{k_0}(\psi_0,z;h) - 2\mathrm{grad}u^i \circ z \cdot h + \widetilde{S}_{k_d}(\eta_d,z) - \widetilde{S}_{k_0}(\eta_0,z)$$

$$= 2u^i \circ z - \widetilde{S}_{k_d}(\psi_d, z) + \widetilde{S}_{k_0}(\psi_0, z)$$

$$(\widetilde{K}'_{k_d})'(\psi_d, z;h) - (\widetilde{K}'_{k_0})'(\psi_0,z;h) - 2\xi(z)\cdot h + \eta_d + \widetilde{K}'_{k_d}(\eta_d,z) + \eta_0 - \widetilde{K}'_{k_0}(\eta_0,z)$$

$$= \frac{2}{|z'|}[z']^{\perp}\cdot \mathrm{grad}u^i \circ z - \psi_d - \widetilde{K}'_{k_d}(\psi_d,z) - \psi_0 + \widetilde{K}'_{k_0}(\psi_0,z)$$

$$\widetilde{S}'_{\infty}(\psi_0, z; h) + \widetilde{S}_{\infty}(\eta_0, z) = u_{\infty} - \widetilde{S}_{\infty}(\psi_0, z)$$

$$(3.2.30)$$

and the matrix form of (3.2.30) can be written as

$$\begin{bmatrix} \widetilde{S}'_{k_d}(\psi_d, z; \cdot) - \widetilde{S}'_{k_0}(\psi_0, z; \cdot) - 2\mathrm{grad}u^i \circ z & \widetilde{S}_{k_d}(\cdot, z) & -\widetilde{S}_{k_0}(\cdot, z) \\ (\widetilde{K}'_{k_d})'(\psi_d, z; \cdot) - (\widetilde{K}'_{k_0})'(\psi_0, z; \cdot) - 2\xi(z) & I + \widetilde{K}'_{k_d}(\cdot, z) & I - \widetilde{K}'_{k_0}(\cdot, z) \\ \widetilde{S}'_{\infty}(\psi_0, z; \cdot) & 0 & \widetilde{S}_{\infty}(\cdot, z) \end{bmatrix} \begin{bmatrix} h \\ \eta_d \\ \eta_0 \end{bmatrix}$$

$$= \begin{bmatrix} 2u^i \circ z - \widetilde{S}_{k_d}(\psi_d, z) + \widetilde{S}_{k_0}(\psi_0, z) \\ \dfrac{2}{|z'|}[z']^{\perp}\cdot \mathrm{grad}u^i \circ z - \psi_d - \widetilde{K}'_{k_d}(\psi_d, z) - \psi_0 + \widetilde{K}'_{k_0}(\psi_0, z) \\ u_{\infty} - \widetilde{S}_{\infty}(\psi_0, z) \end{bmatrix}$$

$$(3.2.31)$$

Now we can describe the method in a short form as follows.

Iterative Scheme for the Simultaneous Linearization Method

Each iteration step of the proposed inverse algorithm consists of one part.

- Given an approximation z for the boundary and densities ψ_d, ψ_0, we solve the linearized (3.2.30), or (3.2.31), for h, η_d, and η_0 to obtain updates $z + h$, $\psi_d + \eta_d$, and $\psi_0 + \eta_0$.

Here we note that only in the first iteration step, it is convenient to start from an approximation z for the boundary and solve the first two equations in (3.2.12) for the densities.

We continue this procedure until some suitable criteria is satisfied. The stopping criterion for the iterative scheme is given by the relative error (3.2.15). Because of the ill-posedness the solution of (3.2.30) requires stabilization, for instance, by Tikhonov regularization. We choose for the boundary H^p penalty term and the regularization parameter $\lambda = (0.8)^j$ decreasing with the iteration step j, and for the densities L^2 penalty term and the regularization parameter $\alpha = 10^{-6}$.

Analogous to the Johannson and Sleeman method, the simultaneously linearization method has an extension for the case of more than one incident wave. Assume that $u_1^i, \ldots, u_M^i$ are M incident waves with different incident directions and $u_{\infty,1}, \ldots, u_{\infty,M}$ the corresponding far field patterns for scattering from ∂D. Then the inverse problem to determine the unknown boundary ∂D from these given far field patterns and incident fields is equivalent to solve (3.2.16) for $m = 1, \ldots, M$. Given an initial guess for the boundary ∂D parametrized by z and for densities $\psi_{d,1}, \ldots, \psi_{d,M}$ and $\psi_{0,1}, \ldots, \psi_{0,M}$, we simultaneously linearize the system (3.2.16) with respect to all $2M+1$ variables. For fixed z, $\psi_{0,m}$ and $\psi_{d,m}$, $m = 1, \ldots, M$ the linearized system of integral equations obtains the form

$$\widetilde{S}'_{k_d}(\psi_{d,m},z;h) - \widetilde{S}'_{k_{0,m}}(\psi_{0,m},z;h) - 2grad\,u_m^i \circ z \cdot h + \widetilde{S}_{k_d}(\eta_{d,m},z) - \widetilde{S}_{k_0}(\eta_{0,m},z)$$

$$= 2u_m^i \circ z - \widetilde{S}_{k_d}(\psi_{d,m},z) + \widetilde{S}_{k_0}(\psi_{0,m},z),$$

$$(\widetilde{K}'_{k_d})'(\psi_{d,m},z;h) - (\widetilde{K}'_{k_0})'(\psi_{0,m},z;h) - 2\xi_m(z) \cdot h + \eta_{d,m} + \widetilde{K}'_{k_d}(\eta_{d,m},z) + \eta_{0,m} - \widetilde{K}'_{k_0}(\eta_{0,m},z)$$

$$= \frac{2}{|z'|}[z']^{\perp} \cdot grad\,u_m^i \circ z - \psi_{d,m} - \widetilde{K}'_{k_d}(\psi_{d,m},z) - \psi_{0,m} + \widetilde{K}'_{k_0}(\psi_{0,m},z),$$

$$\widetilde{S}'_{\infty}(\psi_{0,m},z;h) + \widetilde{S}_{\infty}(\eta_{0,m},z) = u_{\infty,m} - \widetilde{S}_{\infty}(\psi_{0,m},z).$$

$$(3.2.32)$$

Each iteration step of the proposed inverse algorithm also consists of one part.

- Given an approximation z for the boundary and densities $\psi_{d,m}$, $\psi_{0,m}$ we solve the linearized (3.2.32) for h, $\eta_{d,m}$, and $\eta_{0,m}$ to obtain updates $z+h$, $\psi_{d,m}+\eta_{d,m}$, and $\psi_{0,m} + \eta_{0,m}$ for $m = 1, \ldots, M$.

Here we again note that only in the first iteration step, it is convenient to start from an initial guess z for the boundary and solve the first $2M$ equations in (3.2.16) for the densities.

We continue this procedure until some suitable criteria is achieved. The stopping criterion for the iterative scheme is given by the relative error (3.2.18). For the ill-posedness, we choose the same penalty terms and regularization parameters for the case of one incident field.

The simultaneously linearized equations (3.2.25) again exhibit relations to the traditional Newton iteration

$$F'(z;h) = u_\infty - F(z) \tag{3.2.33}$$

obtained by linearization of (3.2.22). The interrelation between simultaneous linearization method and the traditional Newton method was established in the paper published by Ivanyshyn, Kress, and Serranho [18] for impenetrable scatterer. In the following theorem we state an interrelation between these two iterative method for penetrable scatterer.

Theorem 3.2.8 *Assume that k_0^2 is not a Dirichlet eigenvalue of the negative Laplacian in D. Set*

$$\begin{bmatrix} \psi_d \\ \psi_0 \end{bmatrix} := 2 \begin{bmatrix} \widetilde{S}_{k_d}(\cdot,z) & -\widetilde{S}_{k_0}(\cdot,z) \\ I + \widetilde{K}'_{k_d}(\cdot,z) & I - \widetilde{K}'_{k_0}(\cdot,z) \end{bmatrix}^{-1} \begin{bmatrix} u^i \circ z \\ \frac{\partial u^i}{\partial \nu} \circ z \end{bmatrix}$$

Provided h satisfies the linearized boundary to far field equation (3.2.33) then h and the perturbed densities

$$\begin{bmatrix} \eta_d \\ \eta_0 \end{bmatrix} := \begin{bmatrix} \widetilde{S}_{k_d}(\cdot,z) & -\widetilde{S}_{k_0}(\cdot,z) \\ I + \widetilde{K}'_{k_d}(\cdot,z) & I - \widetilde{K}'_{k_0}(\cdot,z) \end{bmatrix}^{-1} \begin{bmatrix} -\widetilde{S}'_{k_d}(\psi_d,z;h) + \widetilde{S}'_{k_0}(\psi_0,z;h) + 2\mathrm{grad}u^i \circ z \cdot h \\ -(\widetilde{K}'_{k_d})'(\psi_d,z;h) + (\widetilde{K}'_{k_0})'(\psi_0,z;h) + 2\xi(z) \cdot h \end{bmatrix}$$

satisfy the linearized field and data equations (3.2.30). Conversely, if h, η_d, and η_0 solve (3.2.30) then h satisfies (3.2.33).

   Proof: Define

$$A(\cdot,z) := \begin{bmatrix} \widetilde{S}_{k_d}(\cdot,z) & -\widetilde{S}_{k_0}(\cdot,z) \\ I + \widetilde{K}'_{k_d}(\cdot,z) & I - \widetilde{K}'_{k_0}(\cdot,z) \end{bmatrix} \quad \text{and} \quad R(z) := 2 \begin{bmatrix} u^i \circ z \\ \frac{\partial u^i}{\partial \nu} \circ z \end{bmatrix}.$$

We also define an operator

$$P_0 : \begin{bmatrix} \psi_d \\ \psi_0 \end{bmatrix} \rightarrow \psi_0$$

and it is mapping from $L^2[0,2\pi] \times L^2[0,2\pi]$ to $L^2[0,2\pi]$. Now, from definition of ψ_0 we can write

$$\psi_0 = P_0(A^{-1}(\cdot,z)R(z)). \tag{3.2.34}$$

From the assumption of the theorem, we have that

$$F'(z;h) = u_\infty - \widetilde{S}_\infty(\psi_0, z). \tag{3.2.35}$$

Since k_0^2 is not Dirichlet eigenvalue of the negative Laplacian in D, we can represent

$$F(z) = \widetilde{S}_\infty(P_0(A^{-1}(\cdot, z)R(z)), z) \tag{3.2.36}$$

By the product and chain rule this implies Fréchet derivative

$$F'(z;h) = \widetilde{S}'_\infty(P_0(A^{-1}(\cdot, z)R(z)), z; h)$$

$$\tag{3.2.37}$$

$$+ \widetilde{S}_\infty(P'_0(A^{-1}(\cdot, z)R(z))(-A^{-1}(\cdot, z)A'(A^{-1}(\cdot, z); h)R(z) + A^{-1}(\cdot, z)R'(z; h), z)$$

If we use the definition of ψ_0 and η_0 in (3.2.37) we arrive at

$$F'(z;h) = \widetilde{S}'_\infty(\psi_0, z; h) + \widetilde{S}_\infty(\eta_0, z). \tag{3.2.38}$$

Finally, from (3.2.35) and (3.2.38) we obtain the last equation of (3.2.30)

$$\widetilde{S}'_\infty(\psi_0, z; h) + \widetilde{S}_\infty(\eta_0, z) = u_\infty - \widetilde{S}_\infty(\psi_0, z). \tag{3.2.39}$$

The definition of η_d and η_0 imply that

$$\widetilde{S}'_{k_d}(\psi_d, z; h) - \widetilde{S}'_{k_0}(\psi_0, z; h) - 2grad u^i \circ z \cdot h + \widetilde{S}_{k_d}(\eta_d, z) - \widetilde{S}_{k_0}(\eta_0, z) = 0$$

$$\tag{3.2.40}$$

$$(\widetilde{K}'_{k_d})'(\psi_d, z; h) - (\widetilde{K}'_{k_0})'(\psi_0, z; h) - 2\xi(z) \cdot h + \eta_d + \widetilde{K}'_{k_d}(\eta_d, z) + \eta_0 - \widetilde{K}'_{k_0}(\eta_0, z) = 0.$$

The definition of ψ_d and ψ_0 also imply that

$$\widetilde{S}_{k_d}(\psi_d, z) - \widetilde{S}_{k_0}(\psi_0, z) - 2u^i \circ z = 0$$

$$\tag{3.2.41}$$

$$\psi_d + \psi_0 + \widetilde{K}'_{k_d}(\psi_d, z) - \widetilde{K}'_{k_0}(\psi_0, z) - 2\frac{\partial u^i}{\partial \nu} \circ z = 0.$$

Therefore in view of (3.2.40) and (3.2.41), the first two equations of (3.2.30) are also satisfied. Conversely, the proof can be obtained by following converse of the above proof.   □

3.2.6   The Hybrid Method

Iterative Scheme

In this section, we describe the extension of the hybrid method [32, 37, 38, 45] from the case of impenetrable scatterer to the case of a dielectric.

1. Given a current approximation to the boundary ∂D, parametrized by z. Find the density ψ_0 from the regularized data equation via Tikhonov regularization

$$(\alpha I + \widetilde{S}^*_\infty \widetilde{S}_\infty)\psi_0 \;=\; \widetilde{S}^*_\infty u_\infty, \tag{3.2.42}$$

where $\widetilde{S}^*_\infty$ is the adjoint operator of $\widetilde{S}_\infty$.

2. Keep ψ_0 fixed and find the density ψ_d from

$$(I + \widetilde{K}'_{k_d})(\psi_d, z) = \frac{2}{|z'|}[z'(t)]^\perp \cdot \mathrm{grad} u^i \circ z - \psi_0 + \widetilde{K}'_{k_0}(\psi_0, z), \tag{3.2.43}$$

3. Keep the densities ψ_d and ψ_0 fixed and find the perturbed boundary h form the linearized equation

$$\widetilde{S}'_{k_d}(\psi_d, z; h) - \widetilde{S}'_{k_0}(\psi_0, z; h) - 2\mathrm{grad} u^i \circ z \cdot h = 2u^i \circ z - \widetilde{S}_{k_d}(\psi_d, z) + \widetilde{S}_{k_0}(\psi_0, z). \tag{3.2.44}$$

4. Update the boundary $z := z + h$ then go to first step. We continue this procedure until some stopping criteria is achieved. The stopping criterion for the iterative scheme is given by the relative error (3.2.15). In the equation (3.2.42) the regularization parameter λ is chosen small such as 10^{-6} and L^2 penalty term is implemented. Since the solution of the equation (3.2.44) is ill-posed, it also requires stabilization, for example, by Tikhonov regularization. We choose H^p penalty term and regularization parameter $(0.9)^j$ decreasing with each iteration step j.(See also [37]).

Analogous to the other methods, the Hybrid method has also an extension for the case of more than one incident wave. Assume that $u^i_1, \ldots, u^i_M$ are M incident waves with different incident directions and $u_{\infty,1}, \ldots, u_{\infty,M}$ the corresponding far field patterns for scattering from ∂D. Then the inverse problem to determine the unknown boundary ∂D from these given far field patterns and incident fields is equivalent to solve

1. Given a current approximation to the boundary ∂D, parametrized by z. Find the densities $\psi_{0,1}, \ldots, \psi_{0,M}$ from the regularized data equations via Tikhonov

$$(\alpha I + \widetilde{S}^*_\infty \widetilde{S}_\infty)\psi_{0,m} \;=\; \widetilde{S}^*_\infty u_{\infty,m}, \quad \text{for} \quad m = 1, \ldots, M. \tag{3.2.45}$$

2. Keep the $\psi_{0,1}, \ldots, \psi_{0,M}$ fixed and find densities $\psi_{d,1}, \ldots, \psi_{d,M}$ from

$$(I + \widetilde{K}'_{k_d})(\psi_{d,m}, z) = \frac{2}{|z'|}[z'(t)]^\perp \cdot \mathrm{grad} u^i_m \circ z - \psi_{0,m} + \widetilde{K}'_{k_0}(\psi_{0,m}, z), \tag{3.2.46}$$

for $m = 1, \ldots, M$.

3. Keep the densities $\psi_{0,1}, \ldots, \psi_{0,M}$ and $\psi_{d,1}, \ldots, \psi_{d,M}$ fixed and find the perturbed boundary h form the linearized equation

$$\widetilde{S}'_{k_d}(\psi_{d,m},z;h) - \widetilde{S}'_{k_0}(\psi_{0,m},z;h) - 2\mathrm{grad}u^i_m \circ z \cdot h = 2u^i_m \circ z - \widetilde{S}_{k_d}(\psi_{d,m}, z) + \widetilde{S}_{k_0}(\psi_{0,m}, z),$$
$$(3.2.47)$$

for $m = 1, \ldots, M$.

4. Update the boundary $z := z + h$ then go to first step. We continue this procedure until some stopping criteria is achieved. The stopping criterion for the iterative scheme is given by the relative error (3.2.18). In the equations (3.2.45) and (3.2.47) we choose as the same regularization parameter and penalty term as in the equations (3.2.42) and (3.2.44) respectively.

3.2.7 Reconstruction the Interior Wave Number via the Hybrid Method

The inverse problem we are interested is that given an incident plane wave u^i, far field pattern u_∞ and the shape of the scatterer, to determine the interior wave number of the field that occurs inside the obstacle. We now proceed describing an iterative algorithm for approximately solving this inverse problem for the interior wave number via the hybrid Method. Now we consider an operator $\widetilde{S}_{k_d} : L^2[0, 2\pi] \times \mathbb{C} \to L^2[0, 2\pi]$.

Iterative Scheme

1. After the boundary ∂D is parametrized by z, find the density ψ_0 from the stabilized data equation,i.e., from

$$(\alpha I + \widetilde{S}^*_\infty \widetilde{S}_\infty)\psi_0 = \widetilde{S}^*_\infty u_\infty \qquad (3.2.48)$$

2. Given a current approximation for the interior wave number k_d. Then find ψ_d from

$$(I + \widetilde{K}'_{k_d})(\psi_d, k_d) = \frac{2}{|z'|}[z'(t)]^\perp \cdot \mathrm{grad}u^i \circ z - \psi_0 + \widetilde{K}'_{k_0}(\psi_0, z), \qquad (3.2.49)$$

3. Linearize the first field equation with respect to interior wave number k_d then keep the density ψ_d fixed and find perturbed interior wave number σ from the linearized equation

$$\widetilde{S}'_{k_d}(\psi_d,k_d;\sigma) = 2u^i \circ z - \widetilde{S}_{k_d}(\psi_d, z) + \widetilde{S}_{k_0}(\psi_0, z). \qquad (3.2.50)$$

The Fréchet derivative of the operator $\widetilde{S}_{k_d}$ with respect to the interior wave number k_d in the direction σ is given by

$$\widetilde{S}'_{k_d}(\psi_d, k_d; \sigma) = -\frac{i\sigma}{2} \int_0^{2\pi} H_1^{(1)}(k_d|z(t) - z(\tau)|)|z(t) - z(\tau)||z'(\tau)|\psi_d(\tau)d\tau,$$

(3.2.51)

for $t \in [0, 2\pi]$.

4. Update the interior wave number as $k_d := k_d + \sigma$ and then go to second step and repeat this procedure until some stopping criteria is achieved. The stopping criterion for the iterative scheme is given by the relative error

$$\frac{|k_{d;N} - k_d|}{|k_d|} \leq \epsilon,$$

(3.2.52)

where $k_{d;N}$ is the computed interior wave number after N iteration steps.

3.2.8   Simultaneous Reconstructions the Boundary and the Interior Wave Number via the Hybrid Method

The inverse problem we are interested is that given an incident plane waves u_m^i and far field patterns $u_{\infty,m}$ for $m = 1, \ldots, M$, to simultaneously determine the boundary ∂D and the interior wave number of the field that occurs inside the obstacle.

Iterative Scheme

1. Given a current approximation to the boundary ∂D, parametrized by z. Find the density $\psi_{0,m}$ from the regularized data equation via Tikhonov regularization

$$(\alpha I + \widetilde{S}_\infty^* \widetilde{S}_\infty)\psi_{0,m} = \widetilde{S}_\infty^* u_{\infty,m},$$

(3.2.53)

2. Given a current approximation to the interior wave number k_d. Then keep the $\psi_{0,m}$ fixed and find density $\psi_{d,m}$ from

$$(I + \widetilde{K}'_{k_d})(\psi_{d,m}, z, k_d) = \frac{2}{|z'|}[z'(t)]^\perp \cdot \mathrm{grad} u_m^i \circ z - \psi_{0,m} + \widetilde{K}'_{k_0}(\psi_{0,m}, z), \quad (3.2.54)$$

3. For fixed densities $\psi_{d,m}$ and $\psi_{0,m}$, simultaneously linearize the first field equation with respect to boundary z in the direction h and interior wave number k_d in the direction σ. Then find perturbed boundary h and perturbed interior wave number σ from the linearized equation of the form

$$\widetilde{S}'_{k_d}(\psi_{d,m}, z, k_d; h) - \widetilde{S}'_{k_0}(\psi_{0,m}, z; h) - 2\mathrm{grad} u_m^i \circ z \cdot h + \widetilde{S}'_{k_d}(\psi_{d,m}, z, k_d; \sigma)$$
$$= 2u_m^i \circ z - \widetilde{S}_{k_d}(\psi_{d,m}, z, k_d) + \widetilde{S}_{k_0}(\psi_{0,m}, z).$$

(3.2.55)

4. Update the boundary $z := z + h$ and the interior wave number $k_d = k_d + \sigma$ then go to first step and repeat this procedure until some stopping criteria is satisfied. The stopping criterion for the iterative scheme is given by the relative errors ϵ_1, ϵ_2

$$\frac{\| u_{\infty,m;N} - u_{\infty,m} \|}{\| u_{\infty,m} \|} \leq \epsilon_1, \quad \text{and} \quad \frac{|k_{d;N} - k_d|}{|k_d|} \leq \epsilon_2, \tag{3.2.56}$$

for $m = 1, \ldots, M$ where $u_{\infty,m;N}$ are the computed far field patterns and $k_{d;N}$ is the computed interior wave number after N iteration steps.

Chapter 4

Numerical Solution and Examples

4.1 Numerical Solution of the Direct Problem

For the numerical solution of (3.1.23) and presentation of our inverse algorithm we assume that the boundary curve ∂D is represented through regular parametrization of the form

$$\partial D := \{z(t) : 0 \le t \le 2\pi\}, \tag{4.1.1}$$

where $z : \mathbb{R} \to \mathbb{R}^2$ is a 2π-periodic and twice continuously differentiable function such that the orientation of ∂D is counter-clockwise. Then the parametrized form of (3.1.23) is given by

$$\widetilde{S}_{k_d}\psi_d - \widetilde{S}_{k_0}\psi_0 = 2u^i o z,$$

$$\psi_d + \psi_0 + \widetilde{K}'_{k_d}\psi_d - \widetilde{K}'_{k_0}\psi_0 = \frac{2}{|z'|}[z']^{\perp} \cdot \mathrm{grad}\, u^i o z, \tag{4.1.2}$$

The kernels,

$$M(t,\tau;k) := \tfrac{i}{2}|z'(\tau)|\, H_0^{(1)}(k|z(t) - z(\tau)|),$$

$$L(t,\tau;k) := \frac{ik}{2}\frac{[z'(t)]^{\perp}.[z(\tau) - z(t)]}{|z'(t)||z(t) - z(\tau)|}|z'(\tau)|\, H_1^{(1)}(k|z(t) - z(\tau)|) \tag{4.1.3}$$

of the operators $\widetilde{S}_k$ and $\widetilde{K}'_k$ can be written in the form

$$M(t,\tau;k) = M_1(t,\tau;k)\ln(4\sin^2\frac{t-\tau}{2}) + M_2(t,\tau;k)$$

$$L(t,\tau;k) \;=\; L_1(t,\tau;k)\ln(4\sin^2\frac{t-\tau}{2}) + L_2(t,\tau;k), \tag{4.1.4}$$

where

$$M_1(t, \tau; k) := -\frac{1}{2\pi}|z'(\tau)|J_0(k|z(t) - z(\tau)|),$$

$$M_2(t, \tau; k) := M(t, \tau; k) - M_1(t, \tau; k)\ln(4\sin^2\frac{t-\tau}{2}),$$

$$L_1(t, \tau; k) := -\frac{k}{2\pi}\frac{[z'(t)]^\perp \cdot [z(\tau) - z(t)]}{|z'(t)||z(t) - z(\tau)|}|z'(\tau)|J_1(k|z(t) - z(\tau)|),$$

$$L_2(t, \tau; k) := L(t, \tau; k) - L_1(t, \tau; k)\ln(4\sin^2\frac{t-\tau}{2}).$$

The functions M_1, M_2, L_1 and L_2 turn out to be smooth with diagonal terms. Their diagonal terms are obtained as

$$M_1(t, t; k) = -\frac{1}{2\pi}|z'(t)| \qquad \& \qquad M_2(t, t; k) = \{\frac{i}{2} - \frac{1}{\pi}\ln(\frac{k}{2}|z'(t)|) - \frac{C_E}{\pi}\}|z'(t)|$$

$$L_1(t, t; k) = 0 \qquad \& \qquad L_2(t, t; k) = -\frac{1}{2\pi}\frac{[z'(t)]^\perp \cdot z''(t)}{|z'(t)|^2}$$

in terms of Euler's constant C_E. The system of integral equations (4.1.2) can be written as the form

$$\int_0^{2\pi} M(t, \tau; k_d)\psi_d(\tau)d\tau - \int_0^{2\pi} M(t, \tau; k_0)\psi_0(\tau)d\tau = 2u^i \circ z(t),$$

$$\psi_d(t) + \psi_0(t) + \int_0^{2\pi} L(t, \tau; k_d)\psi_d(\tau)d\tau - \int_0^{2\pi} L(t, \tau; k_0)\psi_0(\tau)d\tau$$

$$= \frac{2}{|z'(t)|}[z'(t)]^\perp \cdot \mathrm{grad}u^i \circ z(t). \tag{4.1.5}$$

If we insert equations (4.1.4) into (4.1.5) then we obtain

$$\int_0^{2\pi} [M_1(t, \tau; k_d)\ln(4\sin^2\frac{t-\tau}{2}) + M_2(t, \tau; k_d)]\psi_d(\tau)d\tau$$

$$- \int_0^{2\pi} [M_1(t, \tau; k_0)\ln(4\sin^2\frac{t-\tau}{2}) + M_2(t, \tau; k_0)]\psi_0(\tau)d\tau = 2u^i \circ z(t),$$

$$\psi_d(t) + \psi_0(t) + \int_0^{2\pi} [L_1(t, \tau; k_d)\ln(4\sin^2\frac{t-\tau}{2}) + L_2(t, \tau; k_d)]\psi_d(\tau)d\tau$$

$$- \int_0^{2\pi} [L_1(t, \tau; k_0)\ln(4\sin^2\frac{t-\tau}{2}) + L_2(t, \tau; k_0)]\psi_0(\tau)d\tau$$

$$= \frac{2}{|z'(t)|}[z'(t)]^\perp \cdot \mathrm{grad}u^i \circ z(t). \tag{4.1.6}$$

We solve the systems of integral equations approximately via collocation method combined with numerical quadrature as described in Section 3.5 of [7] or in [39] based on approximation by trigonometric polynomials. In our case of 2π-periodic integrals, we choose an equidistant set of knots $t_j := \dfrac{j\pi}{n}$, $j = 0, 1, 2, ...2n - 1$ and use the quadrature rule;

$$\int_0^{2\pi} \ln(4\sin^2\frac{t-\tau}{2})f(\tau)d\tau \approx \sum_{j=0}^{2n-1} R_j^{(n)}(t)f(t_j), \quad 0 \le t \le 2\pi \tag{4.1.7}$$

with quadrature weights given by

$$R_j^{(n)}(t) := -\frac{2\pi}{n}\sum_{m=1}^{n-1}\frac{1}{m}\cos m(t-t_j) - \frac{\pi}{n^2}\cos n(t-t_j), \quad j = 0, 1, 2, ..., 2n-1, \tag{4.1.8}$$

and the trapezoidal rule

$$\int_0^{2\pi} f(\tau)d\tau \approx \frac{\pi}{n}\sum_{j=0}^{2n-1} f(t_j). \tag{4.1.9}$$

The integral equations (4.1.6) are replaced by the approximating equations

$$\sum_{j=0}^{2n-1} R_j^{(n)}(t)M_1(t,t_j;k_d)\psi_d^{(n)}(t_j) + \frac{\pi}{n}\sum_{j=0}^{2n-1} M_2(t,t_j;k_d)\psi_d^{(n)}(t_j)$$

$$- \sum_{j=0}^{2n-1} R_j^{(n)}(t)M_1(t,t_j;k_0)\psi_0^{(n)}(t_j) - \frac{\pi}{n}\sum_{j=0}^{2n-1} M_2(t,t_j;k_0)\psi_0^{(n)}(t_j) = 2u^i \circ z(t),$$

$$\psi_d^{(n)}(t) + \psi_0^{(n)}(t) + \sum_{j=0}^{2n-1} R_j^{(n)}(t)L_1(t,t_j;k_d)\psi_d^{(n)}(t_j) + \frac{\pi}{n}\sum_{j=0}^{2n-1} L_2(t,t_j;k_d)\psi_d^{(n)}(t_j)$$

$$- \sum_{j=0}^{2n-1} R_j^{(n)}(t)L_1(t,t_j;k_0)\psi_0^{(n)}(t_j) - \frac{\pi}{n}\sum_{j=0}^{2n-1} L_2(t,t_j;k_0)\psi_0^{(n)}(t_j)$$

$$= \frac{2}{|z'(t)|}[z'(t)]^\perp \cdot \text{grad}u^i \circ z(t). \tag{4.1.10}$$

The solution of (4.1.10) can be reduced to solve a finite dimensional linear system. For any solutions of (4.1.10) the values $\psi_{i,d}^{(n)} = \psi_d^{(n)}(t_j)$ and $\psi_{i,0}^{(n)} = \psi_0^{(n)}(t_j)$, $i =$

$0, 1, 2, ..., 2n - 1$, at the quadrature points trivially satisfy the linear system,

$$\sum_{j=0}^{2n-1} R^{(n)}|t_i - t_j|)M_1(t_i, t_j; k_d)\psi_d^{(n)}(t_j) + \frac{\pi}{n}\sum_{j=0}^{2n-1} M_2(t_i, t_j; k_d)\psi_d^{(n)}(t_j)$$

$$- \sum_{j=0}^{2n-1} R^{(n)}|t_i - t_j|)M_1(t_i, t_j; k_0)\psi_0^{(n)}(t_j) - \frac{\pi}{n}\sum_{j=0}^{2n-1} M_2(t_i, t_j; k_0)\psi_0^{(n)}(t_j) = 2u^i \circ z(t_i),$$

$$\psi_d^{(n)}(t_i) + \psi_0^{(n)}(t_i) + \sum_{j=0}^{2n-1} R^{(n)}|t_i - t_j|)L_1(t_i, t_j; k_d)\psi_d^{(n)}(t_j) + \frac{\pi}{n}\sum_{j=0}^{2n-1} L_2(t_i, t_j; k_d)\psi_d^{(n)}(t_j)$$

$$- \sum_{j=0}^{2n-1} R^{(n)}|t_i - t_j|)L_1(t_i, t_j; k_0)\psi_0^{(n)}(t_j) - \frac{\pi}{n}\sum_{j=0}^{2n-1} L_2(t_i, t_j; k_0)\psi_0^{(n)}(t_j)$$

$$= \frac{2}{|z'(t_i)|}[z'(t_i)]^{\perp} \cdot \mathrm{grad}\, u^i \circ z(t_i). \tag{4.1.11}$$

for $i = 0, 1, 2, ..., 2n - 1$. It is clear how to modify this system for M incident fields with distinct directions.

Since the integral equation (4.1.2) is uniquely solvable and the kernels M_1, M_2, L_1 and L_2 and right hand sides u^i and $\dfrac{\partial u^i}{\partial \nu}$ are continuous, a rather involved error analysis (for detail we refer to [7]) show that

1. the approximating linear system (4.1.11) is uniquely solvable for all sufficiently large n;

2. as $n \to \infty$ the approximate solutions $\psi_0^{(n)}$ and $\psi_d^{(n)}$ converge uniformly to the solution ψ_0 and ψ_d of the integral equation (4.1.2), respectively;

3. the convergence order of the quadrature error for (4.1.7) and (4.1.9) carries over to the error $\psi_0^{(n)} - \psi_0$ and $\psi_d^{(n)} - \psi_d$.

The latter, in particular, means that since we have analytic kernels M_1, M_2, L_1 and L_2 and analytic right hand sides u^i and $\dfrac{\partial u^i}{\partial \nu}$ the approximation error decreases exponentially, i.e., there exist positive constants C_1, C_2, σ_1 and σ_2 such that

$$|\psi_0^{(n)} - \psi_0| \le C_1 e^{-n\sigma_1} \quad \text{and} \quad |\psi_d^{(n)} - \psi_d| \le C_2 e^{-n\sigma_2}, \quad 0 \le t \le 2\pi, \tag{4.1.12}$$

for all n.

The parametrized form of (3.1.32), i.e., the parametrized far field pattern is given by

$$u_\infty = \gamma \int_0^{2\pi} e^{-ik_0 \hat{x} \cdot z(\tau)}|z'(\tau)|\psi_0(\tau)\, d\tau, \quad \hat{x} \in \Omega. \tag{4.1.13}$$

The expression can be evaluated by the composite trapezoidal rule and after solving the linear system of integral equations (4.1.11) for $\psi_0^{(n)}$, the far field patterns can be obtained as

$$u_\infty = \frac{\gamma\pi}{n} \sum_{j=0}^{2n-1} e^{-ik_0\hat{x}(t_i)\cdot z(t_j)}|z'(t_j)|\psi_0^{(n)} \tag{4.1.14}$$

for $i = 0, 1, \ldots, 2n - 1$.

For a numerical example, we consider the scattering of a plane wave by a dielectric cylinder with a non-convex kite-shaped cross section with boundary ∂D described by the parametric representation

$$z(t) = (\cos t + 0.65\cos 2t - 0.65, 1.5\sin t), \quad 0 \le t \le 2\pi. \tag{4.1.15}$$

Table 4.2 gives some approximate values for the far field pattern $u_\infty(d)$ and $u_\infty(-d)$ in the forward direction d and the backward direction $-d$. The direction d of the incident wave is $d = (1,0)$ and the wave numbers are $k_0 = 1$ and $k_d = 2 + 3i$. Note that the exponential convergence is clearly exhibited.

Table 4.1: Numerical results for direct scattering problem

n	$\operatorname{Re} u_\infty(d)$	$\operatorname{Im} u_\infty(d)$	$\operatorname{Re} u_\infty(-d)$	$\operatorname{Im} u_\infty(-d)$
8	-0.6017247940	-0.0053550779	-0.2460323014	0.3184957768
16	-0.6018967551	-0.0056192337	-0.2461831740	0.3186052686
32	-0.6019018135	-0.0056277492	-0.2461946976	0.3186049949
64	-0.6019018076	-0.0056277397	-0.2461946846	0.3186049951

4.2 Numerical Solution of the Inverse Problem

In order to solve the inverse problem numerically we need parametrization for the unknown boundary ∂D in the form (3.2.8) with non-negative function r representing the radial distance of ∂D from the origin. The perturbed boundary h is of the form

$$h(t) = q(t)(\cos t, \sin t), \qquad \text{for} \qquad 0 \le t \le 2\pi, \tag{4.2.1}$$

with a real function q. In the approximation we assume r and its update q to have the form of a trigonometric polynomial of degree J

$$r(t) = \sum_{j=0}^{J} \alpha_j \cos jt + \sum_{j=1}^{J} \beta_j \sin jt,$$

$$q(t) = \sum_{j=0}^{J} a_j \cos jt + \sum_{j=1}^{J} b_j \sin jt. \tag{4.2.2}$$

The kernels,

$$A(t,\tau;h;k) \quad := \quad -\frac{ik}{2} \frac{(z(t) - z(\tau)) \cdot (h(t) - h(\tau))}{|z(t) - z(\tau)|} |z'(\tau)| \, H_1^{(1)}(k|z(t) - z(\tau)|),$$

$$B(t,\tau;h;k) \quad := \quad \frac{i}{2} \frac{z'(\tau) \cdot h'(\tau)}{|z'(\tau)|} H_0^{(1)}(k|z(t) - z(\tau)|),$$

of the operator (3.2.28) can be written in the form

$$A(t,\tau;h;k) \quad = \quad A_1(t,\tau;h;k) \ln(4 \sin^2 \frac{t - \tau}{2}) + A_2(t,\tau;h;k),$$

$$B(t,\tau;h;k) \quad = \quad B_1(t,\tau;h;k) \ln(4 \sin^2 \frac{t - \tau}{2}) + B_2(t,\tau;h;k), \tag{4.2.3}$$

where,

$$A_1(t,\tau;h;k) \quad := \quad \frac{k}{2\pi} \frac{(z(t) - z(\tau)) \cdot (h(t) - h(\tau))}{|z(t) - z(\tau)|} |z'(\tau)| \, J_1(k|z(t) - z(\tau)|),$$

$$A_2(t,\tau;h;k) \quad := \quad A(t,\tau;h;k) - A_1(t,\tau;h;k) \ln(4 \sin^2 \frac{t - \tau}{2}),$$

$$B_1(t,\tau;h;k) \quad := \quad -\frac{1}{2\pi} \frac{z'(\tau) \cdot h'(\tau)}{|z'(\tau)|} J_0(k|z(t) - z(\tau)|),$$

$$B_2(t,\tau;h;k) \quad := \quad B(t,\tau;h;k) - B_1(t,\tau;h;k) \ln(4 \sin^2 \frac{t - \tau}{2}).$$

The functions A_1, A_2, B_1 and B_2 turn out to be smooth with diagonal terms. Their diagonal terms are in the form

$$A_1(t,t) = 0, \quad \& \quad A_2(t,t;h) = -\frac{1}{\pi} \frac{z'(t) \cdot h'(t)}{|z'(t)|}.$$

$$B_1(t,t;h) = -\frac{1}{2\pi} \frac{z'(t) \cdot h'(t)}{|z'(t)|}, \quad \& \quad B_2(t,t;h;k) = \{\frac{i}{2} - \frac{1}{\pi} ln(\frac{k}{2}|z'(t)|) - \frac{C_E}{\pi}\} z'(t) \cdot h'(t).$$

And the kernels,

$$C(t,\tau;h;k) := \frac{-ik([z'(t)]^{\perp}\cdot(h(t)-h(\tau))+[h'(t)]^{\perp}\cdot(z(t)-z(\tau)))}{2|z'(t)||z(t)-z(\tau)|}|z'(\tau)|H_1^{(1)}(k|z(t)-z(\tau)|).$$

$$D(t,\tau;h;k) := \frac{ik[z'(t)]^{\perp}\cdot(z(t)-z(\tau))(h(t)-h(\tau))\cdot(z(t)-z(\tau))}{|z'(t)||z(t)-z(\tau)|^3}|z'(\tau)|H_1^{(1)}(k|z(t)-z(\tau)|).$$

$$E(t,\tau;h;k) := \frac{-ik^2[z'(t)]^{\perp}\cdot(z(t)-z(\tau))(h(t)-h(\tau))\cdot(z(t)-z(\tau))}{2|z'(t)||z(t)-z(\tau)|^2}|z'(\tau)|H_0^{(1)}(k|z(t)-z(\tau)|).$$

$$F(t,\tau;h;k) := \frac{ik}{2}\frac{h'(t)\cdot z'(t)}{|z'(t)|^2}\frac{[z'(t)]^{\perp}\cdot(z(t)-z(\tau))}{|z(t)-z(\tau)|}|z'(\tau)|H_1^{(1)}(k|z(t)-z(\tau)|).$$

$$G(t,\tau;h;k) := -\frac{ik}{2|z'(t)|}\frac{[z'(t)]^{\perp}\cdot(z(t)-z(\tau))h'(\tau)\cdot z'(\tau)}{|z(t)-z(\tau)||z'(\tau)|}H_1^{(1)}(k|z(t)-z(\tau)|).$$

of the operator (3.2.29) can be written in the form

$$C(t,\tau;h;k) = C_1(t,\tau;h;k)\ln(4\sin^2\frac{t-\tau}{2}) + C_2(t,\tau;h;k),$$

$$D(t,\tau;h;k) = D_1(t,\tau;h;k)\ln(4\sin^2\frac{t-\tau}{2}) + D_2(t,\tau;h;k),$$

$$E(t,\tau;h;k) = E_1(t,\tau;h;k)\ln(4\sin^2\frac{t-\tau}{2}) + E_2(t,\tau;h;k),$$

$$F(t,\tau;h;k) = F_1(t,\tau;h;k)\ln(4\sin^2\frac{t-\tau}{2}) + F_2(t,\tau;h;k),$$

$$G(t,\tau;h;k) = G_1(t,\tau;h;k)\ln(4\sin^2\frac{t-\tau}{2}) + G_2(t,\tau;h;k), \qquad (4.2.4)$$

where

$$C_1(t,\tau;h;k) \quad := \quad \frac{k([z'(t)]^{\perp}\cdot(h(t)-h(\tau))+[h'(t)]^{\perp}\cdot(z(t)-z(\tau)))}{2\pi|z'(t)||z(t)-z(\tau)|}|z'(\tau)|J_1(k|z(t)-z(\tau)|),$$

$$C_2(t,\tau;h;k) \quad := \quad C(t,\tau;h;k) - C_1(t,\tau;h;k)\ln(4\sin^2\frac{t-\tau}{2}).$$

$$D_1(t,\tau;h;k) \quad := \quad \frac{-k[z'(t)]^{\perp}\cdot(z(t)-z(\tau))(h(t)-h(\tau))\cdot(z(t)-z(\tau))}{\pi|z'(t)||z(t)-z(\tau)|^3}|z'(\tau)|J_1(k|z(t)-z(\tau)|),$$

$$D_2(t,\tau;h;k) \quad := \quad D(t,\tau;h;k) - D_1(t,\tau;h;k)\ln(4\sin^2\frac{t-\tau}{2}).$$

$$E_1(t,\tau;h;k) \quad := \quad \frac{k^2[z'(t)]^{\perp}\cdot(z(t)-z(\tau))(h(t)-h(\tau))\cdot(z(t)-z(\tau))}{2\pi|z'(t)||z(t)-z(\tau)|^2}|z'(\tau)|J_0(k|z(t)-z(\tau)|),$$

$$E_2(t,\tau;h;k) \quad := \quad E(t,\tau;h;k) - E_1(t,\tau;h;k)\ln(4\sin^2\frac{t-\tau}{2}).$$

$$F_1(t,\tau;h;k) \quad := \quad -\frac{k}{2\pi}\frac{h'(t)\cdot z'(t)}{|z'(t)|^2}\frac{[z'(t)]^{\perp}\cdot(z(t)-z(\tau))}{|z(t)-z(\tau)|}|z'(\tau)|J_1(k|z(t)-z(\tau)|),$$

$$F_2(t,\tau;h;k) \quad := \quad F(t,\tau;h;k) - F_1(t,\tau;h;k)\ln(4\sin^2\frac{t-\tau}{2}).$$

$$G_1(t,\tau;h;k) \quad := \quad \frac{k}{2\pi}\frac{1}{|z'(t)|}\frac{[z'(t)]^{\perp}\cdot(z(t)-z(\tau))h'(\tau)\cdot z'(\tau)}{|z(t)-z(\tau)||z'(\tau)|}J_1(k|z(t)-z(\tau)|),$$

$$G_2(t,\tau;h;k) \quad := \quad G(t,\tau;h;k) - G_1(t,\tau;h;k)\ln(4\sin^2\frac{t-\tau}{2}).$$

The functions C_1, C_2, D_1, D_2, E_1, E_2, F_1, F_2 G_1, and G_2 turn out to be smooth with diagonal terms. Their diagonal terms are in the form

$$C_1(t,t) = 0, \qquad \& \qquad C_2(t,t;h) = \frac{1}{2\pi}\frac{[z'(t)]^{\perp}\cdot h''(t) + [h'(t)]^{\perp}\cdot z''(t)}{|z'(t)|^2}.$$

$$D_1(t,t) = 0, \qquad \& \qquad D_2(t,t;h) = -\frac{1}{\pi}\frac{[z'(t)]^{\perp}\cdot z''(t)\, z'(t)\cdot h'(t)}{|z'(t)|^4}.$$

$$E_1(t,t) = 0, \qquad \& \qquad E_2(t,t) = 0.$$

$$F_1(t,t) = 0, \qquad \& \qquad F_2(t,t;h) = -\frac{1}{2\pi}\frac{[z'(t)]^{\perp}\cdot z''(t)\, z'(t)\cdot h'(t)}{|z'(t)|^3}.$$

$$G_1(t,t) = 0, \qquad \& \qquad G_2(t,t;h) = \frac{1}{2\pi}\frac{[z'(t)]^{\perp}\cdot z''(t)\, z'(t)\cdot h'(t)}{|z'(t)|^4}.$$

The kernel,

$$P(t,\tau;k_d) := -\frac{i}{2}|z(t)-z(\tau)||z'(\tau)|H_1^{(1)}(k_d|z(t)-z(\tau)|), \qquad (4.2.5)$$

of the operator (3.2.51) can be written in the form

$$P(t,\tau;k_d) = P_1(t,\tau;k_d)\ln(4\sin^2\frac{t-\tau}{2}) + P_2(t,\tau;k_d), \qquad (4.2.6)$$

where

$$P_1(t,\tau;k_d) = \frac{1}{2\pi}|z(t) - z(\tau)||z'(\tau)|J_1(k_d|z(t) - z(\tau)|),$$

$$P_2(t,\tau;k_d) = P(t,\tau;k_d) - P_1(t,\tau;k_d)\ln(4\sin^2\frac{t-\tau}{2}).$$

The functions P_1 and P_2 turn out to be smooth with diagonal terms. Their diagonal terms are in the form

$$P_1(t,t;k_d) = 0 \qquad \& \qquad P_2(t,t;k_d) = -\frac{1}{\pi k_d}|z'(t)|.$$

4.2.1 Numerical Solution of the Johansson and Sleeman Method for Shape Reconstruction

Here, we are now going to shortly describe how the Johansson and Sleeman method can be implemented for the numerical solution of shape reconstruction.

1. We solve the two well-posed field equations in (3.2.12) for the densities by the method described in section 4.1.

2. We solve the ill-posed linearized data equation in (3.2.14) by Tikhonov regularization with the trapezoidal rule. Inserting (4.2.2) into the Tikhonov equation leads to a linear system for the unknown Fourier coefficients a and b.

4.2.2 Numerical Solution of the Simultaneous Linearization Method for Shape Reconstruction

In this subsection, we are going to shortly describe how we apply the simultaneous linearization method for the numerical solution of shape reconstruction.

- We solve the linearized ill-posed equations (3.2.30) by Tikhonov regularization with the method described in section 4.1. Substituting (4.2.2) into the regularized Tikhonov equations lead to a linear system for the unknown Fourier coefficients a and b and unknown densities η_d and η_0.

4.2.3 Numerical Solution of the Hybrid Method

In this subsection, we shortly present how we implement the hybrid method for the numerical solution of shape reconstruction.

1. We solve the regularized equation (3.2.42) via Tikhonov regularization with the trapezoidal rule for the density ψ_0.

2. We find the density ψ_d from the equation (3.2.43) by the method described in section 4.1 for fixed ψ_0.

3. For fixed ψ_0 and ψ_d, we solve the ill-posed linearized equation (3.2.44) by Tikhonov regularization with the method described in section 4.1. Inserting (4.2.2) into the Tikhonov equation leads to a linear system for the unknown Fourier coefficients a and b.

4.2.4   Numerical Solution of Reconstruction the Interior Wave Number via the Hybrid Method

In this subsection, we shortly describe how the hybrid method can be applied for the numerical solution of reconstruction for the interior wave number k_d.

1. We solve the regularized equation (3.2.48) via Tikhonov regularization with the trapezoidal rule for the density ψ_0.

2. We find the density ψ_d from the equation (3.2.49) by the method described in section 4.1.

3. For fixed ψ_d, we solve the ill-posed linearized equation (3.2.50) by Tikhonov regularization with the method described in section 4.1. Inserting (4.2.2) into the Tikhonov equation leads to a linear system for the unknown σ.

4.2.5   Numerical Solution of Simultaneous Reconstructions the Boundary and the Interior Wave Number via the Hybrid Method

This is just combination of the above two last subsections.

4.3   Numerical Examples

For the numerical examples we choose the number of incident plane waves $M = 8$. There are six parameters which effect the quality of the reconstruction. In order to understand the influence of these parameters, we keep five of them fixed and vary the remaining sixth parameter. They are given as fallows;

- initial guess

- interior and exterior wave numbers are represented by k_d and k_0 respectively,

- degree of trigonometric polynomials is represented by J,

- regularization parameter used for the boundary is represented by λ decreasing with each iteration step j,

- regularization parameter used for the densities is represented by α.

- Sobolev norm is represented by H^p,

- Noise level is represented by δ. In order to obtain noisy data, random errors are added point-wise to u_∞,

$$\widetilde{u}_\infty = u_\infty + \delta\xi\frac{||u_\infty||}{|\xi|} \tag{4.3.1}$$

where the random variable $\xi \in C$ and $\{\mathrm{Re}\xi, \mathrm{Im}\xi\} \in (0,1)$

Table 4.2: Parametric representation of boundary curves.

Counter type		Parametric representation
Apple-shaped	:	$z(t) = \{\dfrac{0.5 + 0.4\cos t + 0.1\sin 2t}{1 + 0.7\cos t}(\cos t, \sin t) : t \in [0, 2\pi]\}$
Drop-shaped	:	$z(t) = \{(-0.5 + 0.75\sin\dfrac{t}{2}, -0.75\sin t) : t \in [0, 2\pi]\}$
Ellipse	:	$z(t) = \{(a_1\cos t, a_2\sin t) : t \in [0, 2\pi]\}, a_1, a_2 : \text{constant}$
Kite-shaped	:	$z(t) = \{(\cos t + 1.3\cos^2 t - 1.3, 1.5\sin t) : t \in [0, 2\pi]\}$
Peanut-shaped	:	$z(t) = \{\sqrt{\cos^2 t + 0.25\sin t}\,(\cos t, \sin t) : t \in [0, 2\pi]\}$
Rounded triangle	:	$z(t) = \{(2 + 0.3\cos 3t)(\cos t, \sin t) : t \in [0, 2\pi]\}$

4.3.1 Numerical Examples for the Johansson Sleeman Method with Synthetic Data

In the sequel, the purple curve with stars represents the initial guess, the dashed curve represents the boundary of the scatterer and the red curve represents the reconstruction for all examples.

Firstly, the figures 4.1 and 4.2 show examples of slim ellipse-shaped scatterer. In these examples, we try to understand the influence of the degree J of trigonometric polynomials and of the noise level δ on the quality of the reconstruction.

$k_0 = 1, \ k_d = 10+10i, \ J = 5$
$\lambda = (0.9)^j, \ H^2, \ \delta = 0.$
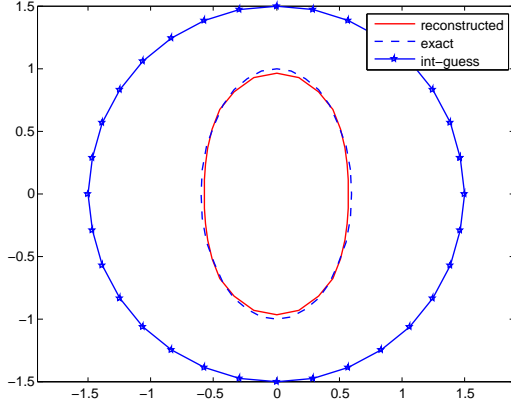
$k_0 = 1, \ k_d = 10 + 10i, \ J = 10,$
$\lambda = (0.9)^j, H^2, \delta = 0.$
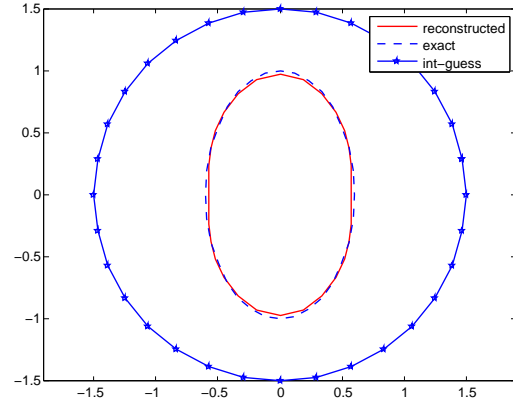
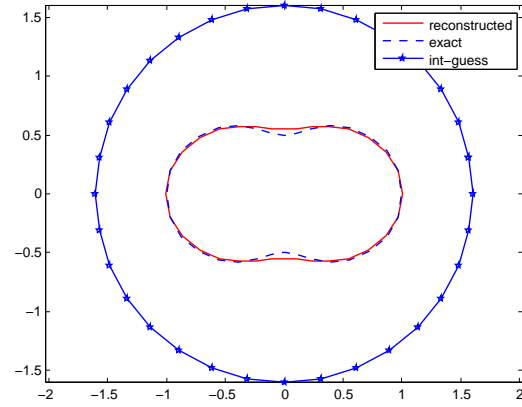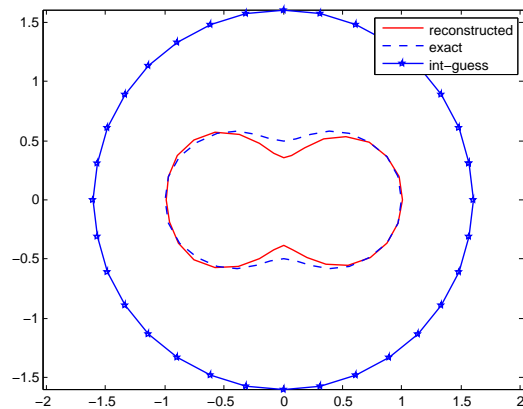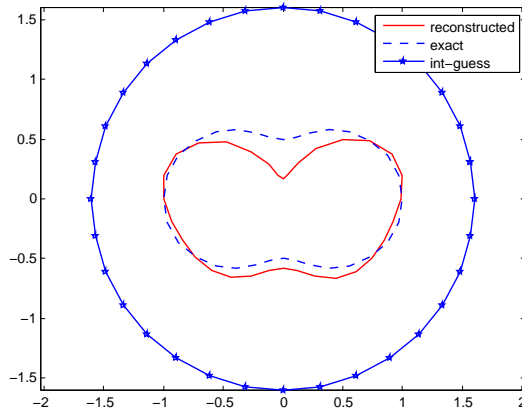Figure 4.1: Dependence on J

Secondly, the figures 4.3–4.9 show examples of an apple-shaped scatterer. In the example 4.3, we illustrate how the reconstructions are influenced when we change the interior wave number k_d. In the example 4.4, we illustrate how the reconstructions are influenced when we increase the degree J of trigonometric polynomials. In the examples 4.5, 4.6 and 4.7, we illustrate how the Sobolev norm H^p effects the quality of the reconstructions. In example 4.8, we investigate how the regularization parameter λ influences the quality of the reconstructions. In the example 4.9, we show how the noise level δ influences the quality of the reconstructions.

Thirdly, the figures 4.10–4.13 show examples of a kite-shaped scatterer. In the example 4.10, we show how the interior wave number k_d influences the quality of the reconstructions. In the example 4.11, we illustrate how the exterior wave number k_0 effects the quality of the reconstructions. In the example 4.12, we show how the degree J of trigonometric polynomials influences the quality of the reconstructions. In the examples 4.13, we illustrate how the noise level δ influences the quality of the reconstructions.

Finally, the figures 4.14 and 4.15 show examples of a peanut-shaped scatterer. In the examples 4.14 and 4.15 we illustrate how the interior wave number k_d and noise level δ influence the quality of the reconstructions, respectively.

$k_0 = 1,\ k_d = 10+10i,\ J = 5$
$\lambda = (0.9)^j,\ H^2,\ \delta = 0.05.$
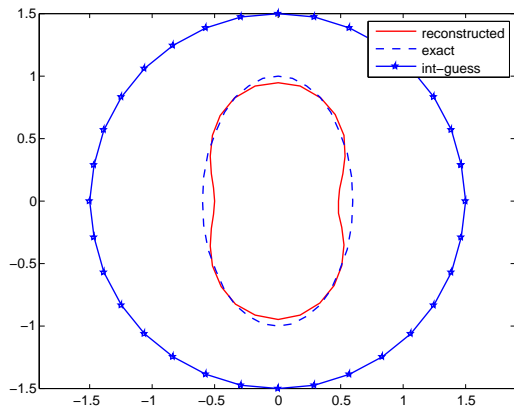
$k_0 = 1,\ k_d = 10+10i,\ J = 5,$
$\lambda = (0.9)^j, H^2, \delta = 0.1.$
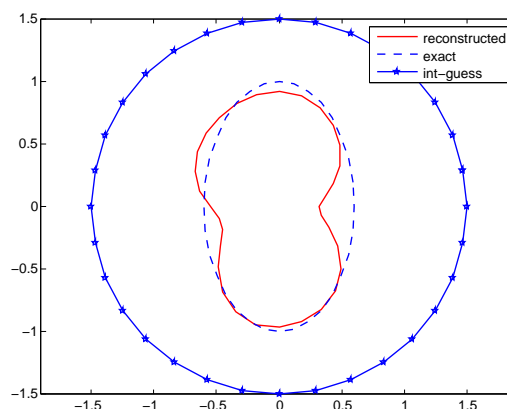
$k_0 = 1,\ k_d = 10+5i,\ J = 5$
$\lambda = (0.8)^j,\ H^2,\ \delta = 0.$

$k_0 = 1,\ k_d = 10+1i,\ J = 5,$
$\lambda = (0.8)^j, H^2, \delta = 0.$
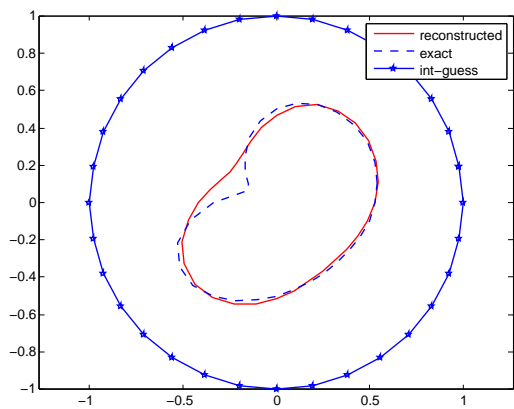
Figure 4.2: Dependence on δ
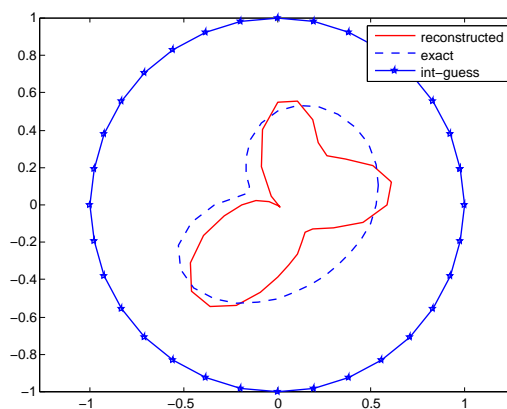
Figure 4.3: Dependence on k_d

$k_0 = 1,\ k_d = 10+5i,\ J = 5$
$\lambda = (0.8)^j,\ H^2,\ \delta = 0.$
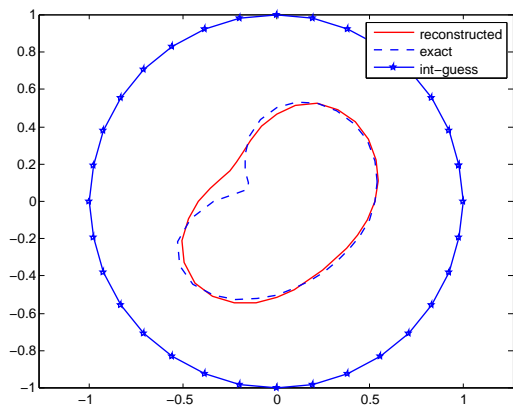
$k_0 = 1,\ k_d = 10+5i,\ J = 20,$
$\lambda = (0.8)^j, H^2, \delta = 0.$
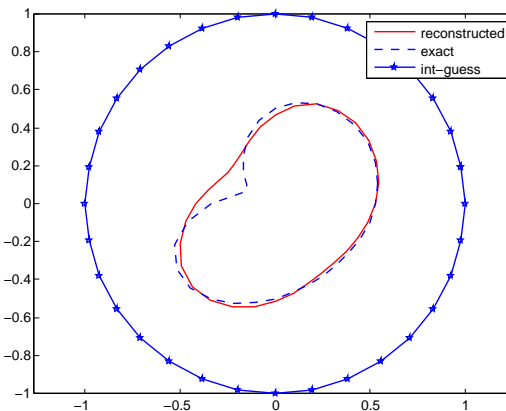
Figure 4.4: Dependence on J

$k_0 = 1,\ k_d = 10+5i,\ J = 5$
$\lambda = (0.8)^j,\ H^2,\ \delta = 0.$
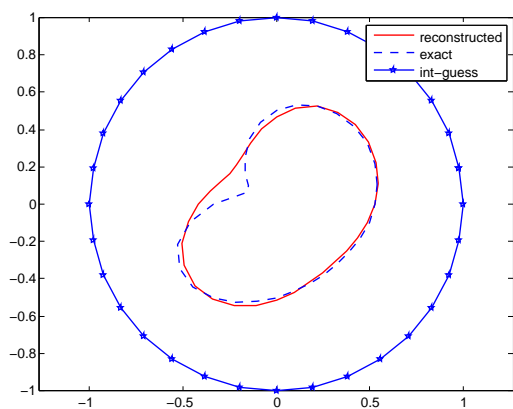
$k_0 = 1,\ k_d = 10+5i,\ J = 5,$
$\lambda = (0.8)^j, L^2, \delta = 0.$
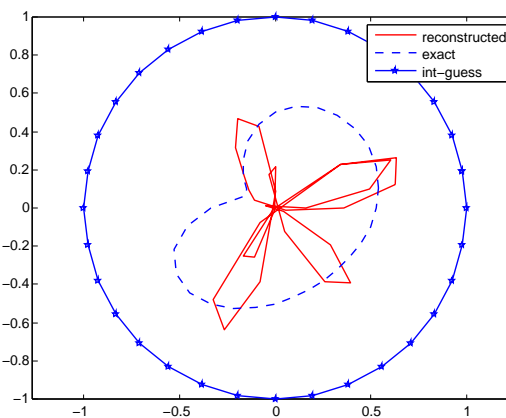
Figure 4.5: Dependence on H^p

$k_0 = 1$, $k_d = 10+5i$, $J = 5$
$\lambda = (0.8)^j$, $H^{1/2}$, $\delta = 0$.
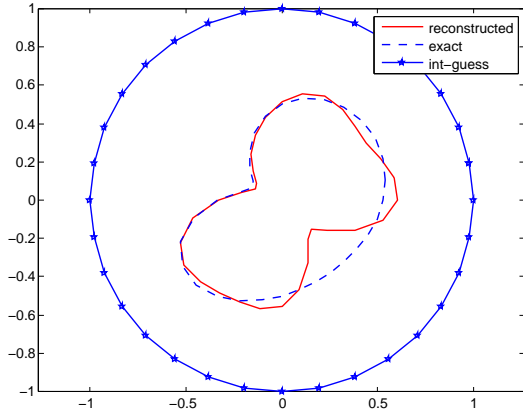
$k_0 = 1$, $k_d = 10+5i$, $J = 5$,
$\lambda = (0.8)^j$, H^1, $\delta = 0$.
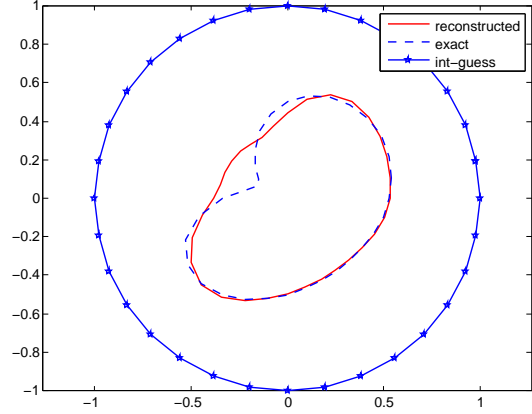
Figure 4.6: Dependence on H^p

$k_0 = 1$, $k_d = 10+5i$, $J = 5$
$\lambda = (0.8)^j$, H^3, $\delta = 0$.
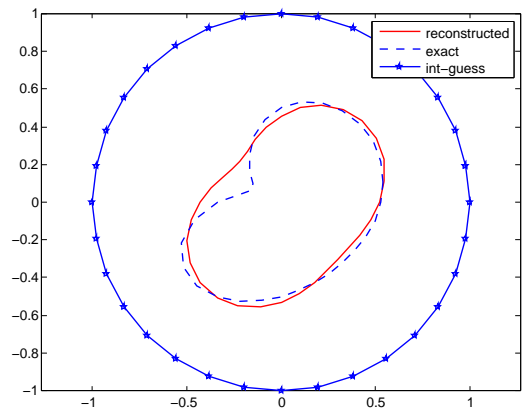
$k_0 = 1$, $k_d = 10+5i$, $J = 5$,
$\lambda = (0.8)^j$, H^4, $\delta = 0$.
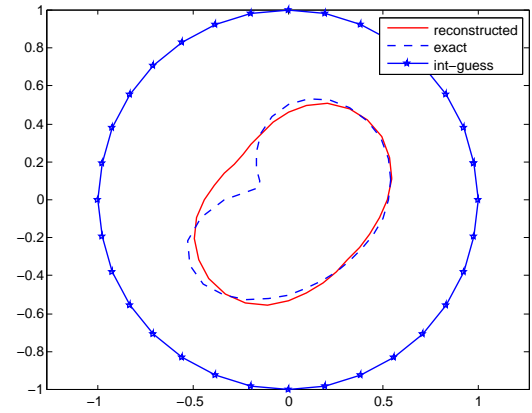
Figure 4.7: Dependence on H^p

$k_0 = 1, \ k_d = 10{+}5i, \ J = 5$
$\lambda = 0.1 * (0.8)^j, \ H^2, \ \delta = 0.$
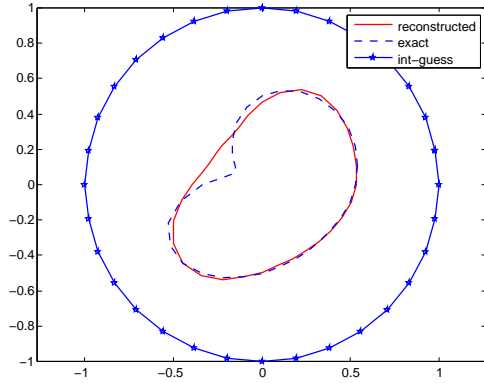
$k_0 = 1, \ k_d = 10 + 5i, \ J = 5,$
$\lambda = 0.01 * (0.8)^j, H^2, \delta = 0.$
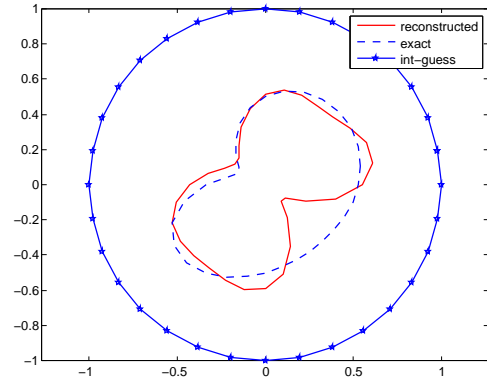
Figure 4.8: Dependence on λ

$k_0 = 1, \ k_d = 10{+}5i, \ J = 5$
$\lambda = (0.8)^j, \ H^2, \ \delta = 0.03.$
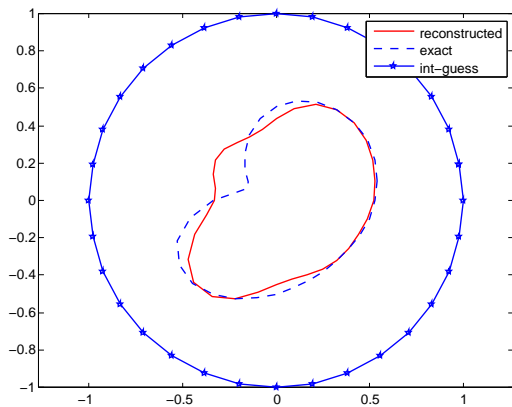
$k_0 = 1, \ k_d = 10 + 5i, \ J = 5,$
$\lambda = (0.8)^j, H^2, \delta = 0.05.$
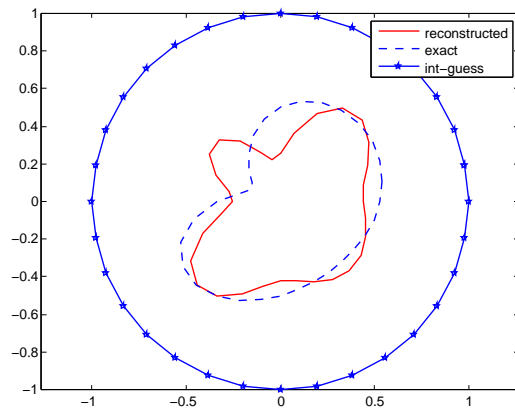
Figure 4.9: Dependence on δ

$k_0 = 1, \ k_d = 10+1i, \ J = 5$
$\lambda = (0.8)^j, \ H^2, \ \delta = 0.$
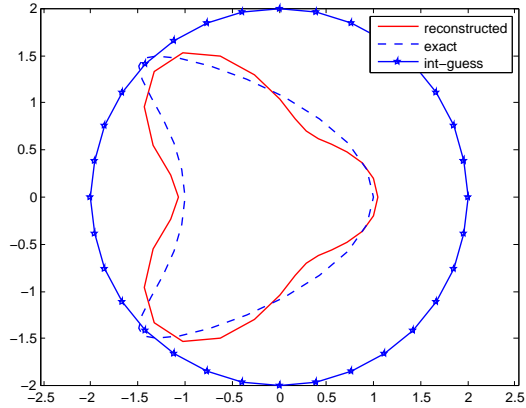
$k_0 = 1, \ k_d = 10+8i, \ J = 5,$
$\lambda = (0.8)^j, H^2, \delta = 0.$
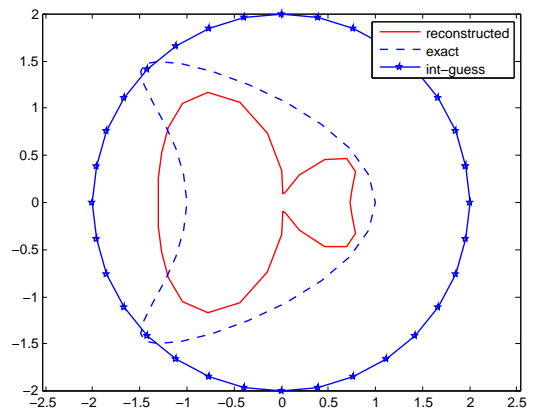
Figure 4.10: Dependence on k_d

$k_0 = 1, \ k_d = 10+1i, \ J = 5$
$\lambda = (0.8)^j, \ H^2, \ \delta = 0.$
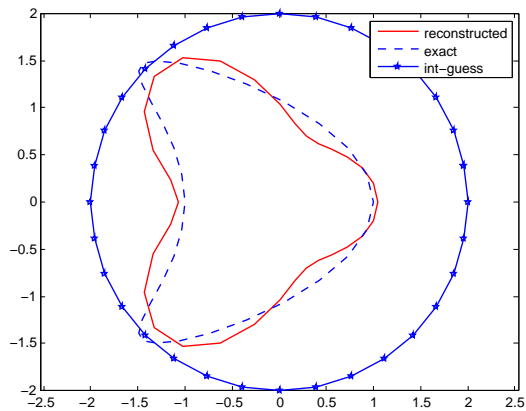
$k_0 = 3, \ k_d = 10+1i, \ J = 5,$
$\lambda = (0.8)^j, H^2, \delta = 0.$
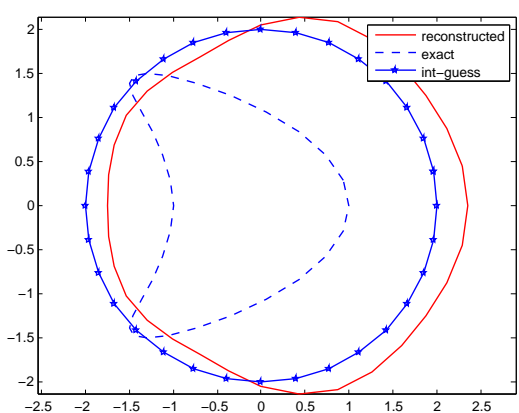
Figure 4.11: Dependence on k_0

$k_0 = 1$, $k_d = 10+1i$, $J = 10$
$(0.8)^j$, H^2, $\delta = 0$.
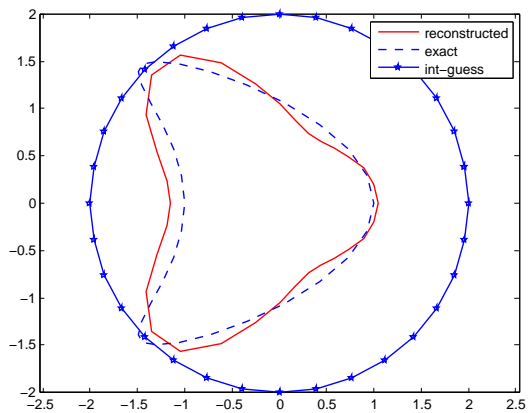
$k_0 = 1$, $k_d = 10 + 1i$, $J = 20$,
$\lambda = (0.8)^j, H^2, \delta = 0$.
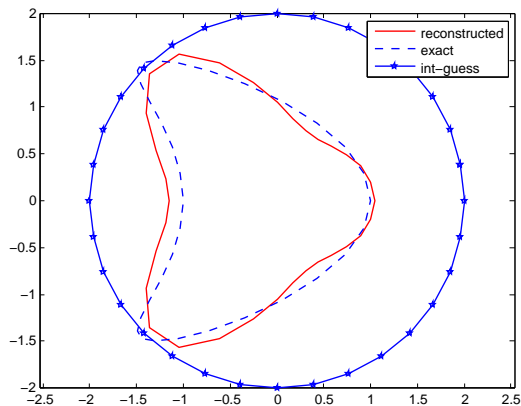
Figure 4.12: Dependence on J

$k_0 = 1$, $k_d = 10+1i$, $J = 5$
$\lambda = (0.8)^j$, H^2, $\delta = 0.03$.
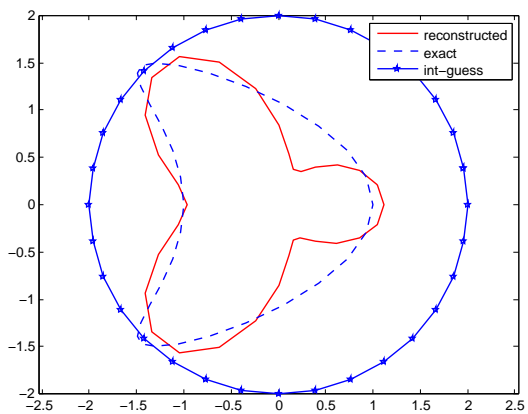
$k_0 = 1$, $k_d = 10 + 1i$, $J = 5$,
$\lambda = (0.8)^j, H^2, \delta = 0.05$.
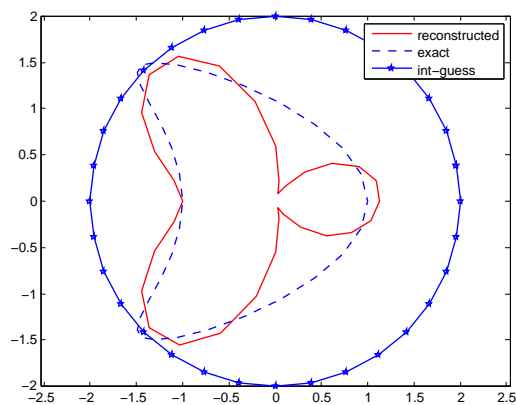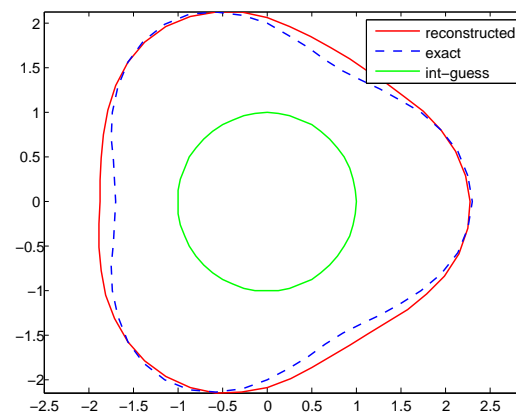
Figure 4.13: Dependence on δ

$k_0 = 1, \ k_d = 10+1i, \ J = 5$
$\lambda = (0.8)^j, \ H^2, \ \delta = 0.$
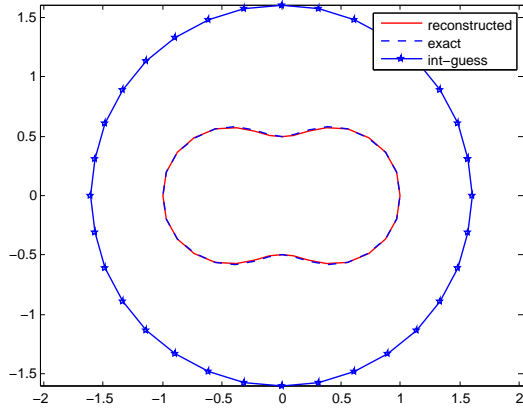
$k_0 = 1, \ k_d = 10 + 5i, \ J = 5,$
$\lambda = (0.8)^j, H^2, \delta = 0.$

Figure 4.14: Dependence on k_d

$k_0 = 1, \ k_d = 10+1i, \ J = 5$
$\lambda = (0.8)^j, \ H^2, \ \delta = 0.03.$

$k_0 = 1, \ k_d = 10 + 1i, \ J = 5,$
$\lambda = (0.8)^j, H^2, \delta = 0.05.$

Figure 4.15: Dependence on δ

From the examples 4.1, 4.4 and 4.12, we observe that the degree J of trigono-metric polynomials has not significant effect on the quality of the reconstructions. Of course this does not mean that the degree J of trigonometric polynomials does not have an influence on the quality of the reconstructions. When we select $J = 1$ we could not obtain a reasonable reconstruction, for instance. From the examples $4.3, 4.10$ and 4.14, we observe that the interior wave number k_d has a significant influence on the quality of the reconstructions. From the example 4.11, we see that the quality of the reconstructions is significantly effected by changing the exterior wave number k_0. From the examples 4.5 and 4.6, we observe that the Sobolev norm H^p has a significant influence on the quality of the reconstruction. From the example 4.7, we also observe that the quality of the reconstructions does not significantly change when we select $p \geq 2$. From the example 4.8, we see that the regularization parameter λ has a significant influence on the quality of the reconstructions. From the examples, $4.2, 4.9, 4.13$ and 4.15, we observe that the Johansson and Sleeman method tolerates noise level up to 5 percentage.

To sum up, in order to have a reasonable reconstruction one has to appropriately select all parameters. There is no theoretical result available for how these parameters should be chosen. We found these parameters by trial and error. However, we keep in mind that since the Johansson and Sleeman method can be viewed as the traditional Newton method (see theorem 3.2.7), this method converges to a local minimum. Therefore, one has to start with a good initial guess. The exterior wave number k_0 should be chosen in the resonance region, i.e., length of the incident plane wave should approximately equal to the diameter of the scatterer.

Comparing with the numerical examples (see Hohage and Schormann [15]) obtained by Newton method for the boundary to far field mapping, we observe that the examples obtained by the Johansson and Sleeman method are not as good as the examples obtained by the Newton method. The main advantage of the Johansson and Sleeman method is that it has a simple implementation.

4.3.2   Numerical Examples for the Simultaneous Lineariza-tion Method with Synthetic data

In the following subsection, the green curve represents initial guess, the dashed curve represents the boundary of the scatterer and the red curve represents the reconstruction for all examples. In order to avoid redundancy, we will only mention what conclusion we obtain from all the following examples for the simultaneous linearization method. In all following examples, we use parameters given above each figures. The figures 4.16 and 4.17 show examples of a peanut-shaped scatterer, the figures 4.18 and 4.19 illustrate examples of a rounded-triangle-shaped scatterer, the figures 4.20 and 4.21 are examples of an apple-shaped scatterer, the figures 4.22 and 4.23 are examples of a dropped-shaped scatterer, and the figures 4.24 and 4.25 are examples of a kite-shaped scatterer.

$k_0 = 1, \ k_d = 10+5i, \ J = 5$
$\alpha = 10^{-8}, \ \lambda = (0.9)^j, \ H^2, \ \delta = 0.$
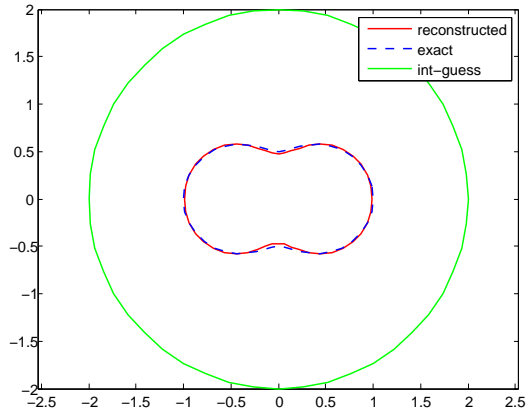
$k_0 = 1, \ k_d = 10 + 5i, \ J = 5,$
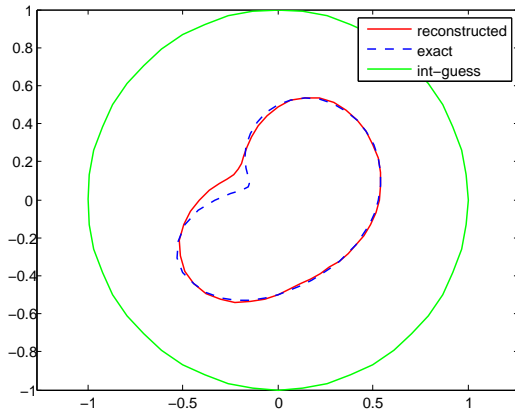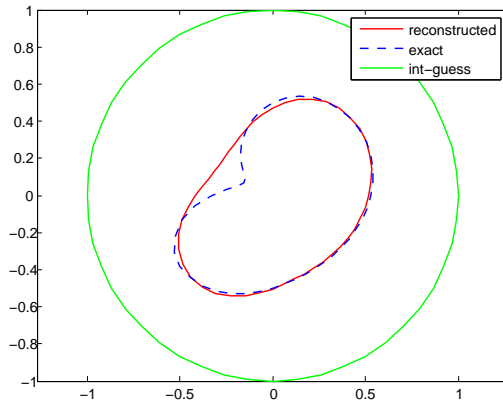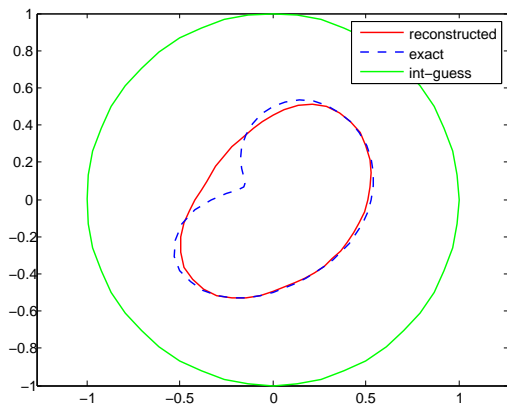$\alpha = 10^{-8}, \ \lambda = (0.9)^j, H^2, \delta = 0.05.$
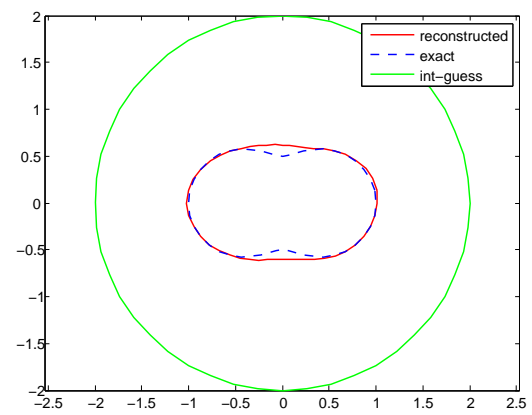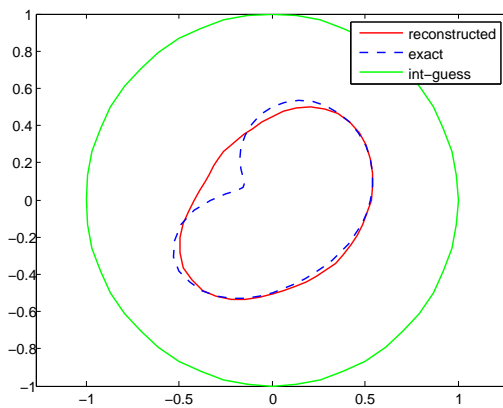
Figure 4.16: Dependence on δ

$k_0 = 1, \ k_d = 10+5i, \ J = 5,$
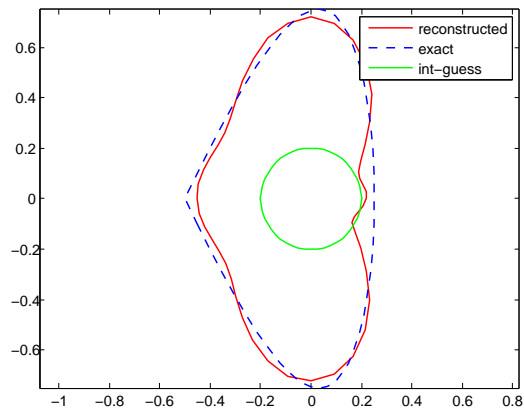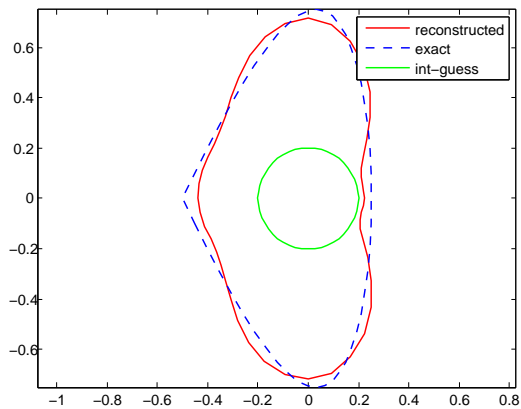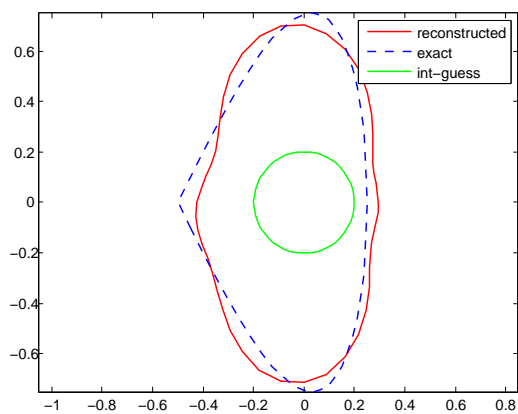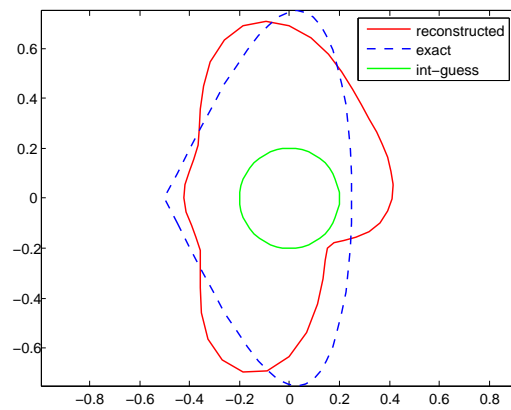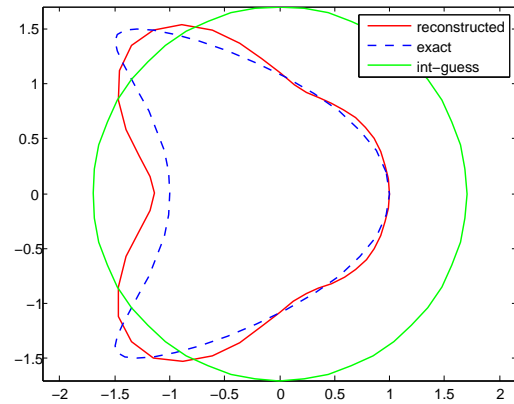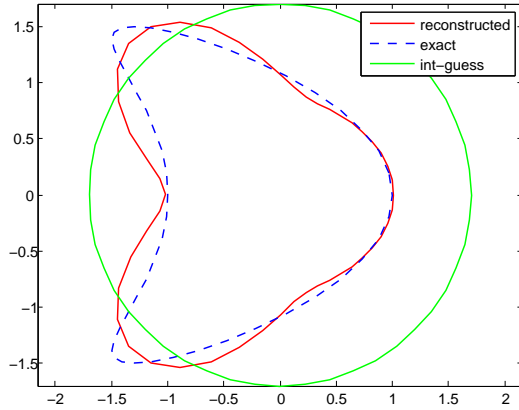$\alpha = 10^{-8}, \lambda = (0.9)^j, \ H^2, \ \delta = 0.1.$
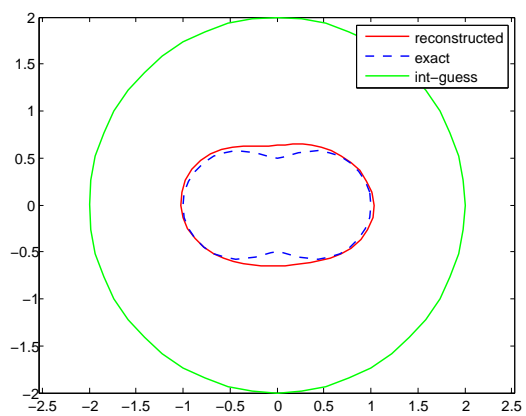
$k_0 = 1, \ k_d = 10 + 5i, \ J = 5,$
$\alpha = 10^{-8}, \ \lambda = (0.9)^j, H^2, \delta = 0.2.$
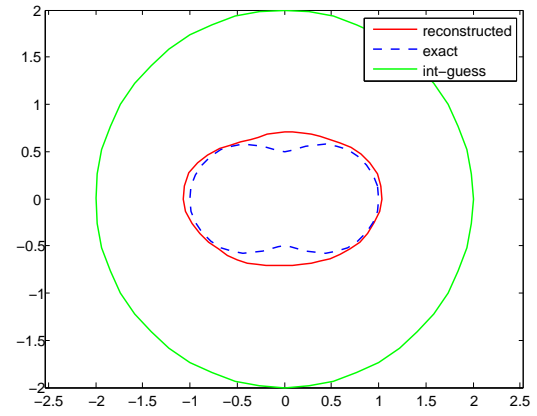
Figure 4.17: Dependence on δ

$k_0 = 1, \ k_d = 10+1i, \ J = 5$
$\alpha = 10^{-7}, \ \lambda = (0.9)^j, \ H^2, \ \delta = 0.$
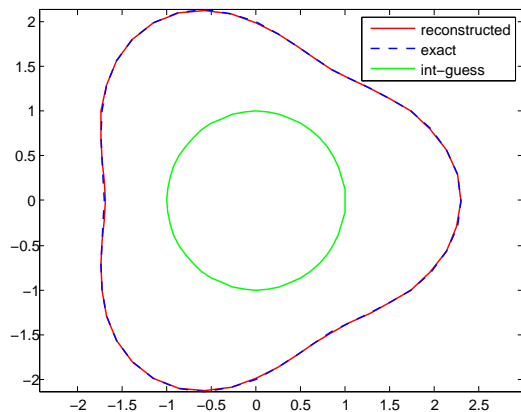
$k_0 = 1, \ k_d = 10 + 1i, \ J = 5,$
$\alpha = 10^{-8}, \ \lambda = (0.9)^j, H^2, \delta = 0.05.$
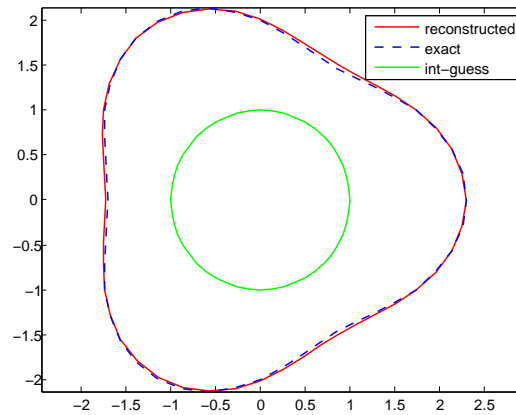
Figure 4.18: Dependence on δ

$k_0 = 1, \ k_d = 10+1i, \ J = 5,$
$\alpha = 10^{-8}, \lambda = (0.9)^j, \ H^2, \ \delta = 0.1.$
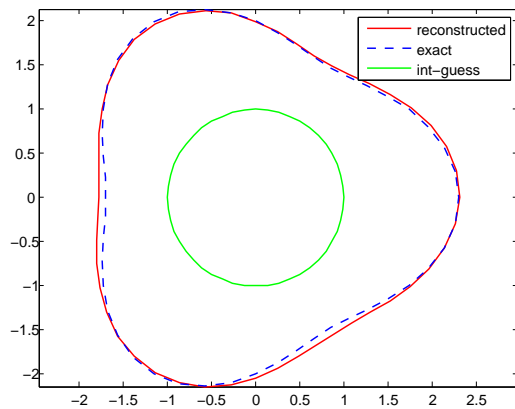
$k_0 = 1, \ k_d = 10 + 1i, \ J = 5,$
$\alpha = 10^{-8}, \ \lambda = (0.9)^j, H^2, \delta = 0.2.$

Figure 4.19: Dependence on δ

$k_0 = 1$, $k_d = 10+10i$, $J = 5$
$\alpha = 10^{-8}$, $\lambda = (0.8)^j$, H^2, $\delta = 0$.

$k_0 = 1$, $k_d = 10 + 10i$, $J = 5$,
$\alpha = 10^{-8}$, $\lambda = (0.8)^j$, H^2, $\delta = 0.05$.

Figure 4.20: Dependence on δ

$k_0 = 1$, $k_d = 10+10i$, $J = 5$,
$\alpha = 10^{-8}$, $\lambda = (0.8)^j$, H^2, $\delta = 0.1$.
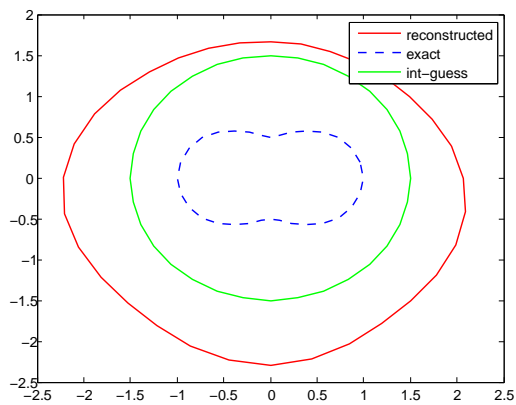
$k_0 = 1$, $k_d = 10 + 10i$, $J = 5$,
$\alpha = 10^{-8}$, $\lambda = (0.8)^j$, H^2, $\delta = 0.2$.

Figure 4.21: Dependence on δ

$k_0 = 1,\ k_d = 10+5i,\ J = 5$
$\alpha = 10^{-5},\ \lambda = (0.9)^j,\ H^2,\ \delta = 0.$

$k_0 = 1,\ k_d = 10 + 5i,\ J = 5,$
$\alpha = 10^{-5},\ \lambda = (0.9)^j, H^2, \delta = 0.05.$

Figure 4.22: Dependence on δ

$k_0 = 1,\ k_d = 10+1i,\ J = 5,$
$\alpha = 10^{-5}, \lambda = (0.9)^j,\ H^2,\ \delta = 0.1.$

$k_0 = 1,\ k_d = 10 + 1i,\ J = 5,$
$\alpha = 10^{-5},\ \lambda = (0.9)^j, H^2, \delta = 0.2.$

Figure 4.23: Dependence on δ

$k_0 = 1, \ k_d = 10+1i, \ J = 5$
$\alpha = 10^{-8}, \ \lambda = (0.9)^j, \ H^2, \ \delta = 0.$

$k_0 = 1, \ k_d = 10 + 1i, \ J = 5,$
$\alpha = 10^{-8}, \ \lambda = (0.9)^j, H^2, \delta = 0.05.$

Figure 4.24: Dependence on δ

$k_0 = 1, \ k_d = 10+1i, \ J = 5,$
$\alpha = 10^{-8}, \lambda = (0.9)^j, \ H^2, \ \delta = 0.1.$

$k_0 = 1, \ k_d = 10 + 1i, \ J = 5,$
$\alpha = 10^{-8}, \ \lambda = (0.9)^j, H^2, \delta = 0.2.$
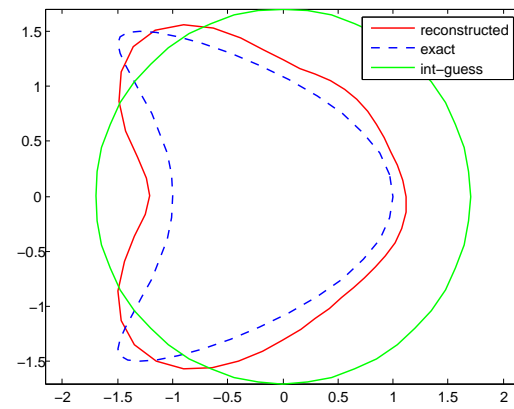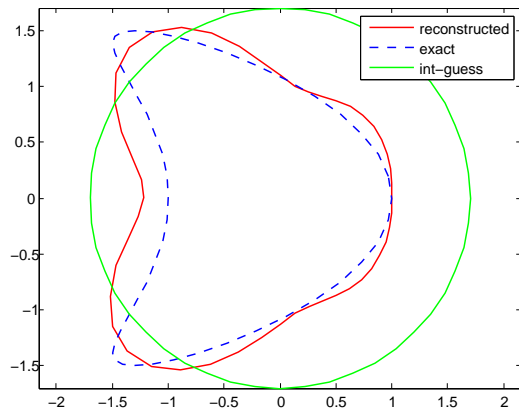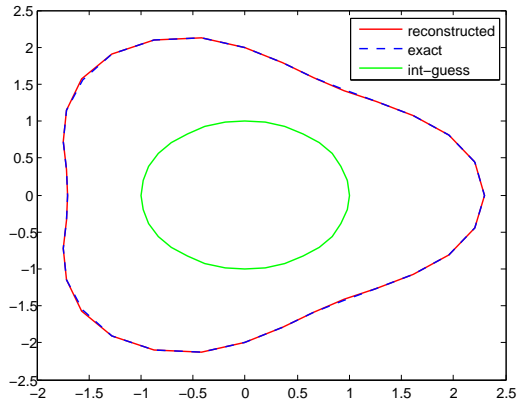
Figure 4.25: Dependence on δ

In conclusion, in the above examples, we focused on the noise level δ in order to prevent redundancy.

Comparing with the numerical examples (see Hohage and Schormann [15]) obtained by the Newton method, we observe that the examples obtained by the simultaneous linearization method compete with the examples obtained by the Newton method. The main advantage of the simultaneous linearization method is the simple form of derivatives. Moreover, it tolerates noise level up to %10, on the other hand, the Newton method tolerates noise level up to %5. In addition, from the all examples, we observe that the simultaneous linearization method is better than the Johansson and Sleeman method since it provides better reconstruction and tolerates higher noise level.

4.3.3   Numerical Examples for the Hybrid Method with Synthetic data

In the following subsection, the color of the curves has the same meaning as described in the simultaneous linearization method. For decreasing the redundancy, we will only mention about what conclusion we obtain for the hybrid method. In all following examples, we use parameters given above each figures.

The figures 4.26 and 4.27 are examples of a peanut-shaped scatterer, the figures 4.28 and 4.29 are examples of a rounded-triangle-shaped scatterer, the figures 4.30 and 4.31 are examples of an apple-shaped scatterer, the figures 4.32 and 4.33 are examples of a dropped-shaped scatter, and the figures 4.34 and 4.35 are examples of a kite-shaped scatterer.

$k_0 = 1,\ k_d = 10+5i,\ J = 5$
$\alpha = 10^{-7},\ \lambda = (0.9)^j,\ H^2,\ \delta = 0.$
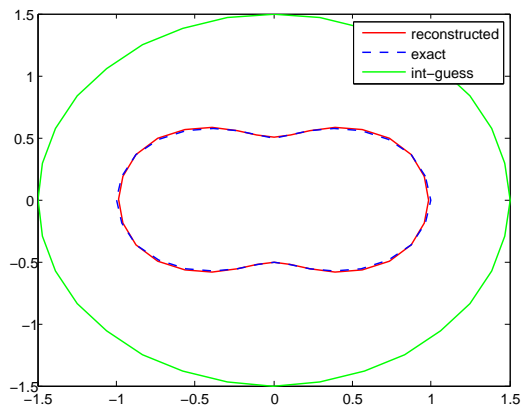
$k_0 = 1,\ k_d = 10+5i,\ J = 5,$
$\alpha = 10^{-7},\ \lambda = (0.9)^j, H^2, \delta = 0.01.$
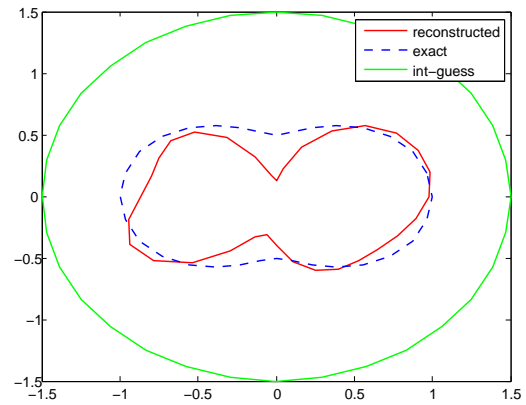
Figure 4.26: Dependence on δ

$k_0 = 1,\ k_d = 10+5i,\ J = 5,$
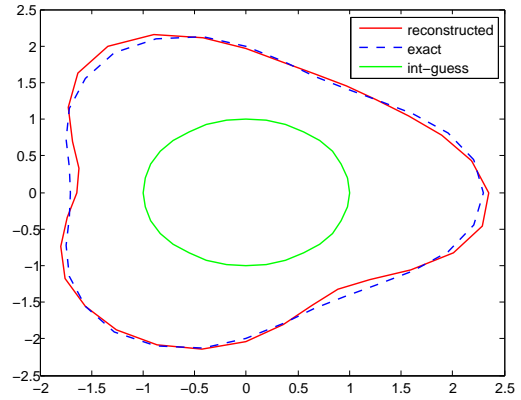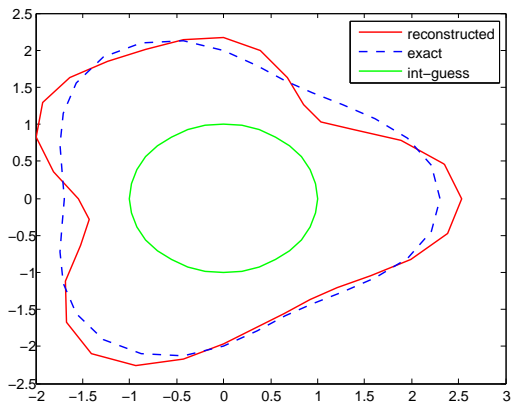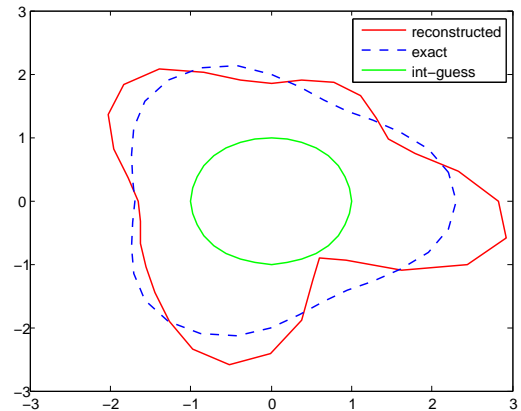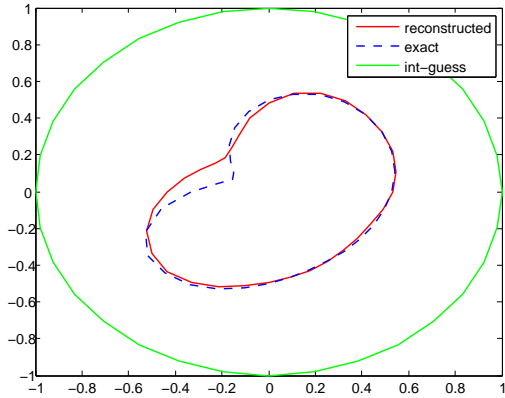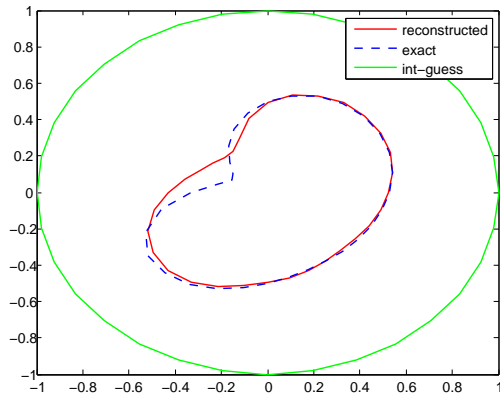$\alpha = 10^{-7}, \lambda = (0.9)^j,\ H^2,\ \delta = 0.02.$

$k_0 = 1,\ k_d = 10+5i,\ J = 5,$
$\alpha = 10^{-7},\ \lambda = (0.9)^j, H^2, \delta = 0.03.$
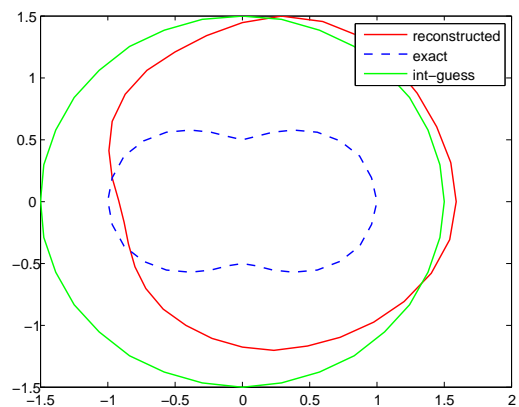
Figure 4.27: Dependence on δ

$k_0 = 1, \; k_d = 10+1i, \; J = 5$
$\alpha = 10^{-7}, \; \lambda = (0.9)^j, \; H^2, \; \delta = 0.$

$k_0 = 1, \; k_d = 10 + 1i, \; J = 5,$
$\alpha = 10^{-7}, \; \lambda = (0.9)^j, H^2, \delta = 0.002.$

Figure 4.28: Dependence on δ

$k_0 = 1, \; k_d = 10+1i, \; J = 5,$
$\alpha = 10^{-7}, \lambda = (0.9)^j, \; H^2, \; \delta = 0.003.$

$k_0 = 1, \; k_d = 10 + 1i, \; J = 5,$
$\alpha = 10^{-7}, \; \lambda = (0.9)^j, H^2, \delta = 0.005.$

Figure 4.29: Dependence on δ

$k_0 = 1, \; k_d = 10{+}10i, \; J = 10$
$\alpha = 10^{-6}, \; \lambda = (0.8)^j, \; H^2, \; \delta = 0.$

$k_0 = 1, \; k_d = 10 + 10i, \; J = 20,$
$\alpha = 10^{-6}, \; \lambda = (0.8)^j, H^2, \delta = 0.$
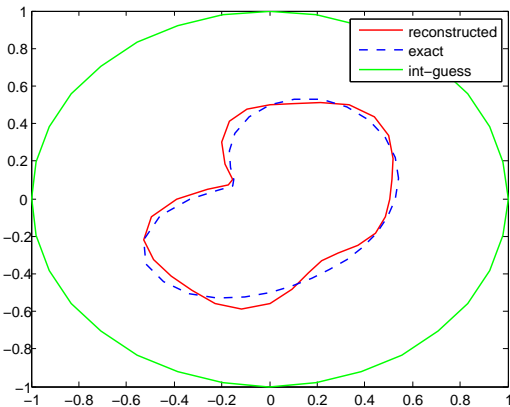
Figure 4.30: Dependence on J

$k_0 = 1, \; k_d = 10{+}10i, \; J = 5,$
$\alpha = 10^{-6}, \lambda = (0.8)^j, \; H^2, \; \delta = 0.01.$
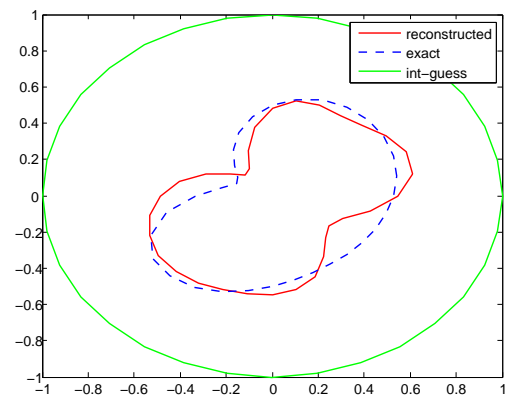
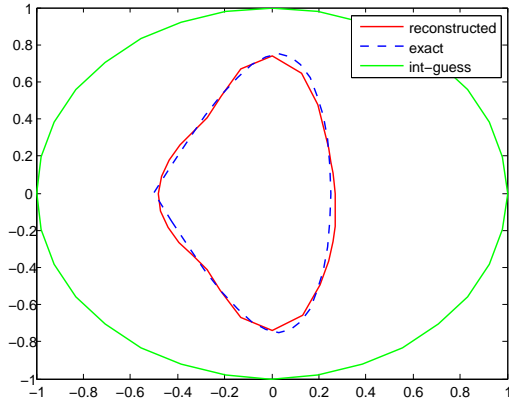$k_0 = 1, \; k_d = 10 + 10i, \; J = 5,$
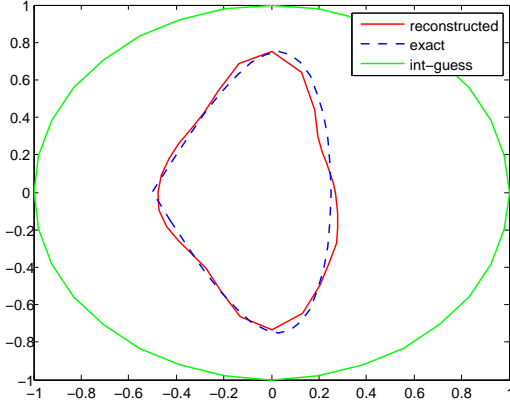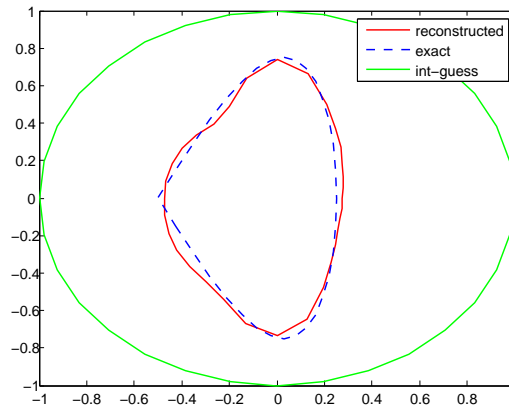$\alpha = 10^{-6}, \; \lambda = (0.8)^j, H^2, \delta = 0.02.$

Figure 4.31: Dependence on δ

$k_0 = 1,\ \ k_d = 10+1i,\ \ J = 5$
$\alpha = 10^{-5},\ \ \lambda = (0.9)^j,\ \ H^2,\ \ \delta = 0.$

$k_0 = 1,\ \ k_d = 10 + 1i,\ \ J = 5,$
$\alpha = 10^{-5},\ \ \lambda = (0.9)^j, H^2, \delta = 0.003.$

Figure 4.32: Dependence on δ

$k_0 = 1,\ \ k_d = 10+1i,\ \ J = 5,$
$\alpha = 10^{-5}, \lambda = (0.9)^j,\ \ H^2,\ \ \delta = 0.005.$

$k_0 = 1,\ \ k_d = 10 + 1i,\ \ J = 5,$
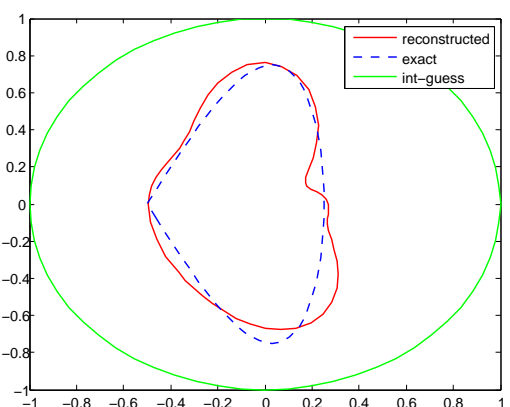$\alpha = 10^{-5},\ \ \lambda = (0.9)^j, H^2, \delta = 0.01.$
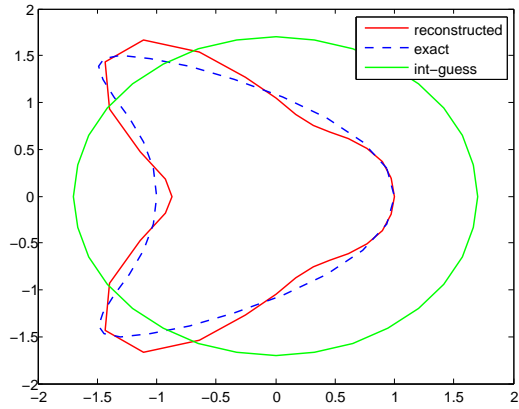

Figure 4.33: Dependence on δ

$k_0 = 1, \ k_d = 10+1i, \ J = 5$
$\alpha = 10^{-5}, \ \lambda = (0.9)^j, \ H^2, \ \delta = 0.$

$k_0 = 1, \ k_d = 10 + 1i, \ J = 20,$
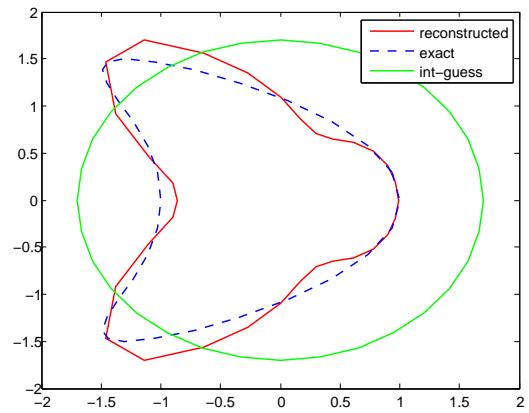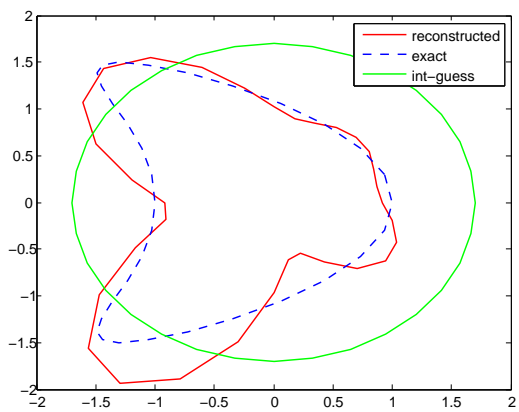$\alpha = 10^{-5}, \ \lambda = (0.9)^j, H^2, \delta = 0.$

Figure 4.34: Dependence on J

$k_0 = 1, \ k_d = 10+1i, \ J = 5,$
$\alpha = 10^{-5}, \lambda = (0.9)^j, \ H^2, \ \delta = 0.005.$

$k_0 = 1, \ k_d = 10 + 1i, \ J = 5,$
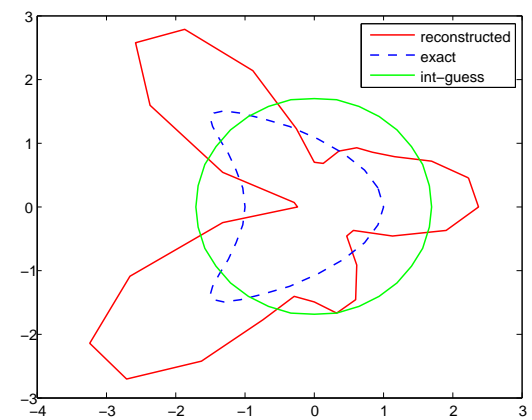$\alpha = 10^{-5}, \ \lambda = (0.9)^j, H^2, \delta = 0.01.$

Figure 4.35: Dependence on δ

To sum up, the quality of the reconstruction depends on the all parameters. To have a reasonable reconstruction, one has to choose suitable parameters and these parameters have to be selected in appropriate manner. We choose these parameters via trial and error.

Comparing the examples that are obtained by the hybrid method with examples that are obtained by Newton method (See Hohage and Schormann [15]) we observe that the hybrid method compete with the Newton method via the quality of the reconstruction. The big drawback of this method is that it is vulnerable to noise level. In the view of the quality of reconstruction, the hybrid method has almost the same quality as the simultaneous linearization method and better quality then the Johansson and Sleeman method.

We now give a general overview on the reconstructions that are obtained by the three methods that we deal with:

- Increasing the number of incident fields, or illuminations, give better reconstruction than one incident field. However, This increase does not have a significant effect on the quality of the reconstruction above some number of incident fields. We obtain almost the same quality of reconstructions with 8 and 16 incident directions, for examples.

- If the directions of incident fields are symmetric to each other then the quality of reconstruction increases.

- Reconstruction depends on initial guess. If we choose initial guess far away from the object then the reconstruction may fail. Moreover, due to the restriction on theorem (3.1.5), we should start initial guess small because of the fact that we decrease the possibility of hitting a Dirichlet eigenvalue and the methods converge to a local minimum.

- Reconstruction depends on wave numbers. The exterior wave number k_0 has to be in resonance region. If you have a dielectric scatterer with 1 meter diameter and use an incident field with 10 meter wave length, you can not obtain a reasonable reconstruction, for example.

- It seems to be enough to select degree of trigonometric polynomials $m = 5$.

- We have got reasonable reconstruction when we choose the regularization parameter λ in the range between 0.1 and 1, and increasing with each iteration step j.

- We need to select the regularization parameter α sufficiently small such as 10^{-6}.

- We have got a reasonable reconstruction when we choose H^2 penalty term.

### 4.3.4 Simultaneously Reconstruction the Shape and the Interior wave number k_d

In the following example, the table shows the reconstruction of the interior wave number k_d and the figure shows the reconstruction of a circle after 15 iteration steps. Initial guess for the interior wave number is $k_d = 5 + 3.5i$ and the exact value of it is $k_d = 6 + 3i$.

j	Re k_d	Im k_d
1	11.0395162371	1.8591428622
2	7.1262095657	0.5910320885
3	7.0605679805	0.6317525981
4	7.1183586985	0.7713567402
5	7.0978164742	1.1142157466
6	6.7877484915	1.7601039965
7	6.4182938086	2.4436691343
8	6.0756484419	2.8851109484
9	6.0007133176	2.9782074624
10	5.9963101217	2.9978738350
11	5.9987548077	3.0003488868
12	5.9997523215	3.0002332761
13	5.9999618896	3.0000776416
14	5.9999839302	3.0000316851
15	5.9999813584	3.0000238253
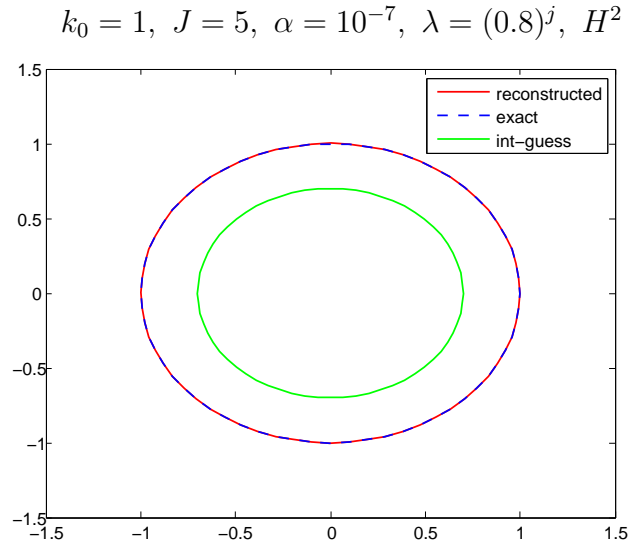
$$k_0 = 1, \ J = 5, \ \alpha = 10^{-7}, \ \lambda = (0.8)^j, \ H^2$$

In the following example, the table shows the reconstruction of the interior wave number k_d and the figure shows the reconstruction of an ellipse after 15 iteration steps. Initial guess for the interior wave number is $k_d = 5 + 3.5i$ and the exact value of it is $k_d = 6 + 3i$.

j	$\mathrm{Re}\,k_d$	$\mathrm{Im}\,k_d$
1	10.3203398376	2.5632097678
2	6.8297190825	0.6248314106
3	6.6350856304	0.7747469455
4	6.5418991220	1.0375083511
5	6.4628680240	1.5967582744
6	6.0633220487	2.4436691343
7	5.7307529586	3.1753741772
8	5.9292088043	3.0873077976
9	5.9953107737	3.0079510245
10	6.0048692420	3.0079510245
11	6.0051298619	3.0043323485
12	6.0049806286	3.0037773471
13	6.0050156114	3.0036649731
14	6.0050693251	3.0036157051
15	6.0050980299	3.0035906292

$$k_0 = 1,\ J = 5,\ \alpha = 10^{-7},\ \lambda = (0.8)^j,\ H^2$$
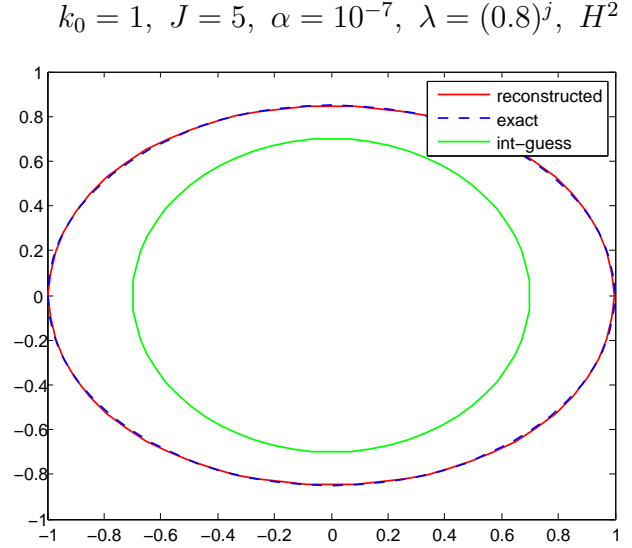
4.4   Numerical Examples via Experimental Data

The experimental system which can be seen in the photo was conducted at the faculty of Electronics and Communication of Istanbul Technical University. For a sufficiently long dielectric obstacle we used a circular cylindrical wood with radius 3 cm. In this system, the transmitter sends electromagnetic plane waves with the frequency one GHz polarized in the direction of the cylinder axis. The distance between the transmitter and the cylinder axis is one meter. The receiver is located one meter away from cylindrical wood and rotates around it and collects data. In order to decrease the reflection of the waves and noise, absorbers are settled around the system.

We used electromagnetic waves with frequency one GHz which means that the exterior wave number k_0 is equal to 20.944 and the interior wave number is taken $k_d = \sqrt{3}k_0$. Since we obtain the data from the near distance, it is required to use near field pattern instead of far field pattern. Now the data equation has to be replaced by

$$S_{k_0}\varphi_0 = A_{\Gamma_R} \tag{4.4.1}$$

where A_{Γ_R} is called near field pattern of scattered field and the index Γ_R represents a circle with radius R. It maps from the boundary ∂D to a circle Γ_R and is given by

$$A_{\Gamma_R}(x) = \int_{\partial D} \Phi_{k_0}(x,y)\varphi_0(y)ds(y) \quad x \in \Gamma_R. \tag{4.4.2}$$

The measured data or the experimental data represented by $A_{measure}$ require some calibration κ. The latter requirement is posed in the least square sense, i.e., the calibration quantity κ is chosen such that

$$g(\kappa) := \sum_{j=1}^{M}[A_{\Gamma_R}(x_j) - \kappa A_{measure}(x_j)]^2, \quad x_j \in \Gamma_R, \tag{4.4.3}$$

attains a minimal value. Here, x_j is given by $x_j = R(\cos t_j, \sin t_j)$, $t_j = \dfrac{2\pi}{M}j$ for $j = 0, \ldots, M-1$ and A_{Γ_R} represents the synthetic data obtained from direct problem for a known scatterer. The calibration factor κ consists of 60 rows and one column and is found of the form

Table 4.3: The value of calibration factor κ

rows $1 - 15$	rows $16 - 30$	rows $31 - 45$	rows $46 - 60$
1.0639 - 0.1096i	1.1242 + 0.0358i	1.0855 + 0.3213i	0.9521 - 0.1206i
1.0157 - 0.0745i	1.0910 + 0.0261i	1.0514 + 0.2847i	0.9494 - 0.1452i
0.9778 - 0.0277i	1.0416 + 0.0553i	1.0047 + 0.2103i	0.9726 - 0.1454i
0.9639 + 0.0107i	1.0051 + 0.0952i	0.9723 + 0.1540i	1.0139 - 0.1187i
0.9805 + 0.0201i	0.9967 + 0.1230i	0.9648 + 0.1278i	1.0503 - 0.0814i
1.0192 - 0.0155i	1.0140 + 0.1299i	0.9768 + 0.1193i	1.0615 - 0.0664i
1.0486 - 0.0910i	1.0354 + 0.1215i	0.9965 + 0.1062i	1.0426 - 0.0919i
1.0412 - 0.1589i	1.0359 + 0.1173i	1.0138 + 0.0715i	1.0021 - 0.1406i
1.0109 - 0.1670i	1.0114 + 0.1335i	1.0229 + 0.0190i	0.9621 - 0.1812i
0.9833 - 0.1111i	0.9811 + 0.1656i	1.0256 - 0.0299i	0.9466 - 0.1975i
0.9659 - 0.0233i	0.9684 + 0.1980i	1.0278 - 0.0559i	0.9660 - 0.1894i
0.9653 + 0.0599i	0.9824 + 0.2154i	1.0288 - 0.0570i	1.0131 - 0.1650i
0.9940 + 0.1129i	1.0010 + 0.2018i	1.0207 - 0.0501i	1.0676 - 0.1390i
1.0525 + 0.1204i	0.9697 + 0.1518i	1.0001 - 0.0572i	1.1032 - 0.1259i
1.1101 + 0.0826i	0.8579 + 0.0914i	0.9734 - 0.0850i	1.1007 - 0.1229i

In the figures 4.36 and 4.37, we compare absolute value of the calibrated measured data and the synthetic data in the direction d evaluated at 60 points. In the figures 4.38 and 4.39, we compare phase of the calibrated measured data and the synthetic data in the direction d evaluated at 60 points. The red and green curves represent the calibrated measured data and the synthetic data, respectively.

In the examples 4.40 and 4.41, we obtain a reconstruction via the calibrated measured data. The red curve represents reconstruction and the blue dashed curve represents the boundary of cross section of the wood cylinder. The left hand side of figure in 4.40 is obtained by simultaneous linearization method for one incident field with incident direction $d = (1, 0)$. From this example, we observe that reconstruction almost coincides with the exact boundary, however, the figure is a little bit shifted along the shadow region. Due to the high noise level in the experimental data, we could not obtain any reasonable reconstruction neither by the Johansson and Sleeman method nor by the hybrid method. The right hand side of 4.40, the left hand side of 4.41, and the right hand side of 4.41 figures represent examples of reconstructions obtained via the simultaneous linearization method, the Johansson and Sleeman method, and the hybrid method for four illuminations, or incident fields, respectively.
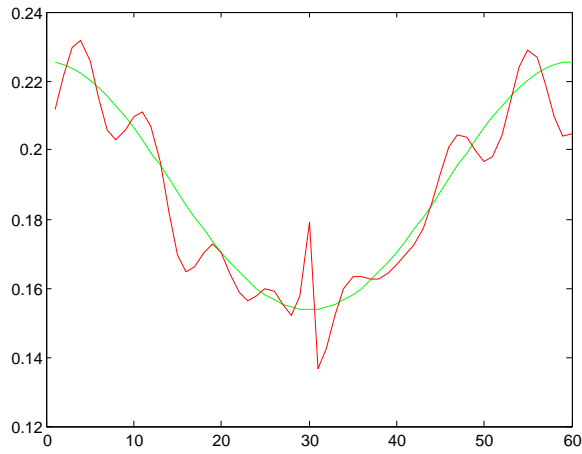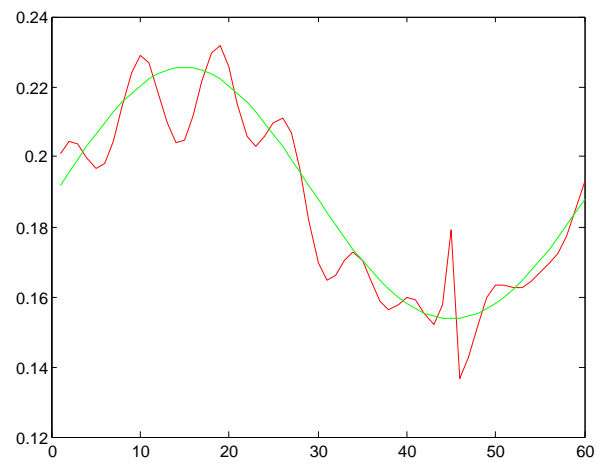
$d = (1, 0)$ $d = (0, 1)$

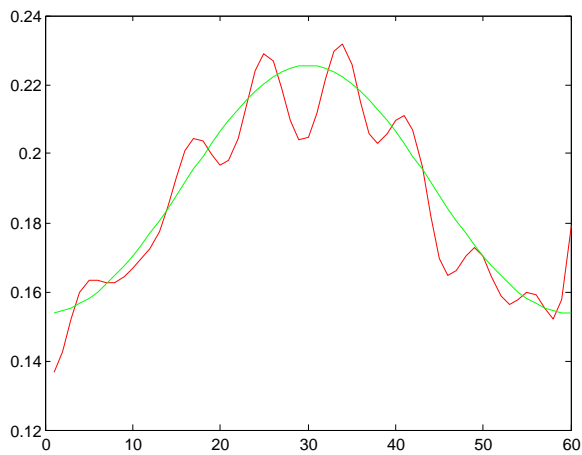Figure 4.36: Comparing absolute value of the measured and synthetic data

$d = (-1, 0)$ $d = (0, -1)$
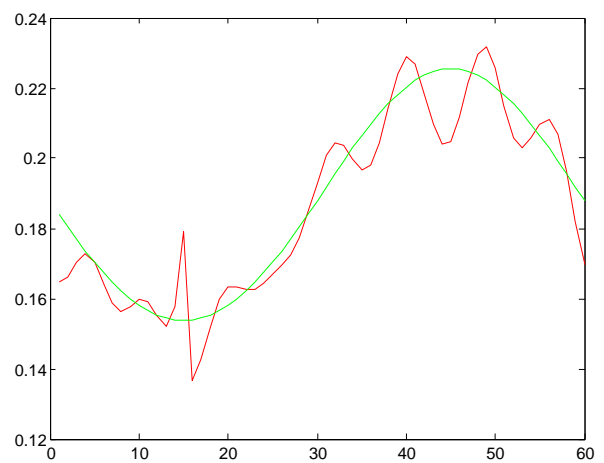
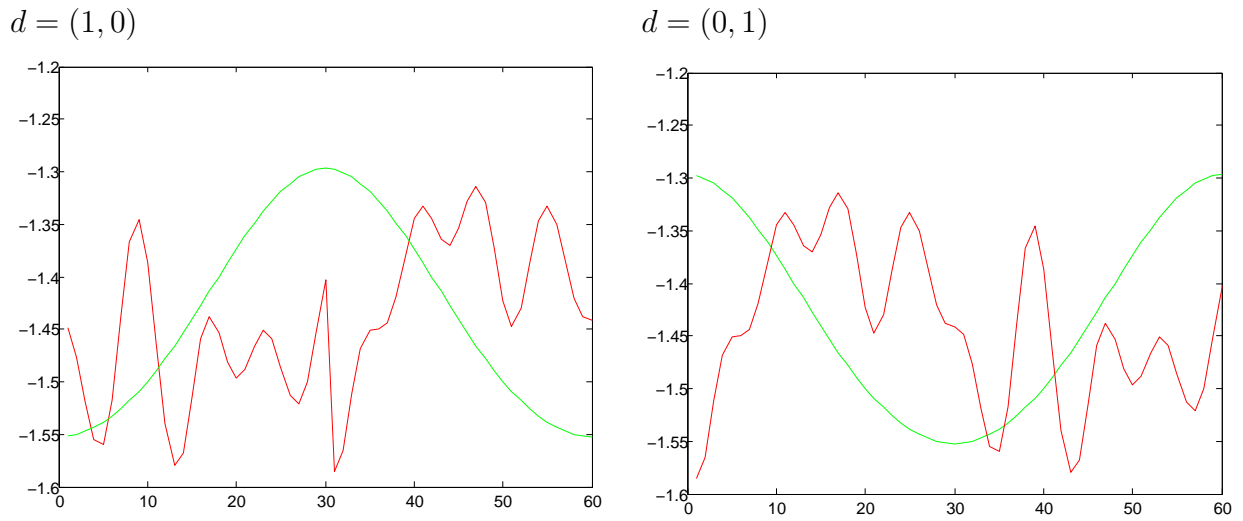Figure 4.37: Comparing absolute value of the measured and synthetic data

$d = (1, 0)$ $d = (0, 1)$

Figure 4.38: Comparing phase of the measured and synthetic data

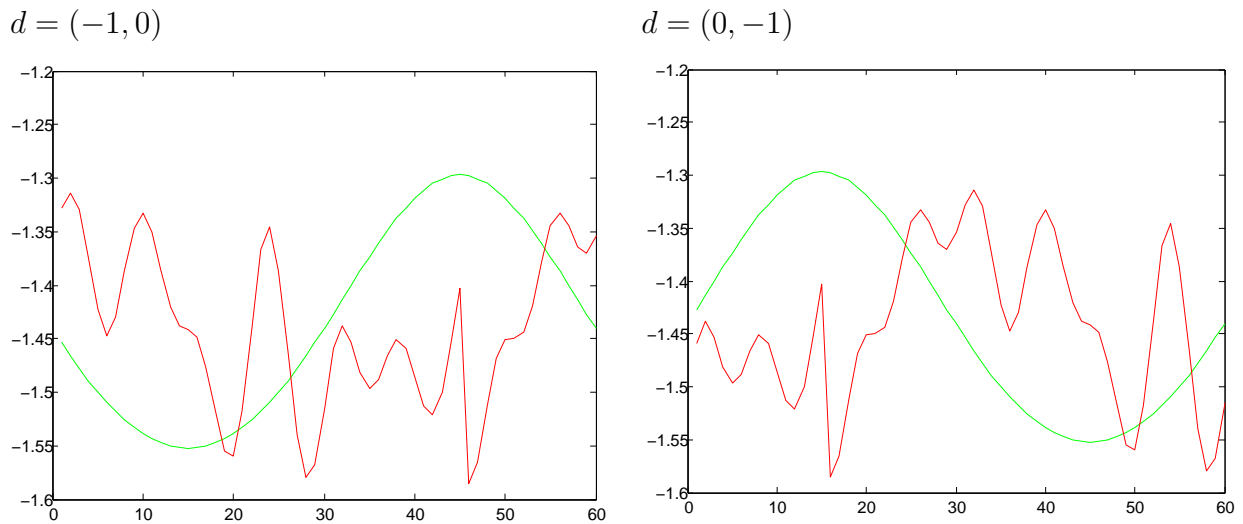$d = (-1, 0)$ $d = (0, -1)$
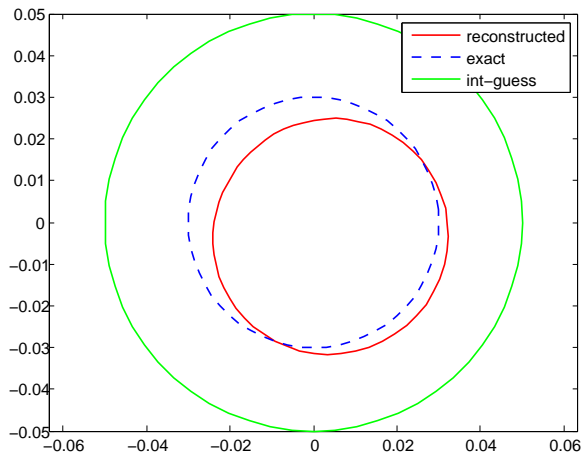

Figure 4.39: Comparing phase of the measured and synthetic data

SLM one illumination
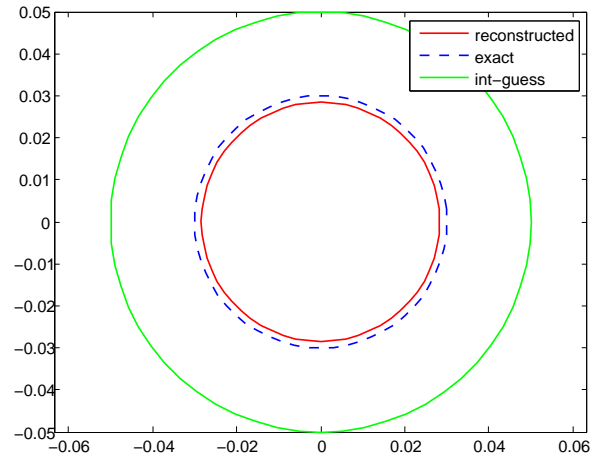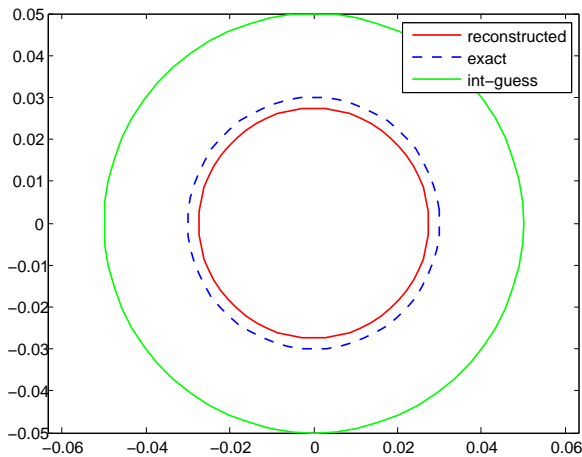
SLM four illuminations

Figure 4.40: Examples of the simultaneous linearization method(SLM) via the calibrated measured data

JS method four illuminations

Hybrid Method four illuminations
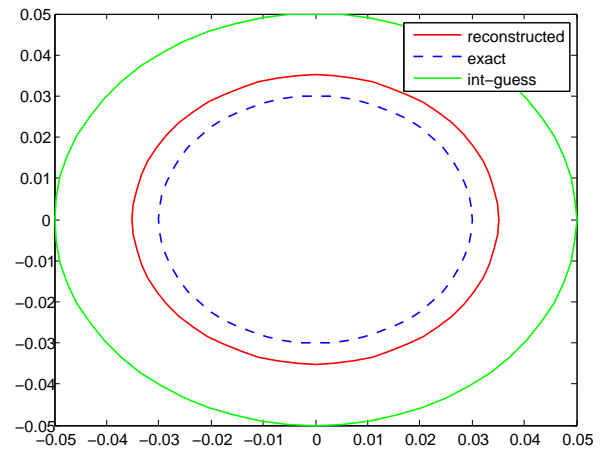

Figure 4.41: Examples of the Johansson and Sleeman(JS) and the hybrid method via the calibrated measured data

From these examples, we observe that the quality of the reconstructions are sufficiently good for all three methods and they almost coincide with exact boundary. In addition, increasing the number of incident direction has a significant effect on the quality of the reconstruction.

Chapter 5

Inverse Obstacle Scattering with Conductive Boundary Condition

5.1 The Direct Problem

Let the simply connected bounded domain $D \subset \mathbb{R}^2$ with C^2 boundary ∂D represent the cross section of an infinitely long homogeneous dielectric cylinder having constant wave number k_d with $Im\{k_d\}, \mathbb{R}e\{k_d\} \geqslant 0$ and denote the exterior wave number of background by $k_0 \in \mathbb{R}$. Denote by ν the outward unit normal vector to ∂D.

Then, given an incident plane wave $u^i = e^{ik_0 x.d}$ with incident direction given by the unit vector d, the direct scattering problem for E-polarized electromagnetic waves by a coated dielectric is modeled by the following *conductive* boundary value problem for the Helmholtz equation: Find solutions u, v to the Helmholtz equations

$$\Delta u + k_0^2 u = 0 \quad \text{in } R^2 \setminus \bar{D}, \qquad \Delta v + k_d^2 v = 0 \quad \text{in } D \qquad (5.1.1)$$

with the conductive boundary conditions

$$u = v, \qquad \frac{\partial u}{\partial \nu} = \frac{\partial v}{\partial \nu} + i\eta v \quad \text{on} \quad \partial D \qquad (5.1.2)$$

for some continuous function defined in one continuously differentiable complex valued function space $\eta \in C^1(\partial D)$ with $Re\{\eta\} \leq 0$ and where the total field is given by $u = u^i + u^s$ with the scattered wave u^s fulfilling the Sommerfeld radiation condition (1.1.3). For a more general case of conductive boundary conditions and for the $\mathbb{R}^3$ version, we refer to Gerlach and Kress [11]. The following theorem is the $\mathbb{R}^2$ version of the uniqueness result in [11].

Theorem 5.1.1 *The direct scattering problem* (5.1.1)-(5.1.2) *has at most one solution.*

Proof: Proceeding as in the proof of theorem 3.1.1, Green's theorem leads to

$$\int_{\partial B_R} u^s \frac{\partial \bar{u}^s}{\partial \nu} ds = -k_0^2 \int_{B_R} |u^s|^2 dx + \int_{B_R} |\nabla u^s|^2 dx$$
$$- \bar{k}_d^2 \int_D |v|^2 dx + \int_D |\nabla v|^2 dx - i \int_{\partial D} \bar{\eta}|v|^2 ds. \tag{5.1.3}$$

instead of (3.1.5). Taking imaginary part of (5.1.3), we obtain

$$\mathrm{Im}\{\int_{\partial B_R} u^s \frac{\partial \bar{u}^s}{\partial \nu} ds\} = 2\mathrm{Re}\{k_d\}\mathrm{Im}\{k_d\} \int_D |v|^2 dx - \int_{\partial D} \mathrm{Re}\{\eta\}|v|^2 ds. \tag{5.1.4}$$

Due to the assumption on η and k_d, the equation (5.1.4) implies that

$$\mathrm{Im}\{\int_{\partial B_R} u^s \frac{\partial \bar{u}^s}{\partial \nu} ds\} \geq 0. \tag{5.1.5}$$

Now the proof is completed as in the theorem 3.1.1. $\square$

Now we try to find the solution in the form of single-layer potentials

$$u^s(x) = \int_{\partial D} \Phi_{k_0}(x, y)\varphi_0(y) ds(y), \quad x \in \mathbb{R}^2 \backslash \bar{D},$$
$$\tag{5.1.6}$$
$$v(x) = \int_{\partial D} \Phi_{k_d}(x, y)\varphi_d(y) ds(y), \quad x \in D,$$

with $\varphi_0, \varphi_d \in H^{-1/2}(\partial D)$. From the jump relation it can be seen that the single layer potentials (5.1.6) satisfy the boundary conditions (5.1.2) provided the densities φ_0, φ_d satisfy the system of integral equation,

$$S_{k_d}\varphi_d - S_{k_0}\varphi_0 = 2u^i, \qquad x \in \partial D,$$
$$\tag{5.1.7}$$
$$\varphi_d + \varphi_0 + i\eta S_{k_d}\varphi_d + K'_{k_d}\varphi_d - K'_{k_0}\varphi_0 = 2\frac{\partial u^i}{\partial \nu}, \quad x \in \partial D.$$

Theorem 5.1.2 *Provided k_0 is not a Dirichlet eigenvalue for the domain D the system of integral equation (5.1.7) has a unique solution in $H^{-1/2}(\partial D) \times H^{-1/2}(\partial D)$.*

Proof: The proof is analogous to the proof of theorem (3.1.5). To establish a solution, we note that due to the assumption on k_0 the inverse operator

$$S_{k_0}^{-1} : H^{1/2}(\partial D) \rightarrow H^{-1/2}(\partial D),$$

exists and bounded. With its aid, if we multiply the equation (5.1.7) by the operator $S_{k_0}^{-1}$ from the left-hand-side, add and subtract φ_d we obtain

$$\varphi_d - \varphi_0 + S_{k_0}^{-1}[S_{k_d} - S_{k_0}]\varphi_d = 2S_{k_0}^{-1}u^i, \quad \text{on} \quad \partial D$$

$$\varphi_d + \varphi_0 + i\eta S_{k_d}\varphi_d + K'_{k_d}\varphi_d - K'_{k_0}\varphi_0 = 2\frac{\partial u^i}{\partial \nu}, \quad \text{on} \quad \partial D$$

(5.1.8)

We can rewrite the equations (5.1.8) in the form of

$$\mathcal{A}\begin{pmatrix} \varphi_d \\ \varphi_0 \end{pmatrix} + \mathcal{R}\begin{pmatrix} \varphi_d \\ \varphi_0 \end{pmatrix} = 2\begin{pmatrix} S_{k_0}^{-1}u^i|_{\partial D} \\ \frac{\partial u^i}{\partial \nu}\Big|_{\partial D} \end{pmatrix}$$

with the matrix operators

$$\mathcal{A}, \mathcal{R} : H^{-1/2}(\partial D) \times H^{-1/2}(\partial D) \to H^{-1/2}(\partial D) \times H^{-1/2}(\partial D)$$

given by

$$\mathcal{A} = \begin{pmatrix} I & -I \\ I & I \end{pmatrix} \quad \text{and} \quad \mathcal{R} = \begin{pmatrix} S_{k_0}^{-1}[S_{k_d} - S_{k_0}] & 0 \\ i\eta S_{k_d} + K'_{k_d} & -K'_{k_0} \end{pmatrix}.$$

Clearly, $\mathcal{A}$ has a bounded inverse (see Theorem 3.1.5). $\mathcal{R}$ is compact since it differs from the operator $\mathcal{K}$ introduced in 3.1.5 only by the additional term $i\eta S_{k_d}$ which is compact from $H^{-1/2}(\partial D)$ into $H^{-1/2}(\partial D)$. Now the proof is completed as in theorem 3.1.5. $\qquad\square$

5.1.1 Numerical Solution of The Direct Problem

For the numerical solution of (5.1.7) and the presentation of our inverse algorithm we assume that the boundary curve ∂D is represented through regular parametrization of the form

$$\partial D := \{z(t) : 0 \le t \le 2\pi\}, \tag{5.1.9}$$

where $z : \mathbb{R} \to \mathbb{R}^2$ is 2π-periodic and twice continuously differentiable function such that the orientation of ∂D is counter-clockwise. Using the parametrized single-layer operator (3.2.9) and the parametrized normal derivative of single layer operator (3.2.10) we obtain parametrized form of (5.1.7) given by

$$\widetilde{S}_{k_d}\psi_d - \widetilde{S}_{k_0}\psi_0 = 2u^i \circ z,$$

$$\psi_d + \psi_0 + i(\eta \circ z)\widetilde{S}_{k_d}\varphi_d + \widetilde{K}'_{k_d}\psi_d - \widetilde{K}'_{k_0}\psi_0 = \frac{2}{|z'|}[z']^\perp \cdot \mathrm{grad}u^i \circ z,$$

(5.1.10)

The difference between the parametrized system of integral equations (4.1.2) and (5.1.10) is that $i(\eta \circ z)\, \widetilde{S}_{k_d} \varphi_d$ additionally appears in (5.1.10). Therefore, the numerical solution of (5.1.10) requires dealing with additional term $i(\eta \circ z)\, \widetilde{S}_{k_d} \varphi_d$. Since this term has also a weakly kernel $M(t, \tau)$ which is defined in (4.1.3), we apply quadrature rules based on trigonometric interpolation and the trapezoidal rule.

We recall that the far field pattern of the single-layer potential u^s with density ψ_0 is given by

$$u_\infty(\hat{x}) = \gamma \int_0^{2\pi} e^{-ik_0\, \hat{x}\cdot z(\tau)} |z'(\tau)| \psi_0(\tau)\, d\tau, \quad \hat{x} \in \Omega, \tag{5.1.11}$$

where $\gamma = \dfrac{e^{i\frac{\pi}{4}}}{\sqrt{8\pi k_0}}$ and ψ_0 is the solution of the system of integral equations (5.1.10).

The following conductive functions are chosen in our experiments.

- $$\eta_1 = -\sin^4(0.5t) + i\cos^4(0.5t) \tag{5.1.12}$$

- $$\eta_2 = -1.5 - \sin^3 t + i\sin t \tag{5.1.13}$$

- $$\eta_3 = -0.5e^{-(t-pi)^2} + i(0.6 + 0.2\sin t) \tag{5.1.14}$$

For a numerical example, we consider the scattering of a plane wave by a dielectric cylinder with a non-convex kite-shaped cross section with boundary ∂D described by the parametric representation

$$z(t) = (\cos t + 0.65\cos 2t - 0.65, 1.5\sin t), \quad 0 \le t \le 2\pi. \tag{5.1.15}$$

Table 5.1 gives some approximate values for the far field pattern $u_\infty(d)$ and $u_\infty(-d)$ in the forward direction d and the backward direction $-d$. The direction d of the incident wave is $d = (1, 0)$ and the wave numbers are $k_0 = 2.8$ and $k_d = 1 + 1i$, and the conductive function η_1 is chosen. Note that the exponential convergence is clearly exhibited.

Table 5.1: Numerical results for direct scattering problem

n	$\operatorname{Re} u_\infty(d)$	$\operatorname{Im} u_\infty(d)$	$\operatorname{Re} u_\infty(-d)$	$\operatorname{Im} u_\infty(-d)$
8	-2.5727739209	0.4381005402	-2.4613551693	0.6118414535
16	-2.6086999117	0.5099897666	-2.4645038927	0.5815194742
32	-2.6087198359	0.5099895695	-2.4645127478	0.5815282913
64	-2.6087198065	0.5099895747	-2.4645127414	0.5815282789

5.2 The Inverse Problem

The inverse scattering problem that we are concerned with is, given the shape of the scatterer, to determine the conductive function η from a knowledge of the far field pattern for one incident wave. The inverse problem is ill-posed since the mapping taking conductive function η into the farfield pattern associated with the scattering problem (5.1.1) and (5.1.2) is highly smoothing, that is, analytic function. We will handle this issue of ill-posedness by using Tikhonov regularization. We note that the far field pattern for one incident plane wave uniquely determine the conductive function η. As a consequence of Rellich's lemma (2.3), the far field pattern uniquely determine u^s in $\mathbb{R}^2 \setminus \bar{D}$. Then from the first condition in (5.1.2) using $\operatorname{Im} k_d > 0$ we observe that v is also uniquely determined in D. From (5.1.2) we can read off the uniqueness of conductive function η. If we assume that ∂D is analytic since in this case v can not vanish on open intervals of ∂D.

The inverse scattering problem is formulated as follows: Given the far field pattern u_∞ for one incident field u^i, determine the conductive function η of the dielectric scatterer D.
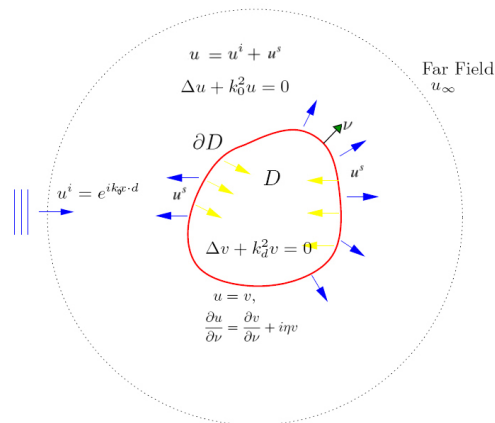
We proceed describing an algorithm for approximately solving the inverse scattering problem by extending the methods proposed by Kress and Serranho[38], and for the reconstruction of the conductive function η we implement the method proposed by Akduman and Kress in [1]. For an conductive cylinder buried in a dielectric cylinder was studied by Akduman, Kress, Yaman, and Yapar [2]. After introducing the far field operator (3.2.5), from (3.1.20) and (5.1.11) we observe that the far field

pattern for the solution to the scattering problem (5.1.1)–(5.1.2) is given by

$$u_\infty = S_\infty \varphi_0 \tag{5.2.1}$$

in terms of the solution to (5.1.7). Therefore we can state the following theorem as theoretical basis of our inverse algorithm.

Theorem 5.2.1 *For a given incident field u^i and a given far field pattern u_∞, assume that conductive function η and the densities φ_d and φ_0 satisfy the system of three integral equations*

$$S_{k_d}\varphi_d - S_{k_0}\varphi_0 = 2u^i,$$

$$\varphi_d + \varphi_0 + i\eta S_{k_d}\varphi_d + K'_{k_d}\varphi_d - K'_{k_0}\varphi_0 = 2\,\frac{\partial u^i}{\partial \nu}\,, \tag{5.2.2}$$

$$S_\infty \varphi_0 = u_\infty.$$

Then η solves the inverse problem.

Given the far field pattern u_∞, the density φ_0 is found by solving the third equation in (5.2.2), i.e., the data equation

$$S_\infty \varphi_0 = u_\infty. \tag{5.2.3}$$

Since the operator $S_\infty : L^2(\partial D) \to L^2(\Omega)$ is compact, it can not have bounded inverse. Therefore the equation (5.2.3) is ill-posed. Moreover, it is severely ill-posed due to analytical kernel of S_∞. Hence the equation (5.2.3) requires stabilization for this we use Tikhonov regularization, i.e., the ill-posed equation (5.2.3) is replaced by

$$\alpha\varphi + S_\infty^* S_\infty \varphi = S_\infty^* u_\infty, \tag{5.2.4}$$

with some positive regularization parameter α and the adjoint operator $S^* : L^2(\Omega) \to L^2(\partial D)$ of S_∞.
After finding the density φ_0 from the (5.2.4) we can now find density φ_d from the first equation of (5.2.2).

$$\varphi_d = S_{k_d}^{-1}(2u^i - S_{k_d}\varphi_0) \tag{5.2.5}$$

Now it remains to find the conductive function η from the second equation of (5.2.2).

$$\eta = -i\frac{2\frac{\partial u^i}{\partial \nu} - \varphi_0 - \varphi_d - K'_{k_d}\varphi_d + K'_{k_0}\varphi_0}{S_{k_d}\varphi_d} \tag{5.2.6}$$

The reconstruction of the conductive function from equation (5.2.6) will be sensitive to errors due to the fact that it blows up in the vicinity of zeros of the $S_{k_d}\varphi_d$. To

obtain a more stable solution (see [1]), we express the unknown conductive function in terms of some basis functions μ_j, $j = 0, \mp 1, \mp 2, \ldots, \mp N$ as a linear combination

$$\eta = \sum_{j=-N}^{N} a_j \mu_j \quad \text{on} \quad \partial D. \tag{5.2.7}$$

A possible choice of basis functions consists of splines or trigonometric polynomials. We satisfy second equation of (5.2.2) in a least square sense, i.e., we determine the coefficients $a_{-N}, \ldots, a_N$ in (5.2.7) such that for a set of grid points $x_1, \ldots, x_M$ on ∂D the least square sum

$$\sum_{m=1}^{M} |\varphi_d(x_m) + \varphi_0(x_m) + i \sum_{j=-N}^{N} a_j \mu_j(x_m) S_{k_d} \varphi_d(x_m) + K'_{k_d} \varphi_d(x_m) - K'_{k_0} \varphi_0(x_m) - \frac{\partial u^i}{\partial \nu}(x_m)|^2$$

$$\tag{5.2.8}$$

is minimized.

5.3 Numerical Result via Synthetic Data

For the numerical examples we choose the number of incident plane wave M. There are six parameters which effect quality of reconstruction. They are given as follows;

- interior and exterior wave numbers are represented by k_d and k_0 respectively,

- degree of trigonometric polynomials is represented by J,

- regularization parameter which uses for the boundary is represented by λ,

- regularization parameter which uses for the densities is represented by α,

- Sobolev norm for conductive function is represented by H^p,

- noise level is represented by δ. In order to obtain noisy data, random errors are added point-wise to u_∞,

$$\widetilde{u}_\infty = u_\infty + \delta\xi\frac{||u_\infty||}{|\xi|} \tag{5.3.1}$$

where the random variable $\xi \in C$ and $\{Re\xi, Im\xi\} \in (0,1)$

In the following all examples, the green curve represents exact graph of conductive function η, the blue curve represents reconstruction that is obtained by noisy data and the red curve represents reconstruction that is obtained by noiseless data.

In the figures 5.1, 5.2, 5.9 and 5.10, the obstacle is apple-shaped scatterer and the conductive functions η_1 and η_2 given in (5.1.12) and (5.1.13) are reconstructed. In the figures 5.3, 5.4, 5.11 and 5.12, the obstacle is kite-shaped and the conductive functions η_1 and η_2 given in (5.1.12) and (5.1.13) are reconstructed. In the examples 5.5, 5.6, 5.13 and 5.14, the obstacle is peanut-shaped and the conductive functions η_1 and η_3 given in (5.1.12) and (5.1.14) are reconstructed, respectively. In the examples 5.7, 5.8, 5.15 and 5.16, the obstacle is rounded-shaped and the conductive functions η_1 and η_2 given in (5.1.12), (5.1.13) and (5.1.14) are reconstructed. The reconstructions are obtained with the parameters which is written above each pair of the figures.

$k_0 = 4.8, \ k_d = 2 + 2.5i, \ J = 10 \quad \alpha = 10^{-7}, \ \lambda = 8, \ H^2, \ \delta = 0.003$

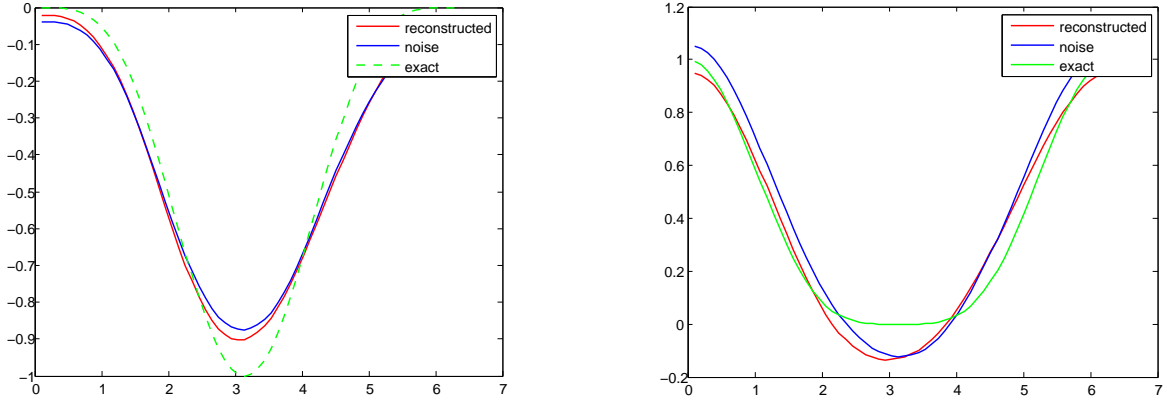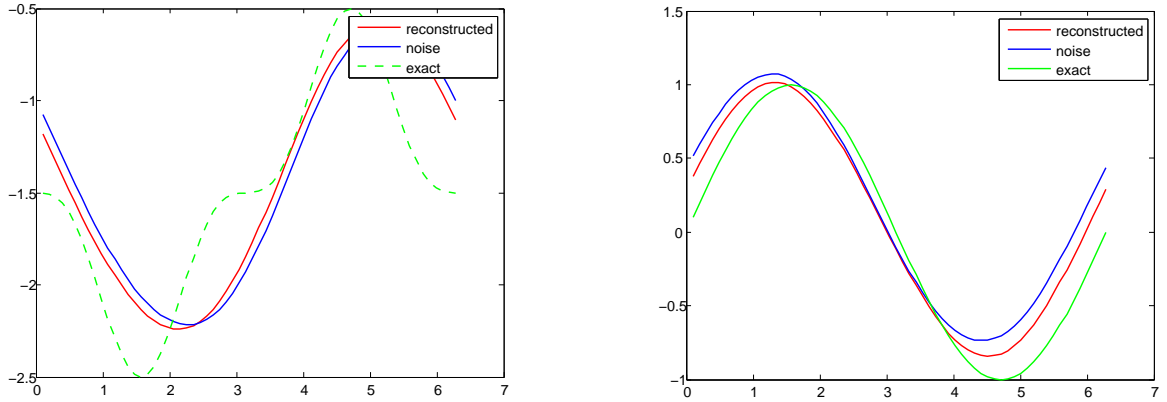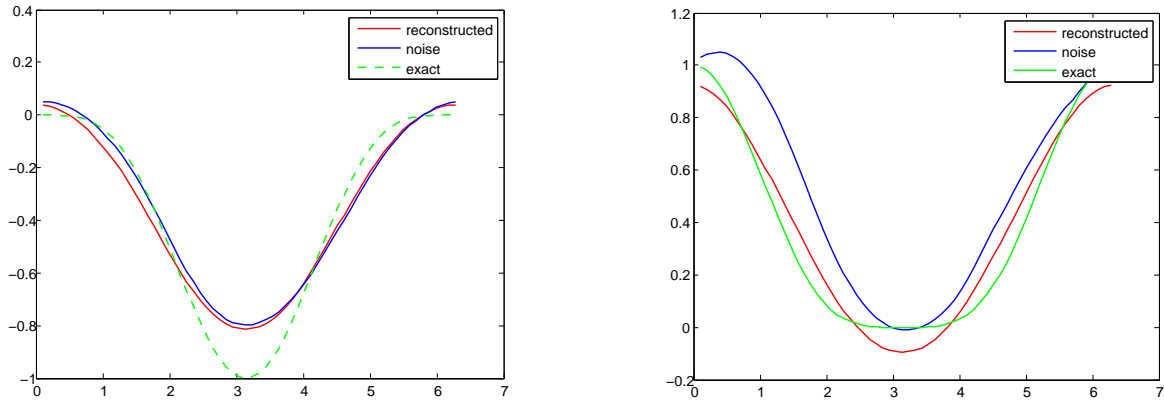Figure 5.1: Real part of η_1 on left & Imaginary part of η_1 on right, which are obtained for one incident field, i.e., M=1

$k_0 = 4.8, \ k_d = 2 + 2.5i, \ J = 10 \quad \alpha = 10^{-7}, \ \lambda = 5, \ H^2, \ \delta = 0.003$

Figure 5.2: Real part of η_2 on left & Imaginary part of η_2 on right, which are obtained for one incident field, i.e., M=1

$k_0 = 4.8, \; k_d = 2 + 2.5i, \; J = 10 \quad \alpha = 10^{-8}, \; \lambda = 6, \; H^2, \; \delta = 0.002$

Figure 5.3:   Real part of η_1 on left & Imaginary part of η_1 on right, which are obtained for one incident field, i.e., M=1

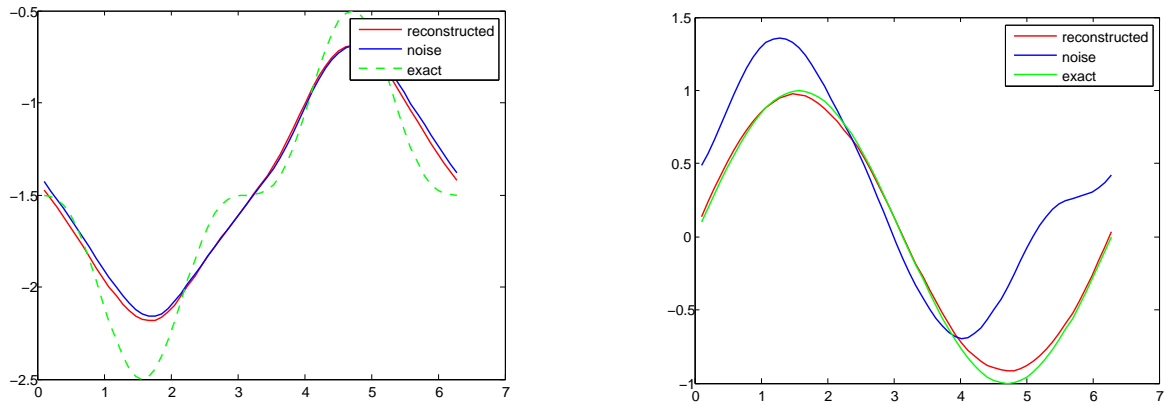$k_0 = 4.8, \; k_d = 2 + 2.5i, \; J = 10 \quad \alpha = 10^{-8}, \; \lambda = 1, \; H^2, \; \delta = 0.002$

Figure 5.4:   Real part of η_2 on left & Imaginary part of η_2 on right, which are obtained for one incident field, i.e., M=1

$k_0 = 5,\ k_d = 2 + 2.5i,\ J = 10\quad \alpha = 10^{-7},\ \lambda = 5,\ H^2,\ \delta = 0.002$
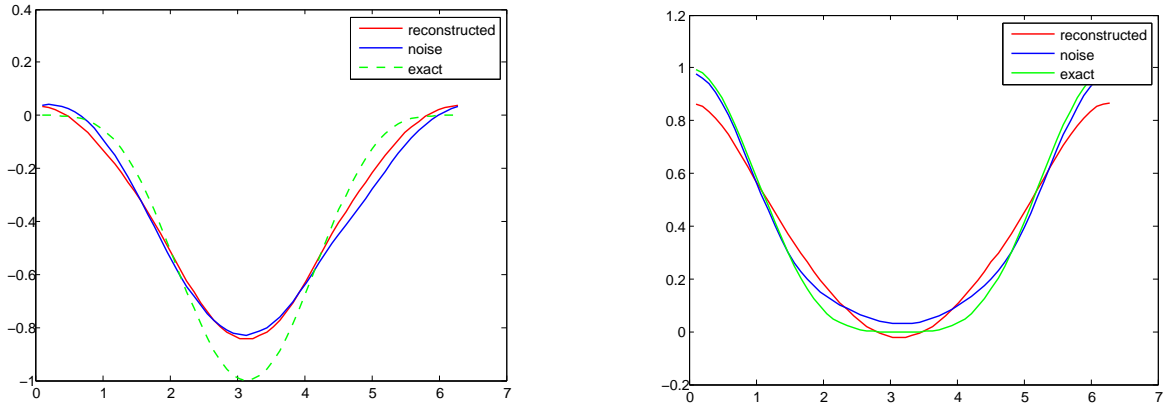

Figure 5.5:   Real part of η_1 on left & Imaginary part of η_1 on right, which are obtained for one incident field, i.e., M=1

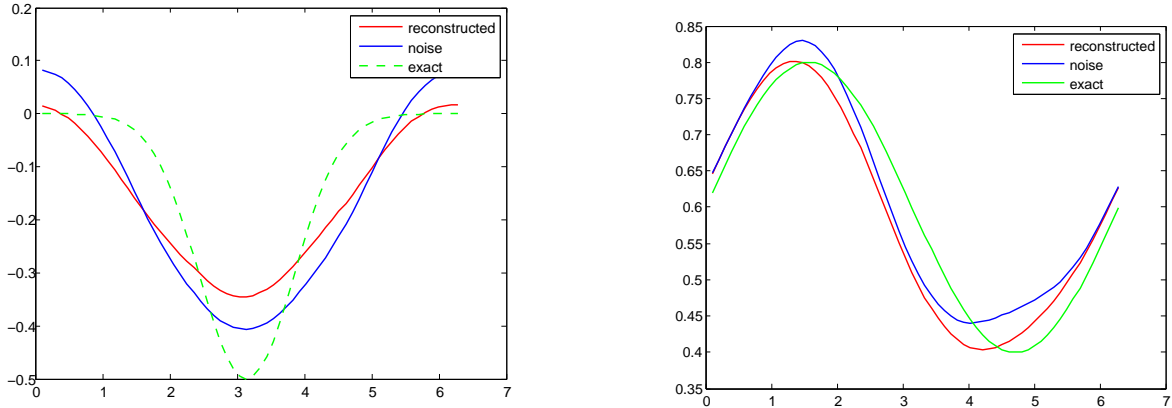$k_0 = 5,\ k_d = 2 + 2.5i,\ J = 10\quad \alpha = 10^{-7},\ \lambda = 5,\ H^2,\ \delta = 0.002$

Figure 5.6:   Real part of η_3 on left & Imaginary part of η_3 on right, which are obtained for one incident field, i.e., M=1

$k_0 = 5, \ k_d = 2.5 + 2i, \ J = 10 \quad \alpha = 10^{-8}, \ \lambda = 1.2, \ H^2, \ \delta = 0.001$

Figure 5.7:   Real part of η_2 on left & Imaginary part of η_2 on right, which are obtained for one incident field, i.e., M=1

$k_0 = 5, \ k_d = 2.5 + 2i, \ J = 10 \quad \alpha = 10^{-8}, \ \lambda = 1.2, \ H^2, \ \delta = 0.001$

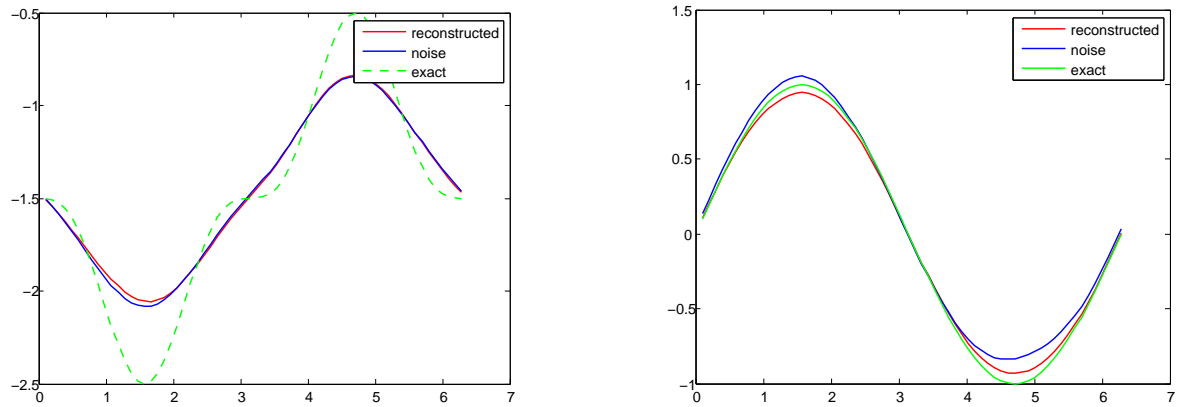Figure 5.8:   Real part of η_3 on left & Imaginary part of η_3 on right, which are obtained for one incident field, i.e., M=1

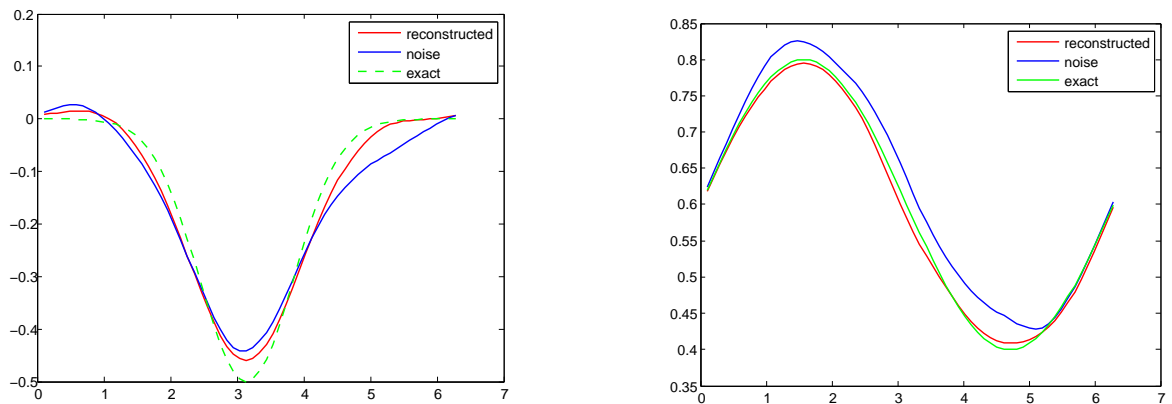$k_0 = 4, \ k_d = 2 + 2i, \ J = 5 \quad \alpha = 10^{-7}, \ \lambda = 1, \ H^2, \ \delta = 0.003$

Figure 5.9:   Real part of η_1 on left & Imaginary part of η_1 on right, which are obtained for one incident field, i.e., M=8

$k_0 = 4, \ k_d = 2 + 2i, \ J = 5 \quad \alpha = 10^{-7}, \ \lambda = 1, \ H^2, \ \delta = 0.003$
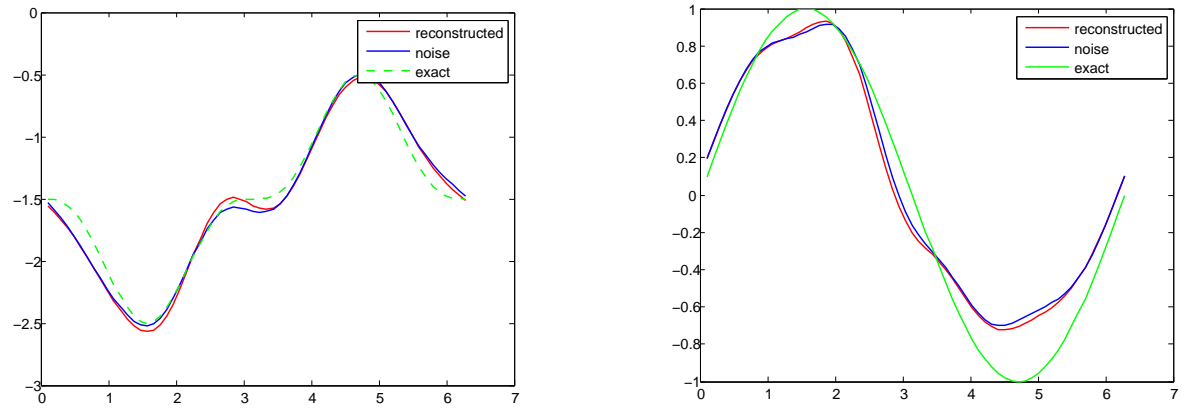
Figure 5.10:   Real part of η_2 on left & Imaginary part of η_2 on right, which are obtained for one incident field, i.e., M=8

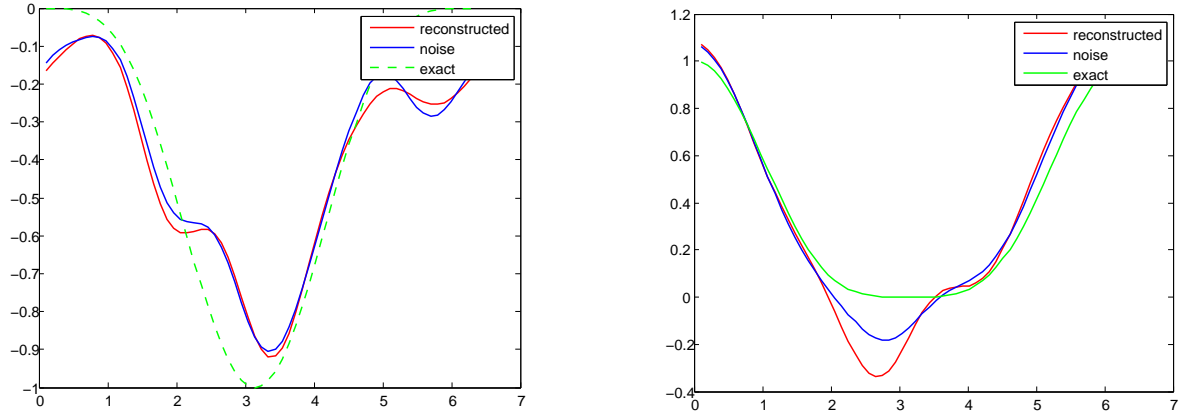$k_0 = 2.8, \; k_d = 1 + 1i, \; J = 5 \;\; \alpha = 10^{-8}, \; \lambda = 0.6, \; H^2, \; \delta = 0.003$

Figure 5.11:   Real part of η_1 on left & Imaginary part of η_1 on right, which are obtained for one incident field, i.e., M=8

$k_0 = 2.8, \; k_d = 1 + 1i, \; J = 5 \;\; \alpha = 10^{-8}, \; \lambda = 0.6, \; H^2, \; \delta = 0.003$

Figure 5.12:   Real part of η_2 on left & Imaginary part of η_2 on right, which are obtained for one incident field, i.e., M=8

$k_0 = 4.5, \; k_d = 1.5 + 1.5i, \; J = 5 \;\; \alpha = 10^{-7}, \; \lambda = 0.8, \; H^2, \; \delta = 0.003$

Figure 5.13:   Real part of η_1 on left & Imaginary part of η_1 on right, which are obtained for one incident field, i.e., M=8

$k_0 = 4.5, \; k_d = 1.5 + 1.5i, \; J = 5 \;\; \alpha = 10^{-7}, \; \lambda = 0.8, \; H^2, \; \delta = 0.003$

Figure 5.14:   Real part of η_3 on left & Imaginary part of η_3 on right, which are obtained for one indent field, i.e., M=8

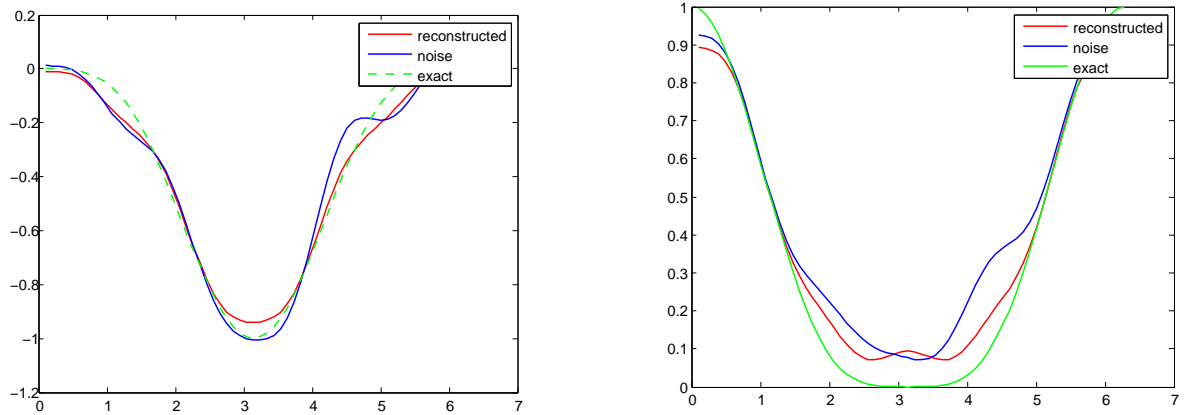$k_0 = 3.5, \ k_d = 2.5 + 2.5i, \ J = 5 \ \ \alpha = 10^{-7}, \ \lambda = 1.2, \ H^2, \ \delta = 0.003$
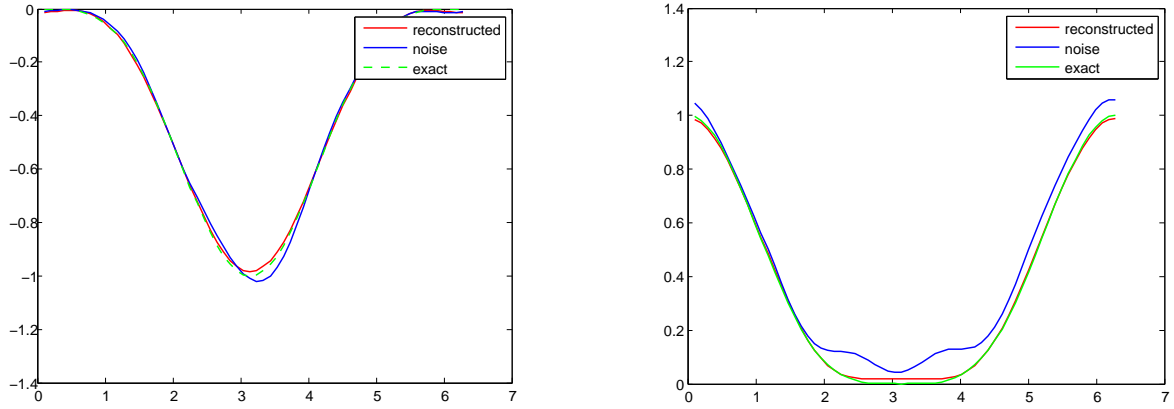
Figure 5.15:   Real part of η_1 on left & Imaginary part of η_1 on right, which are obtained for one indent field, i.e., M=8

$k_0 = 3.5, \ k_d = 2.5 + 2.5i, \ J = 5 \ \ \alpha = 10^{-7}, \ \lambda = 1.2, \ H^2, \ \delta = 0.003$

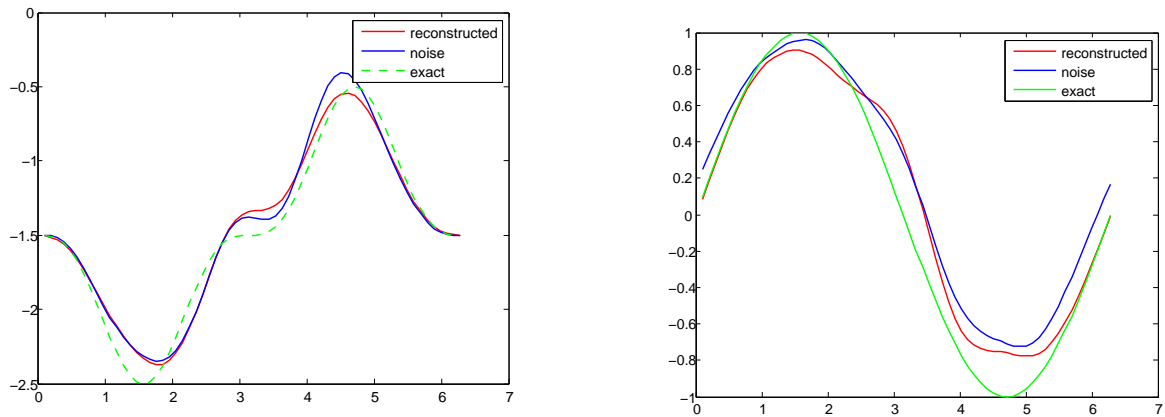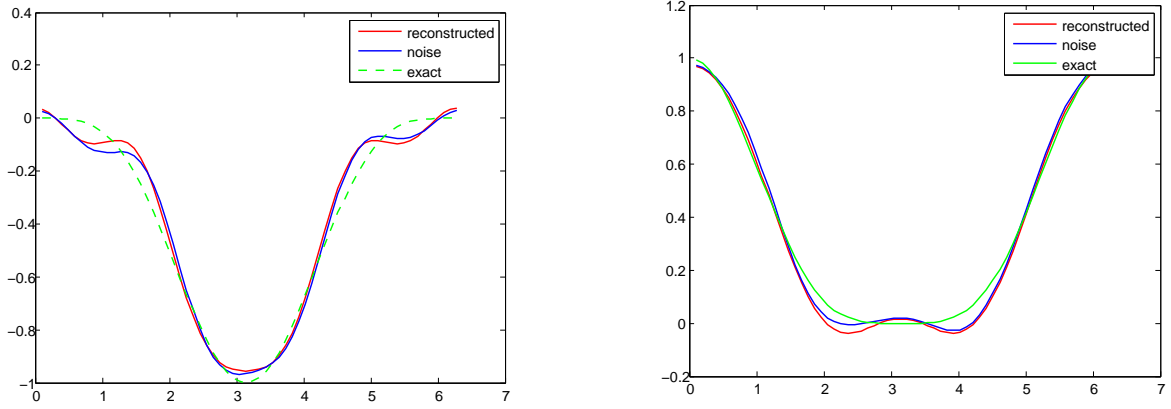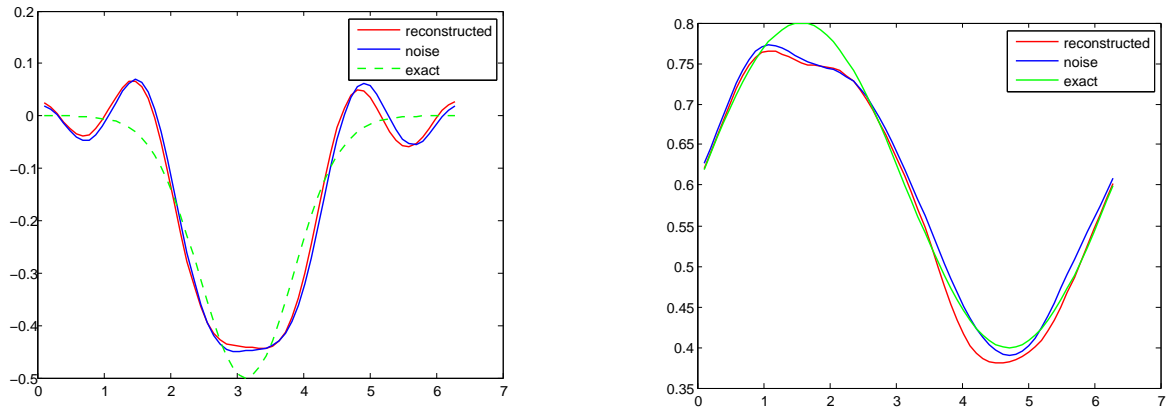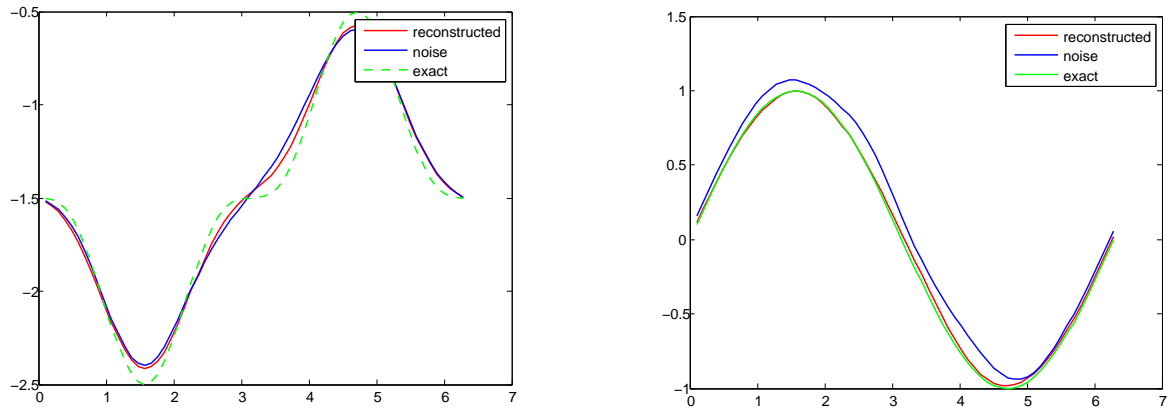Figure 5.16:   Real part of η_2 on left & Imaginary part of η_2 on right, which are obtained for one indent field, i.e., M=8

To sum up, we first note that the quality of reconstruction depends significantly on parameters. In order to obtain a reasonable reconstruction, one has to choose appropriate parameters. We select these parameters by trial and error. Form all examples we observe that quality of reconstructions is satisfactory. We also see that hybrid method is sensitive to noise level for reconstruction a conductive function. From the all examples, we see that the quality of the reconstruction increases when we use 8 incident fields with distinct directions, i.e., M=8.

Chapter 6

Discussion and Outlook

In this thesis, we extended three numerical methods in inverse obstacle scattering from the case of impenetrable obstacles to the case of penetrable obstacles, that is, dielectrics. These three methods are the Johansson and Sleeman method [25], the simultaneous linearization method due to Ivanyshyn, Kress and Rundell [19, 21, 23, 32, 36] and a hybrid method due to Kress and Serranho [32, 37, 38, 45]. In particular, we illustrated the numerical feasibility of these methods by a number of examples. Moreover, we compared the numerical reconstructions obtained from these methods with those from the Newton iteration method [15] for the boundary to far field map. We also investigated interrelations between the Newton type iterations and the above three methods. In addition, we gave a new uniqueness result for recovering a disc from the far field pattern for scattering of one incident plane wave.

All three methods are based on a system of three integral equations for the parameterization of the unknown boundary of the scatterer and two densities on the boundary. The three iterative procedures differ with respect to which of the three equations are linearized and in which order. The Johansson and Sleeman method is the simplest of the three methods and the most easy to implement since it only linearizes the data equation. However, the quality of its reconstructions is not as good as for the hybrid and simultaneous linearization method. In the simultaneous linearization method all three equations are linearized with respect to all three unknowns. From the three methods it yields the best reconstructions and their quality compares well with the reconstructions obtained with the Newton iterations for the boundary to far field map (see [15]) at decreased computational cost because of a simpler form to the Fréchet derivatives that are involved. However, from the three methods considered in this thesis it is the most costly computational wise. The simultaneous linearization method can tolerate more noise than the Johansson and Sleeman method.

The hybrid method linearizes only two equations and therefore is sort of in between both methods from its design and its performance both for accuracy, compu-

tational cost and tolerance to noise. All three methods require good initial guesses for the unknown boundary.

As is mentioned in this manuscript, there are no general uniqueness or even local uniqueness results available for inverse transmission scattering problems for one or a finite number of incident waves. In this thesis, a new uniqueness result is proved for the inverse scattering from a dielectric disc for one incident wave.

The reconstructions obtained for experimental data are sufficiently good when we used four incident fields. However, when we used only one incident direction we could only obtain a reasonable reconstruction by the simultaneous linearization method. This is because the simultaneous linearization tolerates higher noise level then the other methods. Further research is required to make the methods also work for more complex geometries such as apple-shaped or peanut-shaped scatterers via experimental data.

In principle, our methods can be extended to the three-dimensional case and to related problems such as multiple inclusions of dielectric cylinders or buried dielectrics.

In the last problem of this thesis we considered a transmission problem with a conductive boundary condition where the inverse problem was to reconstruct the conductive function. One can also extend this inverse scattering problem to a simultaneous reconstruction of the conductive function and the shape of the scatterer. Similar problems have recently been considered by Kress and Rundell [35] and Serranho [44] for impenetrable scatterers. Uniqueness in inverse obstacle scattering with the conductive boundary condition was established by Gerlach and Kress [11]. However, again there is no uniqueness result for one or finitely many incident fields for conductive transmission problem.

Bibliography

[1] I. AKDUMAN AND R. KRESS, *Direct and inverse scattering problems for in-homogeneuos impedance cylinders of abritrary shape.*, Radio Sci., 38 (2003), pp. 1055–1064.

[2] I. AKDUMAN, R. KRESS, F. YAMAN, AND A. YAPAR, *Inverse scattering for an impedance cylinder buried in a dielectric cylinder*, Inverse Problems in Science and Engineering, 17 (2009), pp. 473–488.

[3] A. ALTUNDAG AND R. KRESS, *On a two-dimensional inverse scatterering problem for a dielectric*, Applicable Analysis, (2011), pp. 1–15.

[4] F. CAKONI, D. GINTIDES, AND H. HADDAR, *The existence of the an infinite discrete set of transmission eigenvalues*, SIAM J. Math. Anal., 42 (2010), pp. 237–255.

[5] D. COLTON AND A. KIRSCH, *A simple method for solving inverse scattering problems in the resonance region*, Inverse Problems, 12 (1996), pp. 383–393.

[6] D. COLTON AND R. KRESS, *Integral equation methods in scattering theory*, Pure and Applied Mathematics (New York), John Wiley & Sons Inc., New York, 1983.

[7] D. COLTON AND R. KRESS, *Inverse acoustic and electromagnetic scattering theory*, vol. 93 of Applied Mathematical Sciences, Springer-Verlag, Berlin, second ed., 1998.

[8] D. COLTON AND P. MONK, *A novel method for solving the inverse scattering problem for time-harmonic acoustic waves in the resonance region*, SIAM J. Appl. Math., 45 (1985), pp. 1039–1053.

[9] D. COLTON AND P. MONK, *A novel method for solving the inverse scattering problem for time-harmonic acoustic waves in the resonance region. II*, SIAM J. Appl. Math., 46 (1986), pp. 506–523.

[10] D. COLTON AND B. D. SLEEMAN, *Uniqueness theorems for the inverse problem of acoustic scattering*, IMA J. Appl. Math., 31 (1983), pp. 253–259.

[11] T. GERLACH AND R. KRESS, *Uniqueness in inverse obstacle scattering with conductive boundary condition*, Inverse Problems, 12 (1996), pp. 619–625.

[12] D. GINTIDES, *Local uniqueness for the inverse scattering problem in acoustics via the Faber-Krahn inequality*, Inverse Problems, 21 (2005), pp. 1195–1205.

[13] T. HOHAGE, *Newton–verfahren beim inversen neumann–problem zur helmholtz–gleichung.*, Göttingen, Univ., Dipl.-Arb., (1996).

[14] T. HOHAGE, *Logarithmic convergence rates of the iteratively regularized Gauss-Newton method for an inverse potential and an inverse scattering problem*, Inverse Problems, 13 (1997), pp. 1279–1299.

[15] T. HOHAGE AND C. SCHORMANN, *A newton-type method for a transmission problem in iverse scattering.*, Inverse Problems, 14 (1998), pp. 1207–1227.

[16] M. IKEHATA, *Reconstruction of an obstacle from the scattering amplitude at a fixed frequency*, Inverse Problems, 14 (1998), pp. 949–954.

[17] V. ISAKOV, *On uniqueness in the inverse transmission scattering problem*, Comm. Partial Differential Equations, 15 (1990), pp. 1565–1587.

[18] I. IVANYSHYN, R. KRESS, AND P. SERRANHO, *Huygens' principle and iterative methods in inverse obstacle scattering*, Adv Comput Math, 33 (2009), pp. 413–429.

[19] O. IVANYSHYN, *Nonlinear boundary integral equations in inverse scattering*, PhD thesis, University of Göttingen, (2007).

[20] O. IVANYSHYN AND T. JOHANSSON, *Boundary integral equations for acoustical inverse sound-soft scattering*, J. Inverse Ill-Posed Probl., 15 (2007), pp. 1–14.

[21] O. IVANYSHYN AND R. KRESS, *Nonlinear integral equations for solving inverse boundary value problems for inclusions and cracks*, J. Integral Equations Appl., 18 (2006), pp. 13–38.

[22] O. IVANYSHYN AND R. KRESS, *Nonlinear integral equations in inverse obstacle scattering*, Mathematical Methods in Scattering Theory and Biomedical Engineering (Fotiatis, Massalas, eds), (2006), pp. 39–50.

[23] O. IVANYSHYN AND R. KRESS, *Inverse scattering for planar cracks via nonlinear integral equations*, Math. Meth. Appl. Sciences, doi (2007), p. 10.1002/mma.970.

[24] J.HADAMARD, *Lectures on Cauchy's Problem in Linear Partial Differential Equations.*, New York , Dover, 1952.

[25] T. JOHANSSON AND B. D. SLEEMAN, *Reconstruction of an acoustically sound-soft obstacle from one incident field and the far field pattern*, IMA J. Appl. Math., 72 (2007), pp. 96–112.

[26] J. JOST, *Postmodern analysis*, Universitext, Springer-Verlag, Berlin, second ed., 2003.

[27] A. KIRSCH, *Characterization of the shape of a scattering obstacle using the spectral data of the far field operator*, Inverse Problems, 14 (1998), pp. 1489–1512.

[28] A. KIRSCH AND R. KRESS, *Uniqueness in inverse obstacle scattering*, Inverse Problems, 9 (1993), pp. 285–299.

[29] R. KRESS, *On the numerical solution of a hypersingular integral equation in scattering theory*, J. Comput. Appl. Math., 61 (1995), pp. 345–360.

[30] R. KRESS, *Integral equation methods in inverse acoustic and electromagnetic scattering*, in Boundary integral formulations for inverse analysis, Adv. Bound. Elem. Ser., Comput. Mech., Southampton, 1997, pp. 67–92.

[31] R. KRESS, *Linear integral equations*, vol. 82 of Applied Mathematical Sciences, Springer-Verlag, New York, second ed., 1999.

[32] R. KRESS, *Newton's method for inverse obstacle scattering meets the method of least squares*, Inverse Problems, 19 (2003), pp. S91–S104. Special section on imaging.

[33] R. KRESS, *Uniqueness and numerical methods in inverse obstacle scattering*, Proceedings of the Conference on Inverse Problems in Applied Sciences, (2006).

[34] R. KRESS AND G. ROACH, *Transmission problem for the helmholtz equation*, J. Math. Phys., 19 (1978), pp. 1433–1437.

[35] R. KRESS AND W. RUNDELL, *Inverse scattering for shape and impedance*, Inverse Problems, 17 (2001), pp. 1075–1085. Special issue to celebrate Pierre Sabatier's 65th birthday (Montpellier, 2000).

[36] R. KRESS AND W. RUNDELL, *Nonlinear integral equations and the iterative solution for an inverse boundary value problem*, Inverse Problems, 21 (2005), pp. 1207–1223.

[37] R. KRESS AND P. SERRANHO, *A hybrid method for two-dimensional crack reconstruction*, Inverse Problems, 21 (2005), pp. 773–784.

[38] R. KRESS AND P. SERRANHO, *A hybrid method for sound-hard obstacle reconstruction*, J. Comput. Appl. Math., 204 (2007), pp. 418–427.

[39] R. KRESS AND I. SLOAN, *On the numerical solution of a logarithmic integral equation of the first kind for the helmholtz equation.*, Numerische Mathematik, 66 (1993), pp. 199–214.

[40] P. LAX AND L. PHILIPS, *Scattering Theory*, Academic Press, London, 1967.

[41] A.-W. MAUE, *Zur Formulierung eines allgemeinen Beugungsproblems durch eine Integralgleichung*, Z. Physik, 126 (1949), pp. 601–618.

[42] R. POTTHAST, *Fréchet differentiability of boundary integral operators in inverse acoustic scattering*, Inverse Problems, 10 (1994), pp. 431–447.

[43] R. POTTHAST, *Fréchet differentiability of the solution to the acoustic Neumann scattering problem with respect to the domain*, J. Inverse Ill-Posed Probl., 4 (1996), pp. 67–84.

[44] P. SERRANHO, *A hybrid method for inverse scattering for shape and impedance*, Inverse Problems, 22 (2006), pp. 663–680.

[45] P. SERRANHO, *A hybrid method for inverse obstacle scattering problems*, PhD thesis, University of Göttingen, (2007).

[46] B. D. SLEEMAN, *The inverse problem of acoustic scattering*, IMA J. Appl. Math., 29 (1982), pp. 113–142.

[47] A. SOMMERFELD, *Partial Differantial Equations.*, Academic Press, New York, 1949.

Curriculum vitae – Lebenslauf

Name: Ahmet Altundag

Geboren: 12.12.1979

Geburtsort: Mardin, Türkei

Familienstand: Verheiratet und habe einen Sohn

Staatsangehörigkeit: Türkisch

Wohnsitz: Göttingen

Akademische Ausbildung

09.'96–06.'99:   Gymnasium, Iskenderun Cumhuriyet Lisesi

09.'01–06.'05:   Bachelor, in Mathematik
                 an der Technischen Universität Yildiz, Istanbul

09.'02–08.'05:   Bachelor, in Physik
                 an der Technischen Universität Yildiz, Istanbul

09.'06–08.'05:   Master, in Mathematik
                 an der Technischen Universität Istanbul

01.'09–01.'12:   Stipendiat im DFG Graduiertenkolleg 1023
01.'12 :   Einreichung der Dissertation

_____   _____
      Datum, Ort   Ahmet Altundag